



Ash-related issues during biomass combustion: Alkali-induced slagging, silicate melt-induced slagging (ash fusion), agglomeration, corrosion, ash utilization, and related countermeasures

Yanqing Niu ^{a,b,c,*}, Houzhang Tan ^{a,c}, Shi'en Hui ^{b,c}

^a Key Laboratory of Thermo-Fluid Science and Engineering of MOE, School of Energy and Power Engineering, Xi'an Jiaotong University, Xi'an, Shaanxi, 710049, China

^b State Key Laboratory of Multiphase Flow in Power Engineering, Xi'an Jiaotong University, Xi'an, Shaanxi, 710049, China

^c Department of Thermal Engineering, School of Energy and Power Engineering, Xi'an Jiaotong University, Xi'an, Shaanxi, 710049, China



ARTICLE INFO

Article history:

Received 22 August 2015

Accepted 10 September 2015

Available online 20 October 2015

Keywords:

Biomass ash

Slagging

Agglomeration

Corrosion

Additives

Leaching

Co-firing

ABSTRACT

Biomass is available from many sources or can be mass-produced. Moreover, biomass has a high energy-generation potential, produces less toxic emissions than some other fuels, is mostly carbon neutrality, and burns easily. Biomass has been widely utilized as a raw material in thermal chemical conversion, replacing coal and oil, including power generation. Biomass firing and co-firing in pulverized coal boilers, fluidized bed boilers, and grate furnaces or stokered boilers have been developed around the world because of the worsening environmental problems and developing energy crisis. However, many issues hinder the efficient and clean utilization of biomass in energy applications. They include preparation, firing and co-firing, and ash-related issues during and after combustion. In particular, ash-related issues, including alkali-induced slagging, silicate melt-induced slagging (ash fusion), agglomeration, corrosion, and ash utilization, are among the most challenging problems. The current review provides a summary of knowledge and research developments concerning these ash-related issues. It also gives an in-depth analysis and discussion on the formation mechanisms, urgent requirements, and potential countermeasures including the use of additives, co-firing, leaching, and alloying.

Alkali species, particularly alkali chlorides and sulfates, cause alkali-induced slagging during biomass combustion. Thus, the mechanisms of generation, transformation, and sequestration of alkali species and the formation and growth of alkali-induced slagging, formed as an alternating overlapping multi-layered structure, are discussed in detail. For silicate melt-induced slagging (ash fusion), the evolutions of chemical composition of both the elements and minerals in the ash during combustion and existing problems in testing are overviewed. Pseudo-4D phase diagrams of $(\text{Mg}_2\text{O})\text{-MaeO-P}_2\text{O}_5\text{-Al}_2\text{O}_3$ and $(\text{Mg}_2\text{O})\text{-MaeO-SiO}_2\text{-Al}_2\text{O}_3$ are proposed as effective tools to predict ash fusion characteristics and the properties of melt-induced slagging. Concerning agglomeration that typically occurs in fluidized bed furnaces, melt-induced and coating-induced agglomeration and coating-forming mechanisms are highlighted. Concerning corrosion, seven corrosion mechanisms associated with Cl_2 , gaseous, solid/deposited, and molten alkali chlorides, molten alkali sulfates and carbonates, and the sulfation/silication of alkali chlorides are comprehensively reviewed. The effects of alloying, salt state (solid, molten, or gaseous), combustion atmosphere, and temperature are also discussed systematically. For ash utilization, potential approaches to the use of fly ash, bottom ash, and biomass/coal co-fired ash as construction and agricultural materials are explored.

Several criteria or evaluation indexes are introduced for alkali-induced slagging and agglomeration, and chemical equilibrium calculation and multicomponent phase diagrams of silicate melt-induced slagging and agglomeration. Meanwhile, remedies, including the use of additives, co-firing, leaching, alloying, and the establishment of regulations, are discussed.

It is suggested that considerable attention should be focused on an understanding of the kinetics of alkali chemistry, which is essential for the transformation and sequestration of alkali species. A combination of heterogeneous chemical kinetics and multiphase equilibrium modeling is critical to estimating the speciation, saturation levels, and the presence of melt of the ash-forming matter. Further practical

* Corresponding author. Key Laboratory of Thermo-Fluid Science and Engineering of MOE, School of Energy and Power Engineering, Xi'an Jiaotong University, Xi'an, Shaanxi, 710049, China. Tel.: +86 137 09181734; Fax: +86 029 82668703.

E-mail address: yqniu85@mail.xjtu.edu.cn (Y. Niu).

evaluation and improvement of the existing criterion numbers of alkali-induced slagging and agglomeration should be improved. The pseudo-4D phase diagrams of $(\text{Mg}_2\text{O})\text{-MgO-P}_2\text{O}_5\text{-Al}_2\text{O}_3$ and $(\text{Mg}_2\text{O})\text{-MgO-SiO}_2\text{-Al}_2\text{O}_3$ should be constructed from the data derived from real biomass ashes rather than those of simulated ashes in order to provide the capability to predict the properties of silicate melt-induced slagging. Apart from Cr, research should be conducted to understand the effects of Si, Al, and Co, which exhibit high corrosion resistance, and heavy metals such as Zn and Pb, which may form low-melting chlorides that accelerate corrosion. Regulations, cooperation among biomass-fired power plants and other industries, potential technical research, and logistics should be strengthened to enable the extensive utilization of biomass ash. Finally, alkali-induced slagging, silicate melt-induced slagging, agglomeration, and corrosion occur concurrently, and thus, these issues should be investigated jointly rather than separately.

© 2015 Elsevier Ltd. All rights reserved.

Contents

1. Introduction	3
2. Part I. Main ash-related issues during combustion: alkali-induced slagging, silicate melt-induced slagging (ash fusion), agglomeration, and customized countermeasures including additives, co-firing, and leaching	4
2.1. Alkali-induced slagging	6
2.1.1. Mechanisms of the generation, transformation, and sequestration of alkali species	6
2.1.2. Mechanisms of the formation and growth of alkali-induced slagging	8
2.1.3. Criterion numbers or evaluation indexes	10
2.2. Silicate melt-induced slagging (ash fusion)	10
2.2.1. Ash fusion test	13
2.2.2. Effects of chemical compositions on AFC	13
2.2.3. Evolution of chemical compositions in ash during combustion	15
2.2.4. Chemical equilibrium calculation	16
2.2.5. Multi-component phase diagram	17
2.3. Agglomeration	19
2.3.1. Effects of bed materials and fuels	19
2.3.2. Agglomeration formation mechanisms	19
2.3.3. Coating forming mechanisms	20
2.3.4. Agglomeration indicator	22
2.4. Countermeasures for the main ash-related issues: additives	23
2.4.1. Effects of single oxide or element additives	23
2.4.2. Effects of mineral additives	25
2.5. Countermeasures for main ash-related issues: co-firing	28
2.5.1. Co-firing benefits and classifications	28
2.5.2. Co-firing in CFB	30
2.5.3. Co-milling co-firing in PC furnace	31
2.5.4. Injection co-firing in PC furnace	31
2.6. Countermeasures for main ash-related issues: leaching	32
2.6.1. Technical water leaching (batch leaching)	33
2.6.2. Technical semi-continuous leaching	33
2.6.3. Natural water leaching by rain and snow	35
2.6.4. Effect of leaching intensity: amount of water and/or time	35
3. Part II. Corrosion	37
3.1. Corrosion mechanisms	37
3.1.1. Corrosion associated with Cl_2	37
3.1.2. Corrosion associated with gaseous alkali chlorides	38
3.1.3. Corrosion associated with solid/deposited alkali chlorides	39
3.1.4. Corrosion associated with sulfation/silication of alkali chlorides	40
3.1.5. Corrosion associated with molten alkali chlorides	40
3.1.6. Corrosion associated with molten alkali sulfates	41
3.1.7. Corrosion associated with molten alkali carbonates	42
3.2. Corrosion countermeasures or influence factors	43
3.2.1. Alloying and salts	43
3.2.2. Atmosphere and temperature	46
4. Part III. Ash utilization	46
4.1. Physico-chemical properties of biomass ash	49
4.2. Utilization for construction materials	51
4.2.1. Relative standard on ash utilization in cement	51
4.2.2. BFA	53
4.2.3. BBA	53
4.2.4. Biomass/coal co-fired ash	54
4.3. Utilization in agriculture and other fields	55
4.4. Barriers and counterplans for the utilization of biomass ash	55
5. Conclusions	55
Acknowledgements	57
References	57

1. Introduction

Biomass as a sufficiently “green” renewable and CO₂-neutral energy source has attracted worldwide attention because of the worsening energy crisis and environmental issues. By switching from coal and natural gas to biomass, the net CO₂ emission per unit heating value can be reduced by 93% and 84%, respectively [1]. In 2004, the total global biomass power installed capacity reached 39 GW, and the annual energy generation achieved was approximately 200 billion kWh [2]. Data show that biomass power installed capacity in the USA has reached 10 GW [3], and a similar increase to 30 GW by 2020 is expected in China [4].

Biomass fuel is defined as any solid organic material that can be burned and used as a source of fuel [5]. Biomass can be classified into four major categories, according to its source, i.e., woody, agricultural, waste, and excrement. Among these, woody biomass is the largest biomass energy source; it covers forest residues (e.g., dead trees, branches and tree stumps, leaves), landscaping residues (yard clippings), industrial wood residue (wood chips, sawdust, etc.), waste wood residues, and so on. Agricultural biomass contains straw and other harvesting residues from agriculture, energy plants from agriculture, residues from the food industry, and grass. Waste includes municipal solid waste, domestic wastewater, commercial waste, and construction waste. Excrement includes farm slurry/excrement and organic waste from households and industry.

Despite its well-known advantages such as high-energy-generation potential and carbon dioxide neutrality that encourage the rapid development of biomass-fired power plants, biomass combustion remains challenging for several reasons. These include problems in the pre-preparation of biofuel (referring to collection, transportation, upgrading by leaching, torrefaction and pelletizing, and milling), firing and co-firing technologies (encompassing direct

firing, injection co-firing, co-milling co-firing, pre-gasification co-firing, and parallel co-firing in pulverized coal (PC) boilers, FB boilers, and grate or fixed bed furnaces), and ash-related issues that occur both during and after combustion [5]. As shown in Fig. 1, ash-related problems, including alkali-induced slagging [6,7,11–14], silicate melt-induced slagging (ash fusion) [3,7,9,14–16], agglomeration [8,14,17–20], corrosion [10,14,21–24], and ash utilization [25,26], are the most intractable issues. Whether in FBs or grate furnaces, high concentrations of Cl and alkali metals (K and Na) in biomass result in the rapid buildup of unmanageable deposits on the fired surfaces, particularly alkali-induced slagging on the superheater [3,6,7,9,11–16,27,28] and silicate melt-induced slagging on the water wall [3], which inhibit heat transfer and reduce boiler efficiency [26,29]. Furthermore, accumulated ash with a high Cl concentration on tube surfaces may lead to corrosion underneath the deposit [14,22,28]. Meanwhile, agglomeration, which originates from fused or partly fused ash, is another major challenge in biomass combustion in FBs and frequently results in defluidization and unscheduled shutdown of the entire power plant [8,14,17–20,28,30]. However, the corresponding mechanisms and countermeasures for alkali-induced slagging, silicate melt-induced slagging (ash fusion), agglomeration, and corrosion, and the utilization/disposal principles of ash residues from biomass-fired power plants remain unclear [28]. Unlike coal, biomass has various sources. For example, woody biomass is low in Si and K, yet high in Ca. Agricultural residues are high in Si and K, yet low in Ca. In contrast, animal residues are high in both P and Ca [28,31]. Furthermore, even for a specific biomass, different planting environments [12,32], harvest seasons [20,33], and different parts of the biomass [34,35] can produce distinct ash contents and compositions. This results in unpredictable and highly variable ash-related issues.



Fig. 1. Images of various ash-related issues in biomass-fired furnaces.

upper left: alkali-induced slagging in a 12 MW grate furnace (reprinted from reference 6, with permission of American Chemical Society)
upper middle: alkali-induced slagging in a commercial fluidized bed (FB) (adapted from reference 7)

upper right: agglomeration in a lab-scale bubbling fluidized bed (reprinted from reference 8, with permission of Elsevier)

bottom left: silicate melt-induced slagging (ash fusion) in a 12 MW grate furnace (reprinted from reference 6, with permission of American Chemical Society)

bottom middle: silicate melt-induced slagging (ash fusion) in a lab-scale furnace (adapted from reference 9)

bottom right: corrosion in a commercial bubbling fluidized bed (BFB) (Adapted from reference 10)

KCl and K₂SO₄ are the dominant alkali-containing substances that influence biomass ash-related issues [36]. While K₂SO₄ is a dominant species that nucleates when the gas temperature is reduced [37], KCl condenses on the K₂SO₄ nuclei at a low temperature [38]. Similar results were reported by Reichelt et al. [39] and Nutalapati et al. [31] from both experimental data and FACTSAGE simulation calculations. They found that K₂SO₄ mainly accumulates on high-temperature heating surfaces, whereas KCl accumulates on low-temperature heating surfaces. In addition, Li et al. [3] and authors [6] have indicated that both K₂Ca(SO₄)₂ and K₃Na(SO₄)₂ play a significant role in slagging.

A number of experimental studies concerning additives [40,41], co-firing [42,43], chemical pretreatment [44,45], and alloying [46,47], all of which change the generation and transformation processes of alkali chlorides and sulfates, have been conducted to solve ash-related problems. However, these are all possible targets because of the variability in biomass species, plant environment, combustion temperature, and atmosphere [40,48–51]; remedial methods that may be effective under one set of conditions may prove ineffective for other types of fuel and under different conditions. As an alternative, to solve these troublesome ash-related problems fundamentally and provide useful guidelines for the selection of co-firing fuels, additives, and biomass fired in utility boilers, several researchers began to focus on criterion numbers or evaluation indexes such as the alkali index (K₂O + Na₂O) kg·GJ⁻¹ [52], (Na + K+2Mg+2Ca)/S ratio [53], (K + Na)/(Ca + Mg) ratio [54], and S/Cl ratio [55].

Aside from the experimental research on additives, co-firing, chemical pretreatment, and evaluation indexes, several researchers studied ash transformation by means of thermal-balance calculation software such as FACTSAGE, which is based on Gibbs free energy minimization [31,56–58]. However, Bostrom et al. [48] pointed out that the ash transformation reactions may be influenced by temperature, residence time, air supply, flue gas velocity, and other factors. Because in the flame of a powder burner or PC furnace, short residence times limit the interactions and encounters between the ash and gases; the system is far from being at equilibrium. The main challenges are not only to predict local compositions and implement relevant transport equations for particles, but also to obtain a reasonable estimate of the speciation of inorganic matter, i.e., ash-forming elements, in each volume cell rather than in the pseudo-final state.

Although several studies including experiments, evaluation index analysis, and thermal-balance calculation/simulations have been conducted, ash-related problems remain unresolved, and knowledge about their causes is fragmentary. Therefore, the focus of this study is to review the progress of research and to reveal the formation

mechanisms, urgent requirements, and potential countermeasures to solve the abovementioned ash-related problems. The paper consists of three main parts, divided according to the amount of research attention they have received and their importance in current practical operations in biomass power generation:

Part I presents the main ash-related issues, including alkali-induced slagging, silicate melt-induced slagging (ash fusion), and agglomeration, as well as countermeasures related to the use of additives, co-firing, and leaching.

Part II presents a discussion of the additional ash-related issues, i.e., corrosion, including various corrosion mechanisms and countermeasures or influence factors.

Part III focuses on biomass ash utilization as construction materials and agricultural soil ameliorants. Limitations and counterplans are also discussed.

2. Part I. Main ash-related issues during combustion: alkali-induced slagging, silicate melt-induced slagging (ash fusion), agglomeration, and customized countermeasures including additives, co-firing, and leaching

A schematic of ash formation and transformation mechanism in biomass combustion is shown in Fig. 2. Similar to pulverized coal combustion [59], during the combustion of biomass particles and the formation of char particles, volatile organo-metallic compounds (containing Cr, V, etc.) are first released followed by devolatilization; then, partial alkali and alkali-earth elements (e.g., K, Na, and Ca) and volatile trace elements (e.g., Hg, As, and Se) diffused out of the char. As the gas temperature decreases, the volatile components nucleate and condense to form submicron-sized particle. Also, some volatile material condenses on residual fly ash. The high concentrations of K and Na (especially K) through nucleation, condensation, and reactions result in a variety of severe ash-related problems such as alkali-induced slagging, silicate melt-induced slagging (ash fusion), and agglomeration (Figs. 1 and 3).

Fig. 3 shows the formation mechanisms of alkali-induced slagging, silicate melt-induced slagging (ash fusion), agglomeration, and fly ash. KCl is considered the most stable gas-phase alkali-metal-containing substance in the entire combustion process and the dominant substance that influences biomass slagging [6,36,60]. During the process of combustion, alkali metals undergo complex chemical reactions and transformation and are released as KOH_{aerosol}, KCl_{aerosol}, K₂SO₄_{aerosol}, NaCl_{aerosol}, Na₂SO₄_{aerosol}, and other compounds [61]. As flue gas temperature decreases, some alkali metal aerosols grow and form submicron ash particles by mechanisms that

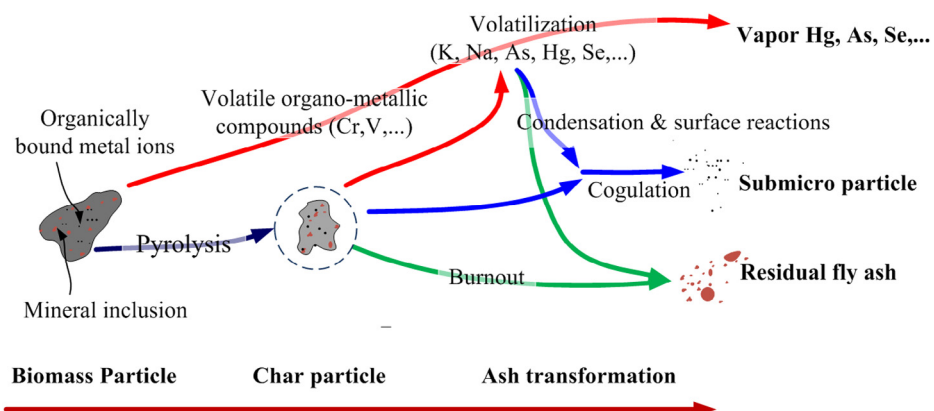


Fig. 2. Schematic diagram of ash formation and transformation mechanisms in biomass combustion (adapted from reference 59).

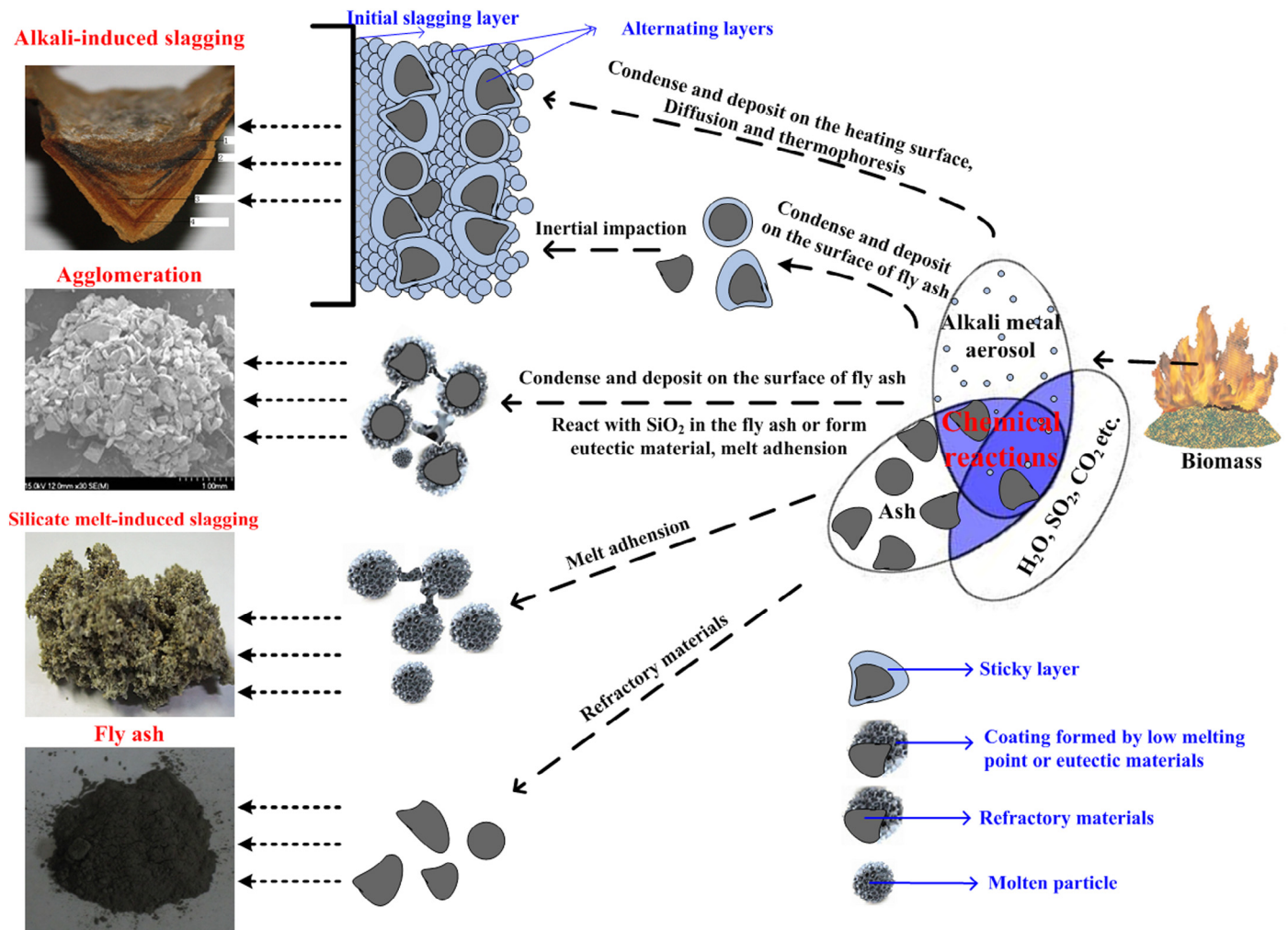


Fig. 3. Schematic of the formation processes of the main ash-related issues in biomass combustion (adapted from reference 12 with permission of Elsevier).

include nucleation, adsorption, condensation, and chemical reaction. These then condense on the heating surfaces and form a sticky initial slagging layer via thermophoresis and turbulent diffusion; this sticky layer serves as an adhesive that bonds subsequent fly ash to the heating surfaces [60,62]. Some alkali metal aerosols condense on the surface of the fly ash and either form a sticky layer or form low-melting substances by reaction with SiO_2 [49] and Fe_2O_3 [62] contained in the fly ash. Furthermore, some alkali metal aerosols form low-temperature eutectic mixtures; for example, $\text{Na}_2\text{SO}_4 + \text{NiSO}_4$, which melts between 944 K and 1157 K [62], and $\text{KCl} + \text{K}_2\text{SO}_4$, which melts at 823 K [63]. Subsequently, coarse fly ash, with or without a self-surface sticky layer, is deposited on the surface of the sticky initial slagging layer by inertial impaction [6,36]. Once the initial slagging layer loses sufficient adhesion to accumulate further coarse fly ash, a new sticky layer, mainly containing submicron ash particles enriched in alkali metals, re-forms. The accumulation of submicron alkali metal ash particles and the capture of coarse ash particles result in the construction of an alternating overlapping multi-layered structure [6]. This process of alkali-induced slagging is shown in the top part of Fig. 3.

Aside from playing a supporting role in the formation of overlapping layered slagging, alkali metals, when combined with SiO_2 , lead to agglomeration, as shown in Fig. 3. Accompanied by alkali-induced slagging, partial alkali metals react with SiO_2 in the fly ash or bed material and transform into molten silicates, typically in FBs or at FB temperatures [64,65]. For woody biomass containing K and

relatively low amounts of Si, a low-temperature K-silicate melt is formed on the bed particle surfaces through a reaction with gaseous, aerosols, or liquid K compounds. For agricultural biomass with high K content and organically bound Si, agglomeration is attributed to the direct adhesion of bed particles by partly molten ash-derived K-silicate particle/droplet [64,65].

Unlike alkali-induced slagging and agglomeration where alkali metals play a dominant role, silicate melt-induced slagging (ash fusion) is more dependent on Si, Al, and other elements present in the ash. Once the furnace temperature exceeds the melting point of the ash, the ash undergoes deformation and melting and then adheres to the heating surface by inertial impaction. Several studies have indicated that the initial deformation temperature (IDT) increases with reduced K_2O and increased MgO , CaO , Fe_2O_3 , Al_2O_3 , and SiO_2 content in the ash [15]. Increased Si/Al leads to a decrease in IDT because Al_2O_3 causes a greater increase than SiO_2 in the ash fusion temperature [7]. Meanwhile, refractory minerals (quartz, metakaolinite, mullite, rutile, etc.) increase the ash fusion temperature, whereas fluxing minerals (anhydrite, calcium silicate, hematite, etc.) reduce it [66].

During combustion, only a small part of the inorganic components are involved in alkali-induced slagging, silicate melt-induced slagging (ash fusion), and agglomeration; most are discharged along with flue gas in the form of fly ash. Additionally, the large quantity of fly ash produces themselves product a problem. Given the detailed schematics and discussions of the main ash-related issues

during biomass combustion shown in Figs. 1 and 3, alkali-induced slagging, silicate melt-induced slagging (ash fusion), and agglomeration may occur concurrently and should be studied in conjunction rather than separately [67].

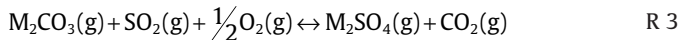
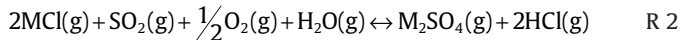
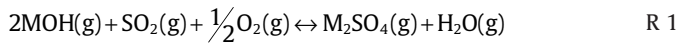
2.1. Alkali-induced slagging

Alkali-induced slagging is mainly associated with alkali metals, especially alkali chlorides and sulfates. Therefore, for alkali-induced slagging, more attention should be paid to the generation, transformation, and sequestration of the corresponding volatile alkali species, formation mechanisms, and criterion numbers or evaluation indexes.

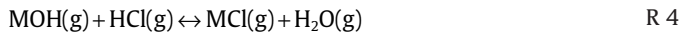
2.1.1. Mechanisms of the generation, transformation, and sequestration of alkali species

During combustion, accompanied by the decomposition of the organic structure (mainly composed of cellulose, hemicelluloses, lignin, lipid, protein, etc.), alkali metals are released and transported either in the form of solid particles or vapor species in the combustion gas. Alkali metals in solid particles exist mainly as M-silicates and M-aluminosilicates (M represents K and Na), and alkali vapor species exist mainly in the forms of M(g), MCl(g), (MCl)₂(g), M₂SO₄(g), and MOH(g) [61]. Initially, alkali metals in the form of both organic and inorganic Na and K compounds enter the gas phase [68]; subsequently, in comparison with all other ash-forming elements, the alkali metals form less stable oxides [48], and the oxides may also be reduced by the carbon-hydrogen fuel matrix into metal vapor at high combustion temperatures. Then these alkali species readily react with water vapor to form more stable and relatively volatile hydroxides [KOH(g) and NaOH(g)]. During the in-flight process, some alkali vapor species encounter a chemical environment that affects the final transfer out of the flame (postflame conditions). Possible gas-phase chemical reactions, including sulfation (R 1–R 3), chlorination (R 4 and R 5), and carbonation (R 6), are listed below [69,70]. Consequently, alkali sulfates, chlorides, and carbonates together with silicates and aluminosilicates enter the postflame flue gas and influence the ash-related issues.

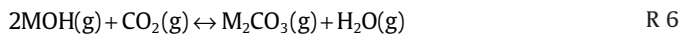
Sulfation reactions:



Chlorination reactions:



Carbonation reactions:



Focusing on different types of biomass, Dayton and Milne [71] identified the alkali vapor species by experiments in a variable-temperature quartz-tube reactor equipped with a molecular beam mass spectrometer (MBMS) system. They found that alkali sulfates are the primary alkali metal species released from the combustion of woody biomass with relatively low alkali metal content. Alkali chlorides are the primary alkali metal species released during the combustion of herbaceous biomass, grasses, and straws with high alkali metal and chlorine contents. Alkali

hydroxides are the most abundant alkali metal species in the vapor during the combustion of biomass with high alkali metal and low chlorine contents. Alkali cyanates are the dominant alkali metal species released from biomass with high alkali content and fuel-bound nitrogen. Similarly, Wei et al. [61] studied K release during the processes of combustion and gasification by means of the thermodynamic calculation tool, FACTSAGE, and showed that for straw biomass with high K, Cl, and Si and low S content, the main potassium species are KCl(g), KOH(g), and K₂Si₄O₉(l) above 1100 K; K₂SO₄(s2) and K₂Si₄O₉(s,s2) from 800 to 1100 K; and KCl(s), K₂SO₄(s), and K₂Si₂O₅(s) from 400 to 900 K. For woody biomass with low K, Cl, and Si and high S content, KCl(g), K₂SO₄(g), and KOH(g) are the primary potassium species above 1100 K; KAlSi₂O₆(s,s2) and K₂SO₄(s2) are the major species from 800 to 1100 K, and K₂SO₄(s) and KAl(SO₄)₂(s) from 400 to 900 K.

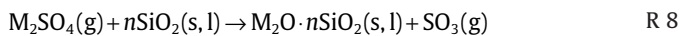
Thermodynamic calculations have also shown that the chlorine content of biomass is an important parameter that facilitates alkali release [61,69,71]. During combustion between 673 and 1273 K and with a constant K(g)/Cl(g) molar ratio of 1.0, KCl(g) is the dominant product based on the calculation using HSC ignoring the condensed phase of the alkali compounds; however, the quantity of KCl(g) decreases with decreased concentrations of Cl(g) and K(g) and results in an increased fraction of KOH(g), which is attributed to the reverse reaction of R 4. When the K(g)/Cl(g) molar ratio is lower than unity, a high chlorine content promotes the release of KCl(g) from R 4 as expected, and there almost no KOH(g) formed because of the presence of excess chlorine that is released as HCl(g). When the K(g)/Cl(g) molar ratio is higher than unity, above 1073 K, the excess potassium is released in the form of KOH(g), whereas, below this temperature, K₂CO₃(g) is formed because of the carbonation of KOH(g) from R 6 as expected [69].

Fig. 4 illustrates the release of chlorine and alkali metals during the combustion of Swedish wood and Danish straw with varying air excess coefficients, up to a temperature of 1800 K, the results are similar with above mentioned [61]. Fig. 4a shows that when the concentrations of Cl and K are low (Swedish wood), the fraction of KOH(g) is high at temperature above 1400 K. KCl(g) and KOH(g) coexist between 1000 and 1800 K, but the concentration of KCl(g) becomes greater than that of KOH(g) below 1400 K. Due to the considerably large S/Cl mole ratio, the quantity of K₂SO₄(g) peaked at 1250 K occurs between 1400 and 1100 K. Detailed analysis of the K balance and the slopes of the curves for KCl(g), KOH(g), HCl(g), and K₂SO₄(g), shown in Fig. 4a, reveals that from 1800 to 1400 K, the chlorination of KOH(g) by R 4 results in an equivalent reduction in KOH(g) and HCl(g) and an equivalent increase in KCl(g). From 1400 to 1250 K, the sulfations of both KCl(g) and KOH(g) (primarily the sulfation of KOH(g) above 1250 K), i.e., R 1 and R 2, increase the amount of K₂SO₄(g) and decrease that of both KOH(g) and KCl(g) proportionally. However, between 1250 and 1100 K, the condensation, silication and alumina-silication reactions shown as R 7–R 9 result in reduced K₂SO₄(g). Alternatively, the continuous decrease in KOH(g) and KCl(g) is attributed to silication and alumina-silication reactions (R 10–R 13) between 1250 and 1000 K.

Condensation of alkali sulfates:



Silication reactions of alkali sulfates:



When n is 1, 2, and 4, the melting points of K₂O_nSiO₂ are below 1073 K [72,73].

Alumina-silication reactions of alkali sulfates:

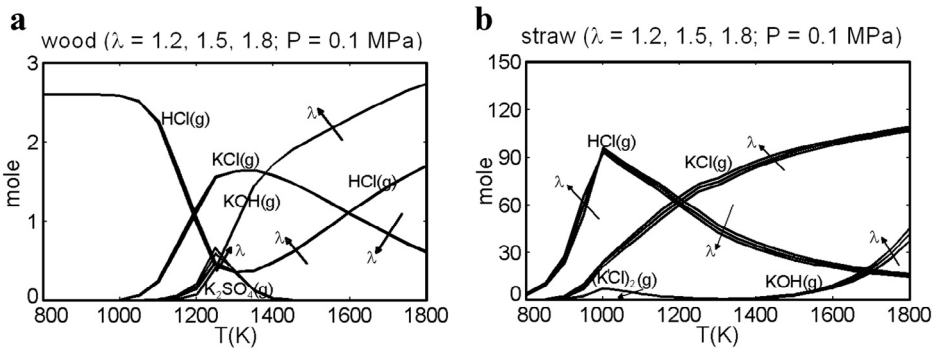
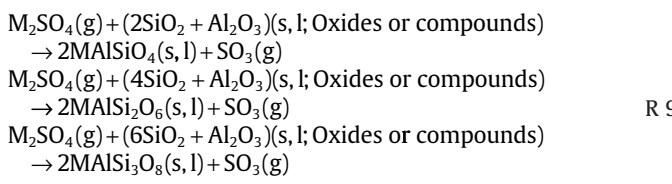


Fig. 4. Release of Cl and alkali metals during the combustion of wood and straw with varying air excess coefficients (reprinted from reference 61, with permission of Elsevier).
a. Swedish wood, b. Danish straw.

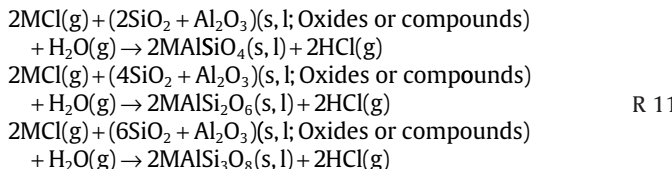
Swedish wood: Cl: 2.60, S:17.26, Si:5.35, K:3.41, unit: mol/1000 kg fuel;
Danish straw: Cl: 132.00, S:27.54, Si:1191.10, K:328.49, unit: mol/1000 kg fuel;
 λ : ratio of oxygen/fuel



Silication reactions of alkali chlorides:



Alumina-silication reactions of alkali chlorides:



Silication reactions of alkali hydroxides:



Alumina-silication reactions of alkali hydroxides:

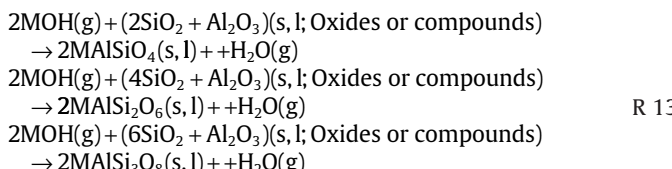


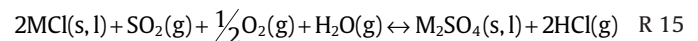
Fig. 4b shows that for straw biomass with high Cl, K, Si, and K/Cl and low S/Cl, KCl(s) and KOH(g) exist above 900 and 1400 K, respectively; these are the primary alkali vapor species in this temperature range. From 1800 to 1000 K, both KCl(g) and KOH(g) decrease because of either silication or alumina-silication reactions, labeled as R 10-R 13, and the amount of produced HCl(g) increases. Below 1000 K, KCl continually decreases because of condensation (R 14). This is good agreement with experiment that indicate that potassium losses are positively correlated with temperature and that the KCl(s,l) in ash disappears completely above 1273 K during combustion or ashing [70]. The authors also found that Cl and KCl exist in ash incinerated

below 1088 K and disappear completely at increased temperatures because of alumina-silication or sulfation or the evaporation of KCl [15].

Condensation of alkali chlorides:



Fig. 4 also shows that oxygen has a certain influence on alkali species transformation. Besides O₂, the concentrations of SO₂(g) and H₂O(g) also have considerable effects on alkali species transformation. R 1-6 indicate that the appearance of SO₂(g), O₂(g), and H₂O(g) promote sulfation and inhibit chlorination and carbonation. The kinetics effects of SO₂(g), O₂(g), and H₂O(g) on KCl(s,l) and K₂SO₄(s,l), i.e., the sulfation of KCl(s,l) expressed by R 15 have been studied in detail. The kinetic parameters are summarized in Table 1. Below 923 K, the reactions are essentially controlled by physical adsorption because of low activation energies; however, at around 923 K, they transform from gas-solid reactions to gas-liquid reactions probably because of phase transition from solid to eutectic mixture of potassium chlorides and sulfates [74,75]. The activation energy for the gas-solid/liquid sulfation of MCl is approximately 146 ± 11 kJ/mol, and the reaction orders of SO₂(g), O₂(g), and H₂O(g) vary with the changing conditions. These global kinetic descriptions provide useful information on the kinetic simulation of sulfation of solid/liquid alkali chlorides.



Focusing on the global gas-solid/liquid sulfation reactions of R 15, Henriksson and Warnqvist [76] proposed detailed reaction mechanisms, which were subsequently adopted and improved by Boonsongsup et al. [77] and Li et al. [78]. Henriksson and Warnqvist [76] reported that SO₂(g), O₂(g), and H₂O(g) are first adsorbed on the surface of MCl. Then SO₂(ads) reacts with O₂(ads) to form SO₃(ads). H₂O(ads) reacts with SO₃(ads) to form H₂SO₄(ads). The products, M₂SO₄(s) and HCl(g), are obtained from the reaction between H₂SO₄(ads) and MCl(g) with NaHSO₃(ads) as an intermediate. The researchers pointed out that adsorption of SO₂(g) on the surface of MCl(s) is the rate-limiting step, and O₂(g) and H₂O(g) are not involved. Similarly, Boonsongsup et al. [77] emphasized that the reaction rate is independent of O₂ and H₂O concentration under the conditions employed (listed in Table 1). That is, oxygen and water vapor are involved in a fast reaction step that does not control the overall rate of reaction. The detailed Henriksson and Warnqvist reaction mechanisms are shown below.



Table 1

Kinetic parameters for R 15 $\frac{dX}{dt} = A \exp(-E/RT)(1-X)^{2/3}(SO_2)^l(O_2)^m(H_2O)^n$.

Authors	MCl	T, K	E, kJ/mol	SO ₂		O ₂		H ₂ O		A, s ⁻¹	Size, μm
				Conc. ppm	l	Conc. Vol. %	m	Conc. Vol. %	n		
Sengelov et al. [74]	KCl (s,l)	873–1023	157	500–1500 500–3000	0.78 0.59	1–20	0.37	4–15	0.15	3.7*10 ^{6a}	90–125
Matsuda et al. [75]	NaCl (s)	623–923	23	3000–13000	0.3	2.5–15	0.6	5–20	0.2	4.31*10 ^{-4b}	75–125
	NaCl (s,l)	923–1123	144		1.4		0.7		0.8	3.18*10 ^{-3b}	
	KCl (s)	623–923	3.46		0.2		0.3		0.3	5.03*10 ^{-6b}	
	KCl (s,l)	923–1123	137		0.5		0.4		0.7	7.35*10 ^{-2b}	
Henriksson and Warnqvist [76]	NaCl (s,l)	873–1073	115 ± 15	1000–500000	0.5	1–10	0.5	2.5–30	Independent	1.4*10 ^{-1c}	250–320
Boonsongsup et al. [77]	NaCl(s)	673–873	17.3	3000–7000 7000–11000	0.67 0.16	3–11	Independent	0.5–20	Independent	1.21*10 ^{-3c}	125–250

^a The value is calculated according to the reactant mole fraction.

^b The value is calculated according to the reactant partial pressure.

^c Unit: mol/(m²·atm·min).

O ₂ (g)↔O ₂ (ads)	R 17
H ₂ O(g)↔H ₂ O(ads)	R 18
SO ₂ (ads)+O ₂ (ads)↔SO ₃ (ads)	R 19
SO ₃ (ads)+H ₂ O(ads)↔H ₂ SO ₄ (ads)	R 20
H ₂ SO ₄ (ads)+NaCl(s)↔NaHSO ₄ (ads)+HCl(g)	R 21
NaHSO ₄ (ads)+NaCl(s)↔Na ₂ SO ₄ (s)+HCl(g)	R 22

Most studies focused only on the gas–solid/liquid sulfation reaction of alkali chlorides R 15. Research into the kinetics of the gas–gas reactions of R 1–R 6 and gas–solid/liquid reactions of R 7–R 14, which are essential to understand the alkali transformations, is scarce. Li et al. [78] recently studied the homogenous sulfation of KCl(g) from 950 to 1400 K in a multi-jet burner by means of spectroscopy and elastic scattering. Experimental and model predictions (Chemkin 4.1.1) showed that the gas-phase sulfation of KCl(g) to K₂SO₄(g) by the homogeneous nucleation of K₂SO₄(g), a mechanism by which aerosols form, is favorable; in addition, the sulfation rate is limited by the oxidation of SO₂ to SO₃. This finding is supported by a recent industrial study conducted by Kassman et al. [79], who reported that the injection of ammonium sulfate, which serves as a source of SO₃, is more efficient than the injection of elemental sulfur in promoting KCl sulfation.

As summarized in Table 2, the preliminary mechanisms of alkali-salts generation and transformation, which clarify the alkali metal chemistry during biomass combustion to a certain extent, are deduced. During the process of combustion, alkali chemistry is affected by the species, temperature, atmosphere, and concentrations of K, Cl, and S. For biomass with high concentrations of Cl and K and fired above 1400 K, KCl(g) is the dominant alkali vapor species. KOH(g) is present when the Cl/K molar ratio is lower than unity. K-silicates and K-aluminosilicates, which originate directly from external mineral sources or are generated by both alumina-silication and silication reactions (R 10–R 13), are the major nonvolatile alkali salts. As the temperature decreases to 1000 K, the concentration of KCl(g), which remains the dominant alkali vapor species, decreases because of alumina-silication and silication reactions (R 10–R 13), whereas KOH(g) disappears completely because of sulfation (R 1 and R 2) and chlorination (R 4) reactions. When the flue gas temperature is less than 1000 K, the remaining KCl(g) is transferred into KCl(s,l) by condensation (R 14) or transferred into K₂SO₄(s,l) through R 15.

For biomass with low concentrations of Cl and K and fired above 1400 K, KCl(g) remains the dominant alkali vapor species regardless of whether the Cl/K molar ratio is higher or lower than unity. By contrast, the fraction of KOH(g) is higher than that of KCl(g) when the Cl/K molar ratio is lower than unity. Meanwhile, the KOH(g) fraction increases with the decrease in Cl(g) and K(g) concentrations, i.e., when the concentrations of Cl and K are low, the KOH(g) fraction is high, and the KCl(g) fraction and the mole ratio of KCl(g)/KOH(g) are low. Between 1400 and 1000 K, KCl(g) and KOH(g) remain the primary alkali vapor species. However, K₂SO₄(g, l) is generated via R 1, R 2, and R 7 when S is present in the fuel. Below 1000 K, the remaining K vapor is transformed into KCl(s,l) and K₂SO₄(s,l).

Although research on the sulfation of MCl is relatively comprehensive, kinetics research, particularly on R 1–R 14, which are essential for the transformation and sequestration of alkali species, requires further investigation. Moreover, the existing kinetics mechanisms should be checked carefully.

2.1.2. Mechanisms of the formation and growth of alkali-induced slagging

Primary deposits form directly on the tube itself very rapidly because of mineralogical reactions. These deposits have a high content of alkali sulfates and chlorides, which, because of their low melting points, both function as glue for the secondary deposits.

Wang et al. [80] conducted a biomass combustion experiment in a drop-tube furnace and pointed out that sulfates and chlorides are the key species that contribute to the formation of ash deposits in a biomass furnace, particularly sulfates. Gaseous KCl and SO₂ are released during high-temperature biomass combustion. Some of the SO₂ is further oxidized into SO₃, which then reacts with KCl to form K₂SO₄ and KHSO₄. The concentration of KCl in the flue gas is significantly reduced after sulfation. As the gas temperature further decreases, alkali sulfates begin to nucleate and condense forming nanoscale aerosols. A part of the K₂SO₄ reacts with SO₃ to form K₂S₂O₇, which has a low melting point. The K₂SO₄ and K₂S₂O₇ aerosols tend to deposit on low-temperature tube surfaces, resulting in an increase in the ash deposition rate, as observed in many biomass-fired power plants. The transformation of SO₂ to SO₃ has a relatively low reaction rate and is a major limiting step in the sulfation and deposition processes. For crop straw, the alkali and chlorine contents are high, and the alkali elements are mainly released as chlorides at high temperatures. The chlorides are then converted into sulfates in the presence of SO₂ and SO₃. A decrease in temperature causes the sulfates to nucleate and condense, form aerosol particles, and finally deposit on the tube wall surface. The alkali content of wood is high but the chlorine content is low; consequently, the alkali elements are mainly released as NaOH and KOH,

Table 2
Alkali-salts generation and transformation mechanisms.

Temp. K	>1400		1400–1000			<900–1000	
Biomass	high Cl, high K Cl/K > 1.0	low Cl, low K Cl/K < 1.0	high Cl, high K Cl/K > 1.0	low Cl, low K Cl/K < 1.0	/	/	/
K-salts, vapor	KCl(g)	KCl(g), KOH(g)	KCl(g)	KOH(g), KCl(g)	KCl(g)	KCl(g), K ₂ SO ₄ (g,l)	KCl(s,l), K ₂ SO ₄ (s,l)
K-salts, non-volatile	K-silicates, K-aluminosilicates						
Principal reactions	<ul style="list-style-type: none"> ● Chlorination reactions of alkali hydroxides: $\text{MOH(g)} + \text{HCl(g)} \leftrightarrow \text{MCl(g)} + \text{H}_2\text{O(g)}$ R 4		<ul style="list-style-type: none"> ● Sulfation reactions of alkali hydroxides: $2\text{MOH(g)} + \text{SO}_2(\text{g}) + \frac{1}{2}\text{O}_2(\text{g}) \leftrightarrow \text{M}_2\text{SO}_4(\text{g}) + \text{H}_2\text{O(g)}$ R 1			<ul style="list-style-type: none"> ● Condensation of alkali sulfates: $\text{M}_2\text{SO}_4(\text{g}) \rightarrow \text{M}_2\text{SO}_4(\text{s}, \text{l})$ R 7	
			<ul style="list-style-type: none"> ● Sulfation reactions of alkali chlorides: $2\text{MCl(g)} + \text{SO}_2(\text{g}) + \frac{1}{2}\text{O}_2(\text{g}) + \text{H}_2\text{O(g)} \leftrightarrow \text{M}_2\text{SO}_4(\text{g}) + 2\text{HCl(g)}$ R 2			<ul style="list-style-type: none"> ● Condensation of alkali chlorides: $\text{MCl(g)} \rightarrow \text{MCl(s, l)}$ R 14	
			<ul style="list-style-type: none"> ● Chlorination reactions of alkali hydroxides: $\text{MOH(g)} + \text{HCl(g)} \leftrightarrow \text{MCl(g)} + \text{H}_2\text{O(g)}$ R 4			<ul style="list-style-type: none"> ● Sulfation reactions of alkali chlorides (Gas-solid or gas-liquid reactions): $2\text{MCl(s, l)} + \text{SO}_2(\text{g}) + \frac{1}{2}\text{O}_2(\text{g}) + \text{H}_2\text{O(g)} \leftrightarrow \text{M}_2\text{SO}_4(\text{s, l}) + 2\text{HCl(g)}$ R 15	
			<ul style="list-style-type: none"> ● Condensation of alkali sulfates $\text{M}_2\text{SO}_4(\text{g}) \rightarrow \text{M}_2\text{SO}_4(\text{s, l})$ R 7				
			<ul style="list-style-type: none"> ● Silication reactions of alkali sulfates: $\text{M}_2\text{SO}_4(\text{g}) + n\text{SiO}_2(\text{s, l}) \rightarrow \text{M}_2\text{O} \cdot n\text{SiO}_2(\text{s, l}) + \text{SO}_3(\text{g})$ R 8				
			<ul style="list-style-type: none"> ● Alumina-silication reactions of alkali sulfates: $\text{M}_2\text{SO}_4(\text{g}) + (2\text{SiO}_2 + \text{Al}_2\text{O}_3)(\text{s, l}; \text{Oxides or compounds}) \rightarrow 2\text{MAlSiO}_4(\text{s, l}) + \text{SO}_3(\text{g})$ $\text{M}_2\text{SO}_4(\text{g}) + (4\text{SiO}_2 + \text{Al}_2\text{O}_3)(\text{s, l}; \text{Oxides or compounds}) \rightarrow 2\text{MAlSi}_2\text{O}_6(\text{s, l}) + \text{SO}_3(\text{g})$ $\text{M}_2\text{SO}_4(\text{g}) + (6\text{SiO}_2 + \text{Al}_2\text{O}_3)(\text{s, l}; \text{Oxides or compounds}) \rightarrow 2\text{MAlSi}_3\text{O}_8(\text{s, l}) + \text{SO}_3(\text{g})$ R 9				
			<p>.....</p>				
	<ul style="list-style-type: none"> ● Silication reactions of alkali chlorides: $2\text{MCl(g)} + n\text{SiO}_2(\text{s, l}) + \text{H}_2\text{O(g)} \rightarrow \text{K}_2\text{O} \cdot n\text{SiO}_2(\text{s, l}) + 2\text{HCl(g)}$ R 10						
	<ul style="list-style-type: none"> ● Alumina-silication reactions of alkali chlorides: $2\text{MCl(g)} + (2\text{SiO}_2 + \text{Al}_2\text{O}_3)(\text{s, l}; \text{Oxides or compounds}) + \text{H}_2\text{O(g)} \rightarrow 2\text{MAlSiO}_4(\text{s, l}) + 2\text{HCl(g)}$ $2\text{MCl(g)} + (4\text{SiO}_2 + \text{Al}_2\text{O}_3)(\text{s, l}; \text{Oxides or compounds}) + \text{H}_2\text{O(g)} \rightarrow 2\text{MAlSi}_2\text{O}_6(\text{s, l}) + 2\text{HCl(g)}$ $2\text{MCl(g)} + (6\text{SiO}_2 + \text{Al}_2\text{O}_3)(\text{s, l}; \text{Oxides or compounds}) + \text{H}_2\text{O(g)} \rightarrow 2\text{MAlSi}_3\text{O}_8(\text{s, l}) + 2\text{HCl(g)}$ R 11						
	<p>.....</p>						
	<ul style="list-style-type: none"> ● Silication reactions of alkali hydroxides: $2\text{MOH(g)} + n\text{SiO}_2(\text{s, l}) \rightarrow \text{K}_2\text{O} \cdot n\text{SiO}_2(\text{s, l}) + \text{H}_2\text{O(g)}$ R 12						
	<ul style="list-style-type: none"> ● Alumina-silication reactions of alkali hydroxides: $2\text{MOH(g)} + (2\text{SiO}_2 + \text{Al}_2\text{O}_3)(\text{s, l}; \text{Oxides or compounds}) \rightarrow 2\text{MAlSiO}_4(\text{s, l}) + \text{H}_2\text{O(g)}$ $2\text{MOH(g)} + (4\text{SiO}_2 + \text{Al}_2\text{O}_3)(\text{s, l}; \text{Oxides or compounds}) \rightarrow 2\text{MAlSi}_2\text{O}_6(\text{s, l}) + \text{H}_2\text{O(g)}$ $2\text{MOH(g)} + (6\text{SiO}_2 + \text{Al}_2\text{O}_3)(\text{s, l}; \text{Oxides or compounds}) \rightarrow 2\text{MAlSi}_3\text{O}_8(\text{s, l}) + \text{H}_2\text{O(g)}$ R 13						
	<p>.....</p>						

which then react with SO_2 and SO_3 to form sulfates. The high silicon content in wood means that there are many silicates nuclei for use as nuclei for the nucleation and condensation of sulfates.

Recently, as shown in Fig. 5, a detailed alkali-induced slagging formation and growth mechanism was proposed [12] based on comparable experimental data from utility furnaces [6,81]. The slagging formation is governed by the re-enrichment of fine particles, re-capturing of coarse particles, and the existence of an initial slagging layer. Fine particles that contain high concentrations of K, Na, Cl, and S, in the forms of KCl and $\text{K}_3\text{Na}(\text{SO}_4)_2$, are initially deposited and enriched on the heating surfaces; then, they trap coarse and large particles containing high Si, Al, and other elements. Fine particles are re-enriched when they are unable to adhere to coarse and large particles, which promotes the layer-by-layer formation and the growth of slagging. A fatal initial layer that primarily contains fine KCl and $\text{K}_3\text{Na}(\text{SO}_4)_2$ particles evidently bonds the slagging tightly onto the heating surface before the formation of the alternating layers. The slagging process will be retarded if the initial layer is destroyed or inhibited.

The slagging growth mechanisms for biomass are further refined by factoring in the alternating layered structure that is observed in biomass utility boiler (Fig. 5). K is released into the gas flow during the combustion process as $\text{KCl}_{(\text{aerosol})}$ and $\text{K}_2\text{SO}_4_{(\text{aerosol})}$, both of which undergo complex chemical reactions and transformations. For example, volatile S is oxidized into SO_2 . Some alkali chloride aerosols are then sulfated or alumina-silicified, whereas some alkali sulfate aerosols generated by the sulfates of alkali chlorides or that originate directly from biomass combustion may also be alumina-silicified. This reduces the concentration of both alkali chloride and sulfate aerosols in the flue gas. When the Cl ratio ($(\text{Cl} + \text{K}_2\text{O} + \text{Na}_2\text{O})/(\text{SiO}_2 + \text{Al}_2\text{O}_3)$) and S ratio ($(\text{S}_{\text{Volatile}} + \text{K}_2\text{O} + \text{Na}_2\text{O})/(\text{SiO}_2 + \text{Al}_2\text{O}_3)$) decrease, the concentration of both alkali chloride and sulfate aerosols in the flue gas decrease, which is advantageous to slagging reduction. However, when both the Cl and S ratios increase, the concentrations of alkali chloride and sulfate aerosols in the flue gas increase, thereby promoting slagging. Some alkali metal aerosols condense on the heating surface at lower flue gas temperatures and form an initial sticky slagging layer by thermophoresis and turbulent diffusion. This sticky layer functions as an adhesive that bonds the subsequent deposits and heating surfaces together. Partial alkali metal aerosols condense on the surface of fly ash and result either in the formation of a sticky layer or further react with SiO_2 and Fe_2O_3 to generate low-temperature melting substances. Coarse fly ashes with or without a sticky layer are then deposited on the surface of the sticky initial slagging layer by inertial impaction. Fine particles that contain high concentrations of K, Na, Cl, and S in the form of KCl and $\text{K}_3\text{Na}(\text{SO}_4)_2$ are initially deposited and enriched; they then capture coarse and large particles that contain higher Si, Al, and other elements. When the fine particles are unable to adhere to coarse large particles, they undergo re-enrichment. This process promotes the layer-by-layer formation and growth of slagging. These alternating overlapping multi-layered slagging structures have also been reported in References 3,6,81,82.

2.1.3. Criterion numbers or evaluation indexes

Several researchers have recently focused on criterion numbers or evaluation indexes to solve alkali-induced slagging fundamentally and provide useful guidelines for the selection of co-firing fuel, additives, and the type of biomass fired in utility boilers. Davidsson et al. [52] estimated the extent of biomass slagging through the alkali index ($\text{AI} = \text{kg}(\text{K}_2\text{O} + \text{Na}_2\text{O})/\text{GJ}$) that is used for the evaluation of coal slagging. Slagging is probable when the AI is in the range 0.17–0.34 kg GJ⁻¹ and is almost certain at greater value. Oleschko and Muller [53], Diaz-Ramirez et al. [54], and Vamvuka et al. [55] proposed $(\text{Na} + \text{K} + 2\text{Mg} + 2\text{Ca})/\text{S}$, $(\text{K} + \text{Na})/(\text{Ca} + \text{Mg})$, and S/Cl as evaluation indexes, respectively. In addition, Jenkins et al. [83] and Jiang et al.

[84] employed the base-to-acid ratio used for coal ($\text{R}_{\text{b/a}} = (\text{Fe}_2\text{O}_3 + \text{CaO} + \text{MgO} + \text{K}_2\text{O} + \text{Na}_2\text{O})/(\text{SiO}_2 + \text{TiO} + \text{Al}_2\text{O}_3)$) to estimate biomass slagging. However, Ye [85] and Hu et al. [86] have emphasized that the evaluation indexes of coal cannot reliably predict the slagging behavior of biomass and proposed a new biomass slagging evaluation index $(\text{MgO} + \text{Al}_2\text{O}_3 + \text{Fe}_2\text{O}_3)/(\text{CaO} + \text{P}_2\text{O}_5)$. When the index value is less than 0.7, the softening temperature (ST) is less than 1000 °C; when it is above 1.7, ST is greater than 1200 °C. Although many evaluation indexes have been investigated, most are based on laboratory data, and few originate from commercial utility boilers or were verified based on industry practice. Moreover, the key elements, Si, Al, K, Cl, and S, which are essential for alkali transformation and alkali-induced slagging, are not accounted for simultaneously.

Alternatively, a set of criterion numbers for alkali-induced slagging (Exp 1), based on a series of experimental results on utility boilers (Table 3 shows a summary of the Cl and S ratios for different fuels burning in different utility boilers), was recently established by the authors [12].

$$\begin{aligned} &\text{While } \text{Cl ratio } (\text{Cl} + \text{K}_2\text{O} + \text{Na}_2\text{O})/(\text{SiO}_2 + \text{Al}_2\text{O}_3) \geq 2.4 \\ &\quad \text{S ratio } (\text{S}_{\text{Volatile}} + \text{K}_2\text{O} + \text{Na}_2\text{O})/(\text{SiO}_2 + \text{Al}_2\text{O}_3) \geq 1.9 \\ &\quad \text{serious slagging} \end{aligned} \quad \text{Exp 1}$$

$$\begin{aligned} &\text{While } \left. \begin{array}{l} \text{Cl ratio} \leq 1.0 \\ \text{S ratio} \leq 0.5 \end{array} \right\} \text{ slight slagging} \end{aligned}$$

Severe slagging occurs when the Cl ratio and S ratio are greater than 2.4 and 1.9, respectively. Slight slagging occurs when the Cl ratio and S ratio are lower than 1.0 and 0.5, respectively. Slagging becomes severe with increasing Cl ratio and S ratio in the ranges of 1.0–2.4 and 0.5–1.9, respectively. Elled et al. [27] and Wang et al. [87] conducted research on deposit by co-firing in utility and small-scale furnaces. They further verified the abovementioned suggestion. Elled et al. [27] conducted deposit research on high potassium fuels (wood and straw) in a 12 MW CFB furnace and reported that the slagging rate decreases by co-firing with sludge that contains high $\text{Si}_2\text{O} + \text{Al}_2\text{O}_3$ and low $\text{K}_2\text{O} + \text{Na}_2\text{O}$ that results in lower Cl and S ratios. Similar results were reported by Wang et al. [87]. They added sewage sludge with low Cl ratio and S ratio to wood to reduce slagging. Therefore, the quantitative criterion numbers (Cl ratio and S ratio) can provide a useful guideline for the selection of biomass, additives, and co-firing fuel fired in utility boilers.

Although the criterion numbers (Cl ratio and S ratio) consider the essential elements (Si, Al, K, Cl, and S) that influence both alkali transformations and alkali-induced slagging, they must be further evaluated and improved because of the limited numbers of surveyed items listed in Table 3. Also, a criterion number that can provide a practical guideline must be repeatedly verified and improved.

2.2. Silicate melt-induced slagging (ash fusion)

Biomass ash-related problems are not only related to chlorine and alkali metals but are also closely related to the biomass ash fusion characteristics (AFC). AFC is an important factor in determining the propensity of fuels to form fused or partly fused slag deposits on heating surfaces in boilers [14]. Although thermal analysis (TGA/DTA), thermochemical calculations, and lab-scale sintering tests [13,54] can be used to predict silicate melt-induced slagging, the ash fusion test is a more useful method to quantitatively provide information on the properties of different biomass. This is especially true for the initial deformation temperature (IDT), which is dependent on the proportions of the elements in the biomass ash, and is employed to guide biomass boiler design [7]. Meanwhile, many AFC assessment methods, such as ternary phase diagrams

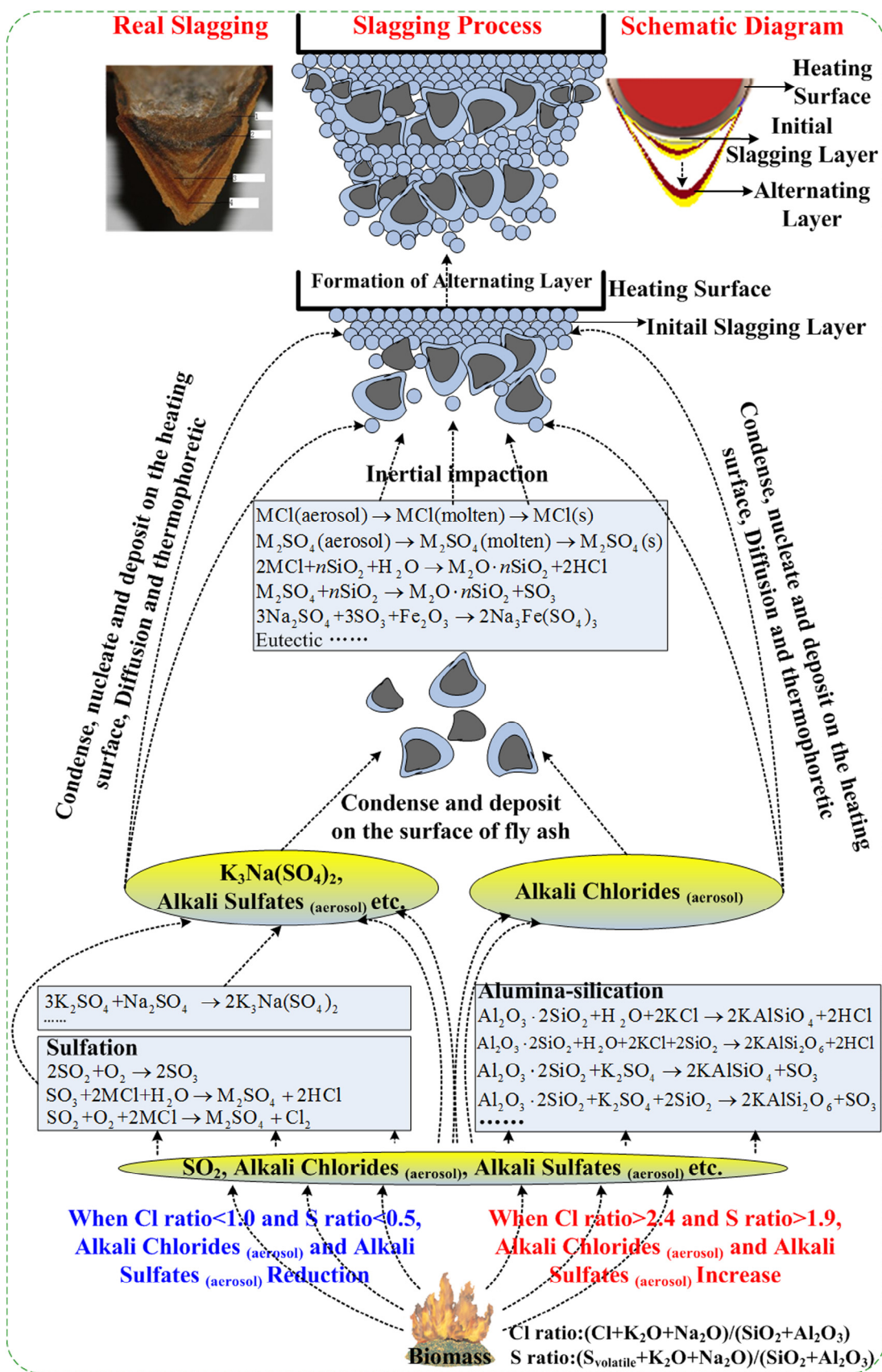


Fig. 5. Alkali-induced slagging formation and growth mechanisms in biomass combustion (reprinted from reference 12, with permission of Elsevier).

Table 3

Summary of Cl ratio and S ratio for different fuels burning in different utility boilers^a (reprinted from reference 12, with permission of Elsevier).

Furnace style	12 MW grate furnace [6]	30 MW grate furnace [81]	12 MW CFB [3]				Industrial incinerator [62]	12MW CFB [27]				1.2MW STEP FIRE boiler [87]				
Fuel	Cotton Stalk 1	Cotton Stalk 2	Cotton Stalk 3	Sawdust	Bamboo	Straw	Bark	Waste-water	Wood	straw	sludge	75% Wood +25% Straw	55% Wood +21% Straw +24% Sludge	Wood	Sewage Sludge	96% Wood +4% Sewage Sludge
Cl	0.41	0.14	0.47	0.33	0.22	0.90	0.74	0.30	0.02	0.25	0.06	0.08	0.08	0.21	0.10	0.21
S _{Volatile}	0.09	0.17	0.20 ^b	0.05 ^b	0.06 ^b	0.14 ^b	0.01 ^b	1.85	0.01 ^b	0.07 ^b	0.82 ^b	0.03 ^b	0.22 ^b	0.13	1.48	0.18
SiO ₂	13.74	51.14	37.87	26.79	39.78	55.25	42.42	1.30	24.86	49.29	33.43	30.96	32.04	22.75	26.71	22.90
Al ₂ O ₃	4.03	9.44	7.47	5.00	4.14	0.98	6.39	22.89	1.27	0.76	21.91	1.14	6.11	6.26	31.74	7.20
SiO ₂ + Al ₂ O ₃	17.77	60.58	45.34	31.79	43.92	56.23	48.81	24.19	26.13	50.05	55.34	32.10	38.15	29.01	58.45	30.10
K ₂ O	25.40	11.72	6.06	5.77	3.44	9.73	3.66	0.00	16.63	18.92	2.24	17.20	13.66	14.47	0.69	13.96
Na ₂ O	6.58	2.36	1.22	6.14	3.01	0.78	2.35	28.59	1.01	0.85	1.00	0.97	0.97	11.37	0.47	10.97
K ₂ O + Na ₂ O	31.98	14.08	7.28	11.91	6.45	10.51	6.01	28.59	17.64	19.77	3.24	18.17	14.63	25.84	1.16	24.93
Ash	3.93	2.57	5.45	1.54	2.30	13.27	4.12	17.71	0.5	7.2	52.3	2.175	14.34	0.71	41.70	2.23
Cl Ratio	2.4	0.3	0.4	1.0	0.4	0.3	0.5	1.3	0.8	0.5	0.1	0.7	0.4	1.9	0.0	1.1
S Ratio	1.9	0.3	0.2	0.5	0.2	0.2	0.1	1.6	0.8	0.4	0.1	0.6	0.4	1.5	0.1	1.1
Slagging Description	Serious, 15–20 days, >900 mm	Slight, 6–12 months <100 mm	Slight, >12 months, <20 mm					Moderate, 30–60days, 70–90 mm	Sludge blends decrease slagging rate				Sludge blends decrease slagging fraction			

^a The units for oxides are wt%; ^b Total S in fuel is defined as volatile S.

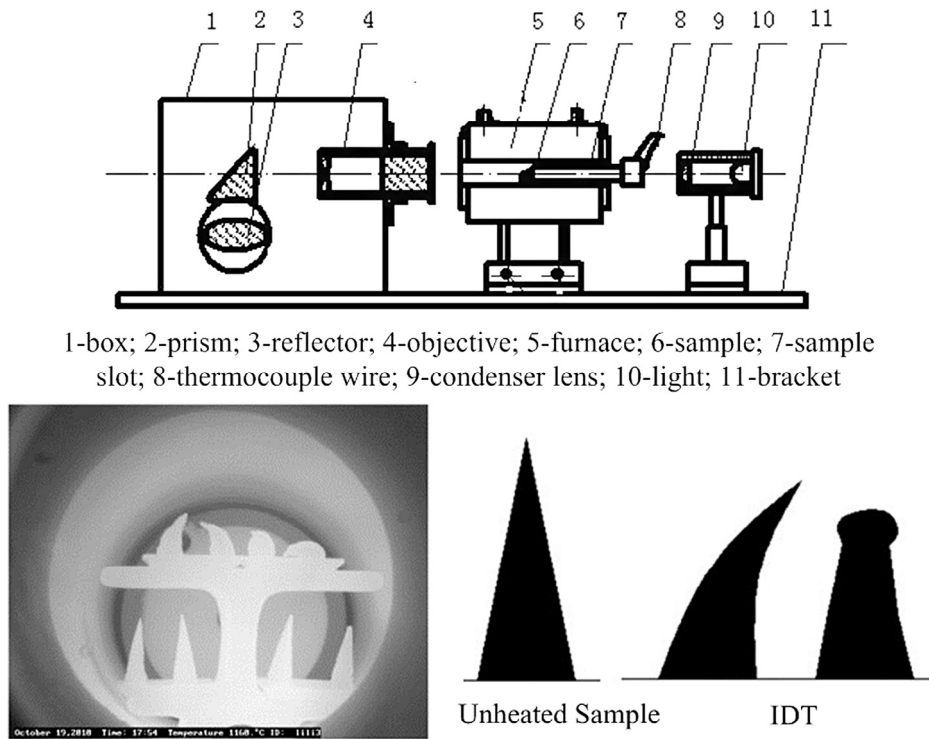


Fig. 6. Schematic of the ash fusion tester and an example for testing (adapted from references 7,15).
Upper image: system diagram of AFC tester; bottom-left image: testing process; bottom-right image: IDT identification

[48,67,88–93] and stepwise regression [94,95] involving a large number of predictors that are expected to influence AFC, can be acquired from the results of ash fusion test and ash composition analysis.

2.2.1. Ash fusion test

Ash fusion temperatures (AFT), including IDT, ST, hemisphere temperature (HT), and fluidized temperature (FT), comprise the most effective and direct methods of AFC evaluation. Generally, ash fusion testing is conducted with an automatic ash fusion temperature analyzer, which mainly consists of a temperature controllable electric heating furnace and a high-precision digital read-out and photographic record camera (Fig. 6). IDT, ST, HT, and FT are identified from the ash cone with the camera.

In ashing, which is the first step in biomass AFC research, the selection of the correct ashing temperature is vital. For example, a low ashing temperature results in unburned carbon in the ash and affects the AFC assessment; in contrast, a high ashing temperature leads to over-volatilization and sintering, and these also influence the AFC assessment. Unfortunately, the ideal ashing temperature for biomass remains uncertain to date. For example, the America ASTM/E870-82 employs 600 °C, European SS-ISO540 employs 550 °C [96], and Chinese GB/T212-2001 adopts 815 °C that is used for the coal ashing process because of the lack of biomass ashing standard. Thy et al. [70], as individuals, used an ashing temperature of 525 °C. With the aim of establishing a consistent biomass ashing temperature, Xiao et al. [97] recommended the adoption of 600 °C through analysis of the physicochemical properties of biomass at different ashing temperatures. Wang et al. [84] studied the fusion characteristics of three seaweed ashes and reported that neither 600 °C nor 815 °C was suitable for seaweed biomass because the generation of high-melting material at these temperatures influences the identification of ash fusion points. Consequently, they proposed that a lower ashing temperature (530 °C) is a more suitable.

Although the ashing fusion test can provide information on the propensity of silicate melt-induced slagging for a specified fuel, the testing procedure used has considerable effects on the results [90]. Firstly, an aluminous cement tile is usually employed to support the specimen, but it is attacked by the basic ash that forms after the experiment, which may lead to unreliable readings. The ASTM standard specifies the adoption of a kaolin/aluminum oxide support and ignores altogether the problem of its being attacked by ash. Meanwhile, the DIN standard specifies the use of a platinum tile. Secondly, several samples display swelling during melting because of the continuous combustion of unburned carbon in the ash, which affects the identification of IDT. Therefore, all observations showing swelling and measurement on re-ignited ash should be discarded.

Although ash fusion testing as an effective method to predict silicate melt-induced slagging during combustion has many problems (including identifying the ashing temperature, selection of the ashing container or specimen support, and even the choice of an ashing standard) that must be overcome, the method remains in wide application.

2.2.2. Effects of chemical compositions on AFC

As a major inducing factor for melt-induced slagging and bed agglomeration, AFCs depend not only on chemical composition but also on mineral composition [88]. For example, IDT as an evaluation index for AFC increases as MgO, CaO, Fe₂O₃, and Al₂O₃ content increase, and decreases with increasing K₂O content in ash [15]. Refractory minerals (quartz, metakaolinite, mullite, rutile, etc.) increase AFTs, whereas fluxing minerals (anhydrite, calcium silicate, hematite, etc.) reduce them [66]. The main elements in the slag are silicon, aluminum, calcium, potassium, and oxygen, and the principal mineral components are Ca₂MgSi₂O₇, KAlSiO₄, SiO₂, and others [13,15,16]. Hence, related research has mainly focused on the analysis of the elemental and mineral compositions of ashes prepared by the ashing of pure biomass or simulated ash by adding various metal oxides

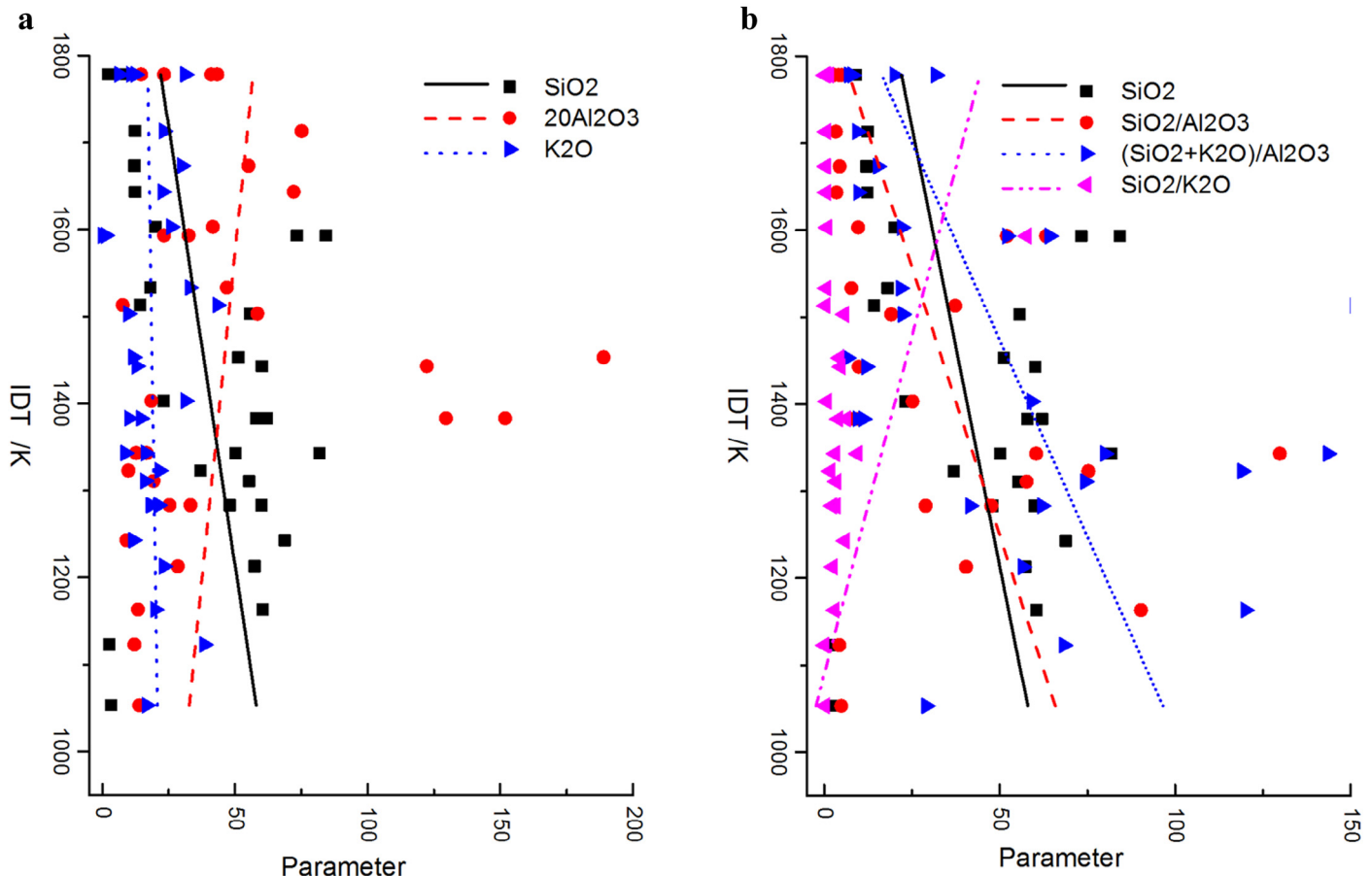


Fig. 7. Effects of various components on IDT. Symbols: experiment value; line: trend line based on the experimental values (reprinted from reference 67, with permission of Elsevier).

- a. Effects of single components
- b. Effects of combined components

into biomass or mixing various metal oxides directly at a certain temperature by XRF, ICP, SEM-EDS, XRD, TG and AFC testing instruments [7,15,16,84].

For coal analysis, ST is widely used as an evaluation index. For biomass, it is suggested that IDT should be adopted because of the lack of sensitivity of ST, HT, and FT to the elements present in biomass ash [15,16]. Ashing experiments conducted on three agricultural residues at 400, 600, 815, 1000, 1200, and 1400 °C showed that IDT increases as K₂O concentration decreases and as MgO, CaO, Fe₂O₃, and Al₂O₃ concentrations in the ash increase. ST, HT, and FT are obviously unaffected by both the concentrations of each element and the ashing temperature. Li et al. [7] further extended the biomass species or corresponding ash species by means of 8 biomass ashes and 27 simulated ashes prepared by mixing organic and inorganic oxides at 580 and 815 °C, respectively, and obtained similar results. Recently, the authors [67] conducted research on silicate melt-induced slagging on basis of the ash properties of 30 biomasses burned in operating power plants and found that IDT can be used as the evaluation index for silicate melt-induced slagging. IDT increases as Al₂O₃ and SiO₂/K₂O increase, but decreases as K₂O, SiO₂, SiO₂/Al₂O₃, and (SiO₂ + K₂O)/Al₂O₃ increase. As shown in Fig. 7, which presents a statistical analysis of the effects of various components on IDT, these compounds can be arranged in order of their decreasing effect on IDT: Al₂O₃>K₂O>SiO₂>SiO₂/K₂O>SiO₂/Al₂O₃>(SiO₂ + K₂O)/Al₂O₃. However, because of the limited number of samples, more research is required before the use of IDT in a practical setting.

On the other hand, the authors [15] pointed out that the evaluation of biomass AFC should not be based simply on their elemental composition, except IDT, but also on the high-temperature molten material that provides structural support for the skeleton-like structure in biomass ash. Neither the high-temperature molten material nor the skeleton structure in biomass ash is influenced by ashing temperature. Fig. 8 shows the TG-DTG curves of capsicum straw ashed at 400, 600, and 815 °C, respectively. The ashes prepared by ashing at 400, 600, and 815 °C experience three, two, and one weight loss peaks, respectively, and these weight loss peaks overlap. Regardless of the ashing temperature, when the heating temperature is higher than a certain value (860 °C for the ashes of capsicum straw), the compositions of the ash are found to be either similar or to contain the same high-temperature molten material. The authors [16] further pointed out that the skeleton structure consists of quartz, potassium iron oxide, and silicates through crystal identification in the corresponding ashes further ashed at 1000, 1200, and 1400 °C. The silicates mainly exist in the form of potassium magnesium silicate, potassium aluminum silicate, potassium calcium silicate, calcium silicate, mullite, diopside, pyrope, monticellite, and other minerals. Therefore, aside from the elemental compositions, we should also pay attention to the mineral species present in the ash. Furthermore, Vassilev et al. [66] reported that refractory minerals (quartz, metakaolinite, mullite, rutile, etc.) increase AFTs, whereas fluxing minerals (anhydrite, calcium silicate, hematite, etc) reduce them.

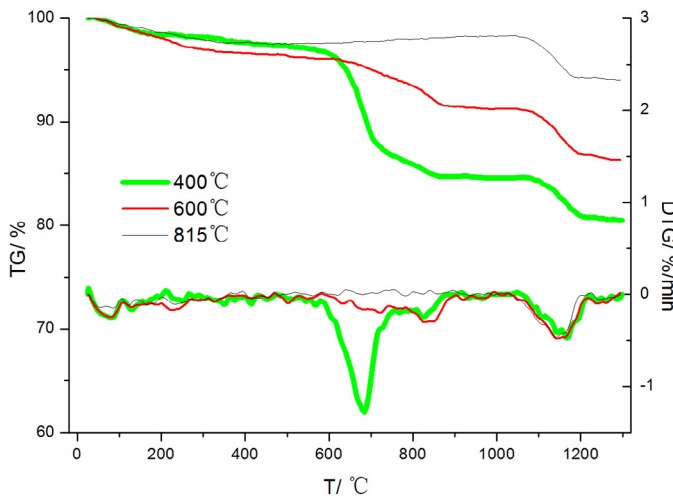


Fig. 8. TG/DTG curves of the ashes of capsicum straw ashed at 400, 600 and 815 °C (reprinted from reference 15, with permission of Elsevier).

2.2.3. Evolution of chemical compositions in ash during combustion

To determine the effects of both elemental and mineral compositions on AFC, the evolution of the chemical composition of the ash during combustion has been widely investigated [15,98].

2.2.3.1. Effects of temperature on mineral compositions.

In the past five years, our research group has devoted considerable attention to the evolution of the chemical composition of the ashes over different ashing temperatures and presented the substances existing forms and provided detailed reactions by analyzing the ash composition from different combustion temperatures [15,16]. The identification of the crystalline phases of capsicum straw ashed at 400, 600, 815, 1000, 1200, and 1400 °C is shown in Fig. 9. The main components of capsicum straw ashes formed at 400 °C are quartz, sylvite, arcanite, fairchildite, calcite, potassium iron oxide, and magnesium oxide. As the ashing temperature increases, calcite and fairchildite disappear and calcium silicide is generated at 600 °C by R 23 and R 24; meanwhile, at 600 °C when carbon is completely burned off, Ca_2SiO_4 is substituted by CaSi_2 through R 25. At 815 °C, sylvite disappears and this is accompanied by the appearance of zeolite (R 26) and leucite (R 27). At 1000 °C, periclase and calcium

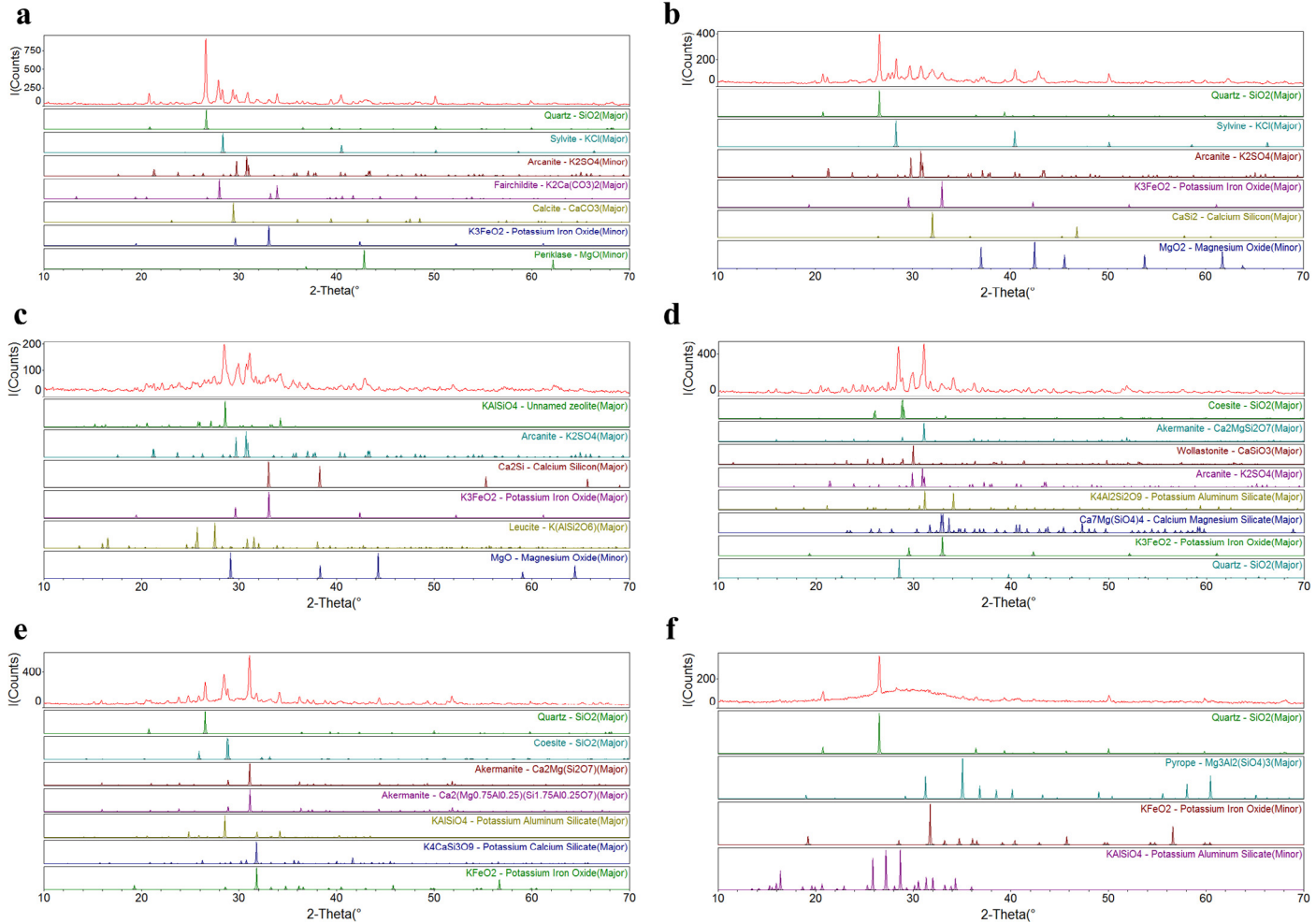


Fig. 9. XRD analysis results of capsicum straw ashed at 400, 600, 815, 1000, 1200, and 1400 °C (adapted from references 15,16).

- 400 °C
- 600 °C
- 815 °C
- 1000 °C
- 1200 °C
- 1400 °C

Table 4

Summary of the evolution of mineral composition of the ashes at increasing ashing temperatures [15,16].

Temperature /°C	Changes of mineral compositions	Reactions	
400	SiO ₂ , KCl, K ₂ SO ₄ , K ₂ Ca(CO ₃) ₂ , CaCO ₃ , K ₃ FeO ₂ , Mg O		
600	Out:K ₂ Ca(CO ₃) ₂ , CaCO ₃ In:CaSi ₂ , Ca ₂ SiO ₄	MCO ₃ → MO + CO ₂ ↑ 2SiO ₂ + CaO + 5C → CaSi ₂ + 5CO ↑ SiO ₂ + 2CaO → Ca ₂ SiO ₄	R 23 R 24 R 25
815	Out: KCl In:KAlSiO ₄ , K(AlSi ₂ O ₆)	2KCl + Al ₂ O ₃ + 2SiO ₂ + H ₂ O → 2KAlSiO ₄ + 2HCl ↑ 2KCl + Al ₂ O ₃ + 4SiO ₂ + H ₂ O → 2K(AlSi ₂ O ₆) + 2HCl ↑	R 26 R 27
1000	Out: MgO, CaSi ₂ In:Ca ₂ MgSi ₂ O ₇ , Ca ₇ Mg(SiO ₄) ₄ , CaSiO ₃	2CaSi ₂ + 5O ₂ → 2CaSiO ₃ + 2SiO ₂ 2CaSiO ₃ + MgO → Ca ₂ MgSi ₂ O ₇ 2CaSi ₂ + MgO + 5O ₂ → Ca ₂ MgSi ₂ O ₇ + 2SiO ₂ 14CaSi ₂ + 2MgO + 35O ₂ → 2Ca ₇ Mg(SiO ₄) ₄ + 20SiO ₂ 14CaSiO ₃ + 2MgO + 21O ₂ → 2Ca ₇ Mg(SiO ₄) ₄ + 6SiO ₂	R 28 R 29 R 30 R 31 R 32
1200	Out:CaSiO ₃ ,K ₂ SO ₄ In:K ₄ CaSi ₃ O ₉ , SO ₂	CaSiO ₃ + 2K ₂ SO ₄ + 2SiO ₂ → K ₄ CaSi ₃ O ₉ + 2SO ₂ + O ₂	R 33
1400	SiO ₂ , Mg ₃ Al ₂ (SiO ₄) ₃ , KFeO ₂ , KAlSiO ₄ , Molten amorphous phase		

silicate disappear and are converted into akermanite (R 28–R 30) and calcium magnesium silicate (R 28, R 31, and R 32), respectively. At 1200 °C, arcanite and calcium silicate react together to form potassium calcium silicate and SO₂ (R 33). At 1400 °C, the ash is fully molten, and quartz, pyrope, and monticellite are identified as the major components. In addition, potassium aluminum silicate and potassium iron oxide are identified as the minor components. This is summarized in detail in Table 4. Li et al. [7] also reported that K₂Ca(CO₃)₂ and KCl are the major phases at 580 °C, and KCl, CaO and MgO at 815 °C.

For low-temperature ash properties, Vamvuka and Zografos [99] conducted similar research at 600, 780, and 900 °C. They reported that both calcium and fairchildite exist in the ash prepared at 600 °C and disappeared at temperature greater than 600 °C; potassium vaporizes between 780 and 900 °C. The results are consistent with the above observation. Thy et al. [70] conducted similar research using wood, rice straw, and wheat straw ashed between 525 and 1425 °C and reported that larnite emerges at 718 °C accompanying the disappearance of calcium. Furthermore, aluminum silicate periclase forms at approximately 815 °C, and sylvite completely disappears at 1011 °C. Overall, the research results are similar except for the temperature at which sylvite disappears. However, this may be caused by the lack of precision of XRD analysis or the experimental conditions. Consequently, further studies are required.

2.2.3.2. Effects of temperature on elemental compositions.

Accompanied by the changes in mineral compositions of the ash, the elemental content of the ash also change significantly; in particular, the changes in the presence of volatile elements directly influence the formation of submicron particles that accelerate alkali-induced slagging.

Johansen et al. [100] studied the release of K, Cl, and S during the pyrolysis and combustion of corn. The results showed that the release of K and Cl is closely related. K is released in significant quantities in the temperature range of 700–800 °C in the form of KCl, and only 5%–10% of mass loss occurs at temperature below 700 °C. Cl is fully released at 800 °C, and Cl in excess of K is released in the form of HCl. Organic S is released below 500 °C, and inorganic S is released above 900 °C in the form of aerosolized K₂SO₄ and SO₂, which is formed by the decomposition of K₂SO₄. A similar result was achieved by analyzing the elemental concentrations of the ash by

XRF. The release properties of the volatile element K, S, and Cl are illustrated in Fig. 10 [15,16].

Fig. 10 shows that because K, S and Cl are increasingly released as the temperature increases, the ashing ratios of the three straws decrease until 1200 °C. Then they remain either unchanged or decrease slightly between 1200 °C and 1400 °C. Below 600 °C, the reduced ashing ratios are mainly attributed to the release of K and organic S. Between 600 °C and 815 °C, the reduction is mainly caused by the release of K and Cl, possibly in the forms of KCl aerosol [100] and HCl (via R 26 and R 27). Cl concentration is essentially zero at 815 °C. However, between 815 °C and 1200 °C, K concentration decreases because of the volatility of KOH and K₂SO₄ aerosols [100]. Meanwhile, inorganic S is released in the form of SO₂ by the decomposition of K₂SO₄ (R 33). All these conditions result in the continuing decrease of the ashing ratio as temperature increase until 1200 °C. At temperature above 1200 °C, ash melts and the ashing ratios remain constant or decrease slightly.

2.2.4. Chemical equilibrium calculation

Compared with experiment, chemical equilibrium calculations are economically feasible and quick. They can also provide systematic information on the behavior of different fuels and can be further utilized to reduce or prevent ash-related issues inherent in the thermo-conversion of biofuels [18]. Therefore, simulation tools such as FACTSAGE [31,56–58,70] and HSC [69] have been used extensively. Utilizing FACTSAGE, Brus et al. [56] and Chen et al. [57] reported that during biomass combustion, K exists mainly in the forms of KOH(g), K₂SO₄(g), KAlSiO₄(s), KAlSi₂O₆(s), and KCl(s,g). Similarly, Nutalapati et al. [31] employed FACTSAGE to study the effect of temperature on the existing forms of K, and pointed out that gaseous potassium mainly exists as KCl(g) below 900 °C, whereas KCl(g) and KOH(g) co-exist between 900 °C and 1600 °C, and K₂SO₄(g) only exists at approximately 1200 °C. The KOH(g) concentration decreases as temperature decreases.

However, Thy et al. [70], who compared the results of FACTSAGE simulation calculations and experiment concerning the high-temperature elemental loss of rice straw ash, wheat straw ash, and wood ash from 525 °C to 1425 °C, reported that FACTSAGE has significant drawbacks. For example, for wood ash, FACTSAGE fails to predict the formation of phosphor-nearing larnite that is observed experimentally; In addition, the release of potassium is

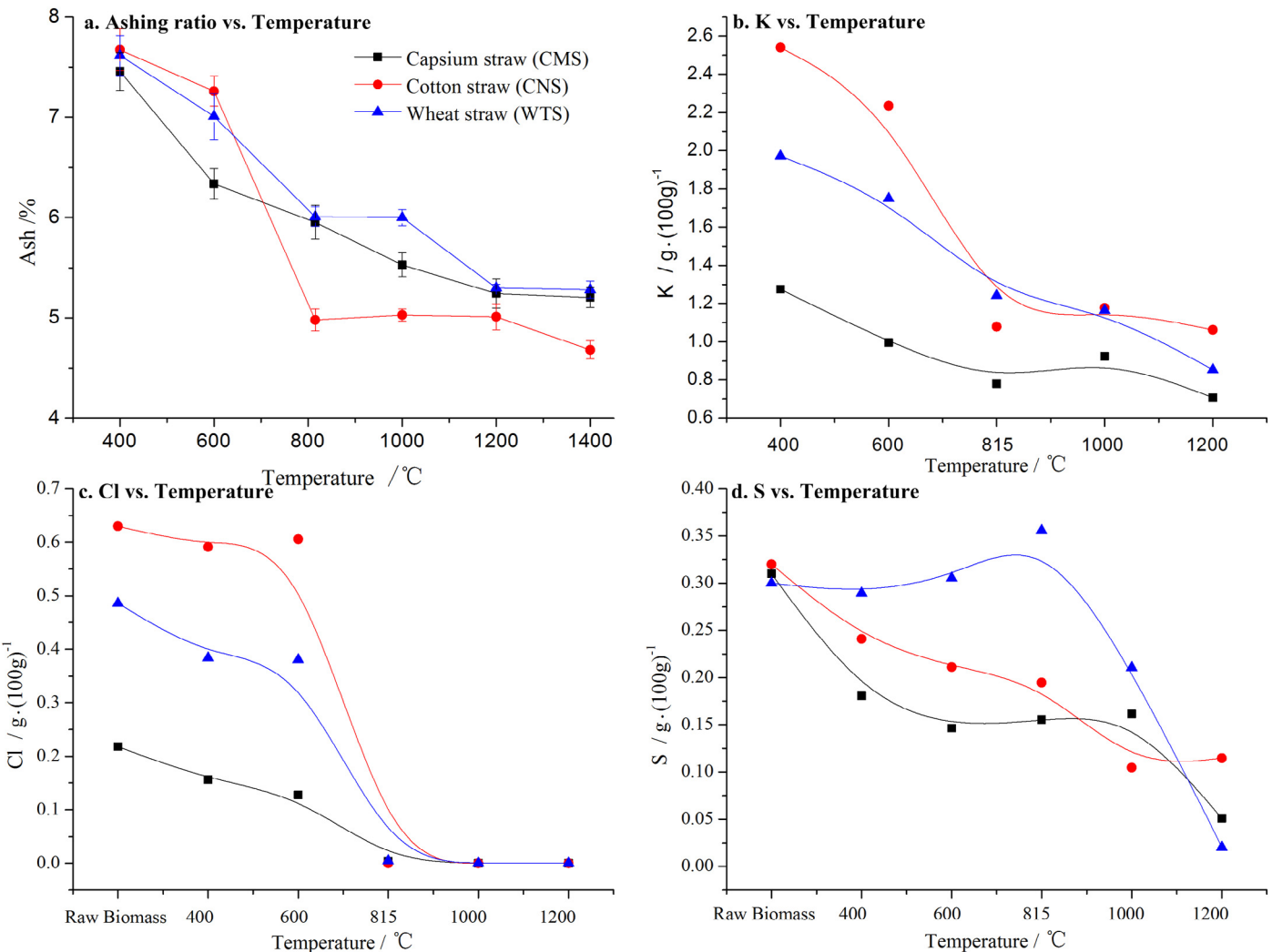


Fig. 10. Effects of ashing temperature on the ashing ratio and the release properties of K, S, and Cl (adapted from references 15,16).

restricted to temperatures near or above its liquidus; in contrast, low temperature release is experimentally observed. Furthermore, for rice straw, the FACTSAGE results are in contrast with experiment. Additionally, for wheat ash, FACTSAGE calculation suggests a very low initial melting temperature and a high liquidus in comparison with the experimental results [70].

The ash transformation reactions during slagging may be influenced by temperature, residence time, air supply, flue gas velocity, and other factors [48]. Ash transformation reactions in both grate furnace and FB environments can reach equilibrium because of their long residence time and the good contact between gaseous materials and solid initial ash. However, in the flame of a powder burner, although the gas-phase reactions are promoted because of high temperature and turbulence that favor the formation of chlorides, sulfates, and carbonates, the interactions between ash and gas are limited because of their limited residence times; the system is far from being in equilibrium [48].

Simulation tools can provide guidance, but should be further perfected because deviations from experiment results. A combination of heterogeneous chemical kinetics and multiphase equilibrium models is essential, and good chemical estimates of the speciation, saturation levels, and the presence of a melt of the ash-forming matter must be available to obtain reliable results [48].

2.2.5. Multi-component phase diagram

Multi-component phase diagrams have been proposed as an effective tool to forecast AFC, i.e., the propensity of an ash with a given composition to form a molten slagging. Phase diagram allow rapid assessment of the AFC of a particular fuel in comparison with duplicate AFC experiments. They can also provide a general guide to the major mineral phases present via comparison with the phase diagrams of the major oxides [90]. Many phase diagrams, including those of $\text{SiO}_2\text{-CaO-Al}_2\text{O}_3$ [88], $\text{SiO}_2\text{-CaO-Fe}_2\text{O}_3$ [88], $\text{SiO}_2\text{-Al}_2\text{O}_3\text{-K}_2\text{O}$ [67], $\text{K}_2\text{O-Na}_2\text{O-CaO-MgO-SiO}_2$ [48], $\text{K}_2\text{O-CaO-SiO}_2$ [48], $\text{Al}_2\text{O}_3\text{-SiO}_2\text{-TiO}_2$ [89], $\text{Al}_2\text{O}_3\text{-Fe}_2\text{O}_3\text{-SiO}_2$ [89], $\text{Al}_2\text{O}_3\text{-CaO-SiO}_2$ [89], and $\text{CaO-SiO}_2\text{-Al}_2\text{O}_3\text{-Fe}_2\text{O}_3$ [90], have been proposed. Given the limited dimensions of the multi-component phase diagrams, Bostrom et al. [48] employed a pseudo-ternary phase diagram, $\text{K}_2\text{O-CaO-SiO}_2$, as a substitute for the $\text{K}_2\text{O-Na}_2\text{O-CaO-MgO-SiO}_2$ phase diagram and used this to predict the molten slagging tendencies of woody biomass (shown in Fig. 11). Owing to the high melting temperature, the propensity to form silicate-based molten slagging is low for fuel that has a relatively high basic oxide/silica ratio, i.e., $((\text{K}_2\text{O} + \text{Na}_2\text{O} + \text{CaO} + \text{MgO})/\text{SiO}_2)$. However, fine particle formation increases toward the “ $\text{K}_2\text{O}(\text{+Na}_2\text{O})$ ” corner of the triangle, particularly close to the basic oxide binary component. This may be the reason that Li et al. [7] found that, for high potassium samples, the

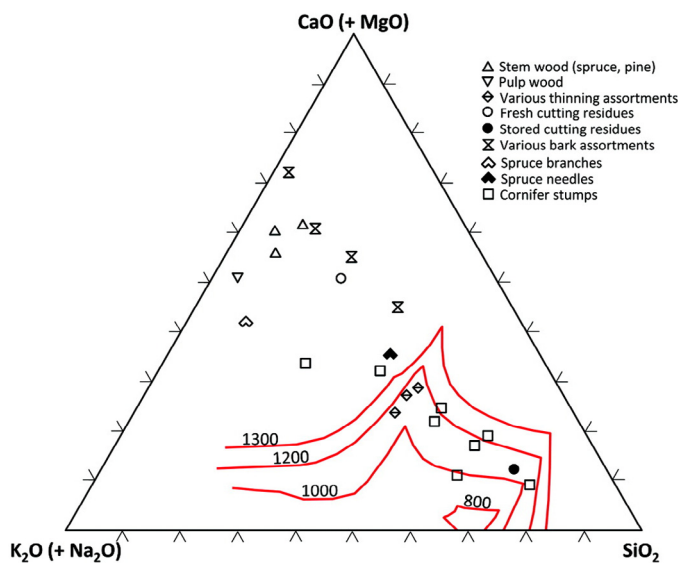


Fig. 11. Application example of the pseudo-ternary diagram of K_2O - Na_2O - CaO - MgO - SiO_2 in predicting the fusion characteristics of fuels (reprinted from reference 48, with permission of American Chemical Society).

ash fusion test cannot correctly predict ash slagging and deposition trends because potassium is released during the ashing procedure under the ash fusion testing conditions.

For coal, Gray [90] also considered all the components and proposed a ternary diagram where the vertical axes are percent base ((CaO + MgO + FeO + Na_2O + K_2O + etc.) for reducing atmosphere and (CaO + MgO + Na_2O + K_2O + etc.) for oxidizing atmosphere)), percent fluxing acidic oxides (SiO_2 + TiO_2 + P_2O_5 + B_2O_3), and percent non-fluxing acidic oxides (Al_2O_3 for reducing and Al_2O_3 + Fe_2O_3 for oxidizing). Al_2O_3 always behaves as a non-fluxing acid. Fe behaves as a non-fluxing acid for the oxidizing condition in the form of Fe_2O_3 and as a basic oxide under a reducing atmosphere in the form of FeO . Unfortunately, no experimental determination of such a phase diagram exists, and further specification and simplification are necessary. However, according to the research results of Li et al. [7] and our previous study

[15], IDT is mainly related to the concentrations of K_2O , MgO , CaO , Fe_2O_3 , Al_2O_3 , and SiO_2 . Therefore, multicomponent phase diagram that includes the major components K_2O - Na_2O - CaO - MgO - SiO_2 - Al_2O_3 - Fe_2O_3 - TiO_2 will be more accurate.

As indicated by the abovementioned proposed ternary phase diagrams, biomass AFC evaluation diagrams can be expressed by alkali metals or fluxing basic oxides (K_2O + Na_2O for oxidizing and K_2O + Na_2O + FeO for reducing)-alkali earth metals or non-fluxing basic oxides (CaO + MgO)-fluxing acidic oxides (SiO_2 + TiO_2 + P_2O_5)-non-fluxing acidic oxides (Al_2O_3 + Fe_2O_3 for oxidizing and Al_2O_3 for reducing). Indeed, several other components, such as the fluxing acidic oxide B_2O_3 , fluxing basic oxide Mn_2O_4 , and the non-fluxing basic oxides BaO and SrO , are ignored because of their minor or trace concentrations. Therefore, two triangular prism AFC phase diagrams, namely, (K_2O + Na_2O)-(CaO + MgO)-(SiO_2 + TiO_2 + P_2O_5)-(Al_2O_3 + Fe_2O_3) for oxidation and (K_2O + Na_2O + FeO)-(CaO + MgO)-(SiO_2 + TiO_2 + P_2O_5)- Al_2O_3 for reduction, can be used to reveal the propensity to form melt-induced slagging for ashes with a given composition and predict their mineral composition determined by crystalline phase identification from experiment.

Although (K_2O + Na_2O)-(CaO + MgO)-(SiO_2 + TiO_2 + P_2O_5)-(Al_2O_3 + Fe_2O_3) for oxidizing conditions and (K_2O + Na_2O + FeO)-(CaO + MgO)-(SiO_2 + TiO_2 + P_2O_5)- Al_2O_3 for reducing conditions can effectively predict the AFC, having the phases cover all elements with weight or mole percentages from 0% to 100% is unrealistic. Therefore, further simplification is necessary by approximating the behaviors of Mg and Na to be similar to those of Ca and K, respectively. Considering that both Fe_2O_3 and Al_2O_3 increase IDT [7,15,101] and the lower concentration of Fe_2O_3 in ash than that of Al_2O_3 , the phase diagram can be expressed as (Ma_2O)- $MaeO$ - P_2O_5 - Al_2O_3 and (Ma_2O)- $MaeO$ - SiO_2 - Al_2O_3 . Ma denotes alkali metals, including K and Na. Mae denotes alkaline earth metals, including Ca and Mg. Al is the sum of Al and Fe. Therefore, the acquisition of the pseudo 4D phase diagrams (Ma_2O)- $MaeO$ - P_2O_5 - Al_2O_3 and (Ma_2O)- $MaeO$ - SiO_2 - Al_2O_3 can provide a more effective guideline for AFC than a simple ternary phase diagram. Acquisition of the data to build this phase diagram, of course, requires much experimental work.

As shown in Fig. 12, the authors [67] recently constructed a SiO_2 - Al_2O_3 - K_2O ternary phase diagram based on the ash properties of 30

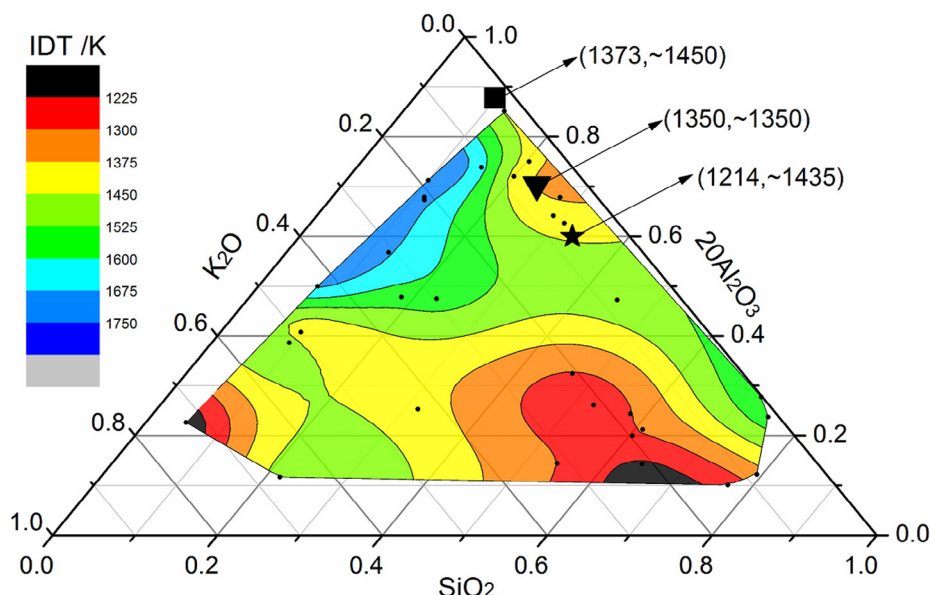


Fig. 12. K_2O - SiO_2 - Al_2O_3 ternary phase diagram (reprinted from reference 67, with permission of Elsevier).

■ Biomass + Kaolin; ▼ Biomass; ★ Biomass + SiO_2 ; · Experimental value; unit: weight ratio; data (A,B) present (experimental value, predicted value).

biomasses burned in operating power plants. Surprisingly, the ternary phase diagrams well predicted the IDT of the pure biomass, and the predicted values of pure biomass based on the ternary phase diagram are consistent with the experimental values; however, the experimental IDTs of biomass containing additional SiO_2 and kaolin are approximately 220 and 80 K lower than the predicted values, respectively. Therefore, although both pure biomass and biomass containing additional aluminosilicate compounds share the same $\text{K}_2\text{O}-\text{SiO}_2-\text{Al}_2\text{O}_3$ construction, the latter has a lower IDT because of the additional low-melting substances generated from the silication reaction (R 8) induced by the addition of aluminosilicate compounds. As a result, the $\text{K}_2\text{O}-\text{SiO}_2-\text{Al}_2\text{O}_3$ ternary diagram constructed based on pure K_2O , SiO_2 , and Al_2O_3 underestimates the IDT and is unsuitable for predicting the AFC of pure biomass because of the excessive generation of low-melting substances.

To easily predict the AFC or potential melt-induced slagging properties, the pseudo-4D phase diagrams, both $(\text{Ma}_2\text{O})-\text{MaeO}-\text{P}_2\text{O}_5-\text{Al}_2\text{O}_3$ and $(\text{Ma}_2\text{O})-\text{MaeO}-\text{SiO}_2-\text{Al}_2\text{O}_3$, which provide a more effective guideline for AFC than the simple ternary phase diagrams, should be constructed based on statistical data from real biomass ashes rather than from simulated ashes obtained by the addition of certain metal oxides to the biomass/biomass ashes or by the direct mixing of different metal oxides.

2.3. Agglomeration

With the advantages of being insensitive to changes in fuel properties and having low operating temperatures, fluidized bed boilers are particularly suitable for biomass combustion. However, bed agglomeration induced by the inorganic fuel components is a major problem. In the worst case, it results in defluidization and unscheduled shutdown of the entire power plant [30]. Generally, the agglomeration tendency depends on the bed material [20,91,102], fuel [17,19,20,91], and operating conditions [20,91].

2.3.1. Effects of bed materials and fuels

The chemical composition of the bed particle layer exhibits a strong dependence on the bed material and the fuel ash composition. An agglomerated bed particle generally consists of several superimposed layers with different properties and compositions [19,56]; the inner layers are more dependent on the bed material composition, and the outer layers have a composition that is more similar to those of the fuel ash [56,91,102]. Generally, the thickness of the coating around the bed material grains is approximately 2–50 μm , whether measured in a laboratory reactor or a commercial-scale FB [19,103,104]. The elemental composition of the homogeneous inner layer formed on the quartz bed materials is dominated by Si, K, and Ca, which are responsible for the agglomeration of quartz sand [56,102]. For an olivine bed, the inner composition layer consists mainly of Mg, Si, and Ca [102]; in comparison with a quartz bed, the agglomeration is slight because Mg increases the melting temperature of pure potassium silicate [17]. For blast-furnace slag as the bed material, the granular outer coating layer is the main component of the “glue” in the formed bed agglomeration necks and melts at the higher temperature range of 800 °C to 1000 °C; thus, it can reduce agglomeration to a certain extent. According to chemical equilibrium calculations using FACTSAGE, the reduced agglomeration tendency of olivine and blast-furnace slag, when used as the bed materials, is due to the low chemical driving force for K to react with and be retained on the bed materials [56,102]. Otherwise, K-feldspars and plagioclase, which are the two main components of natural sand, have distinct influence on the agglomeration tendency of different fuels [17]. They do not influence the agglomeration of K- and Si-rich fuels (such as wheat straw); however, plagioclase reacts with fuel potassium increasing the initial defluidization temperature for K-rich biomass residues

by forming leucite. K-feldspars aggravates the agglomeration of K- and Ca-rich fuels (such as bark) because the introduction of Al to a potassium silicate melt lowers the melting temperature at high K/Al and low $(\text{K}_2+\text{Al}_2)/\text{Si}$ ratios [17].

Ohman et al. [19] reported that the layers covering the bed particles are homogenous, but that the elemental distributions of the coating vary significantly between bed samples from different fuels. Generally, compared with trace amounts of Na, Mg, and Al, the dominant elements are Si, K, and Ca in all coatings, as shown in Fig. 13. The distribution of Si, K, and Ca matches that of the sample well. The light regions in the SEM-EDS images represent the element distribution. A $\text{SiO}_2-\text{CaO}-\text{K}_2\text{O}$ ternary system is therefore proposed to evaluate the melt behavior of typical woody biomass fuels that contain high Ca and K and low Si [102]. For K- and Si-rich agricultural residues such as wheat straw, agglomeration is not influenced by the bed material; the major coating elements are Si and K, and the fuel ash itself melts causing the bed agglomerate before layer can develop [17]. For P-rich fuels, alkali and alkali earth phosphates should be formed first followed by sulfates, chlorides, silicates, carbonates, and hydroxides. This is probably because of the greater acidity of $\text{P}_2\text{O}_5(\text{g})$ than $\text{SO}_2(\text{g})/\text{SO}_3(\text{g})$, $\text{HCl}(\text{g})$, $\text{SiO}_2(\text{g})$, and $\text{CO}_2(\text{g})$ in the competition for the basic components, i.e., $\text{KOH}(\text{l,g})$, $\text{NaOH}(\text{l,g})$, $\text{CaO}(\text{s})$, and $\text{MgO}(\text{s})$. K-Ca phosphates and K-Mg phosphates favor agglomeration reduction because of the high stability of phosphate compounds [65].

2.3.2. Agglomeration formation mechanisms

Agglomeration is dependent on the chemical characteristics and melting behavior of the coating, which are sensitive to the relative amount of calcium and potassium in the fuel [19]. Increasing Ca content moves the composition toward regions with high melting temperatures, whereas increasing K concentration moves the composition toward regions with low eutectic temperatures [92]. Grimm et al. [102] reported that bed particle layer formation and bed agglomeration are associated with the direct adhesion of particles by partly molten fuel ash derived from K-Mg phosphates in fuels rich in S, P, K, and Mg, and from K-silicates in fuels rich in Si and K. Melissari [14] agreed with these reports and defined agglomeration as a result of two phenomena: (1) accumulation of low-melting salts of potassium and phosphorous, and (2) reaction of potassium phosphate with Si and Ca to generate low-melting silicates of potassium and calcium.

As shown in Fig. 14, Visser et al. [20,105] summarized two different routes for agglomeration, namely, “melt-induced” agglomeration (a) and “coating-induced” agglomeration (b). In “melt-induced” agglomeration, the bed particles adhere together via a molten phase because of the high local peak temperature, which roughly matches the chemical composition of the ash. In “coating-induced” agglomeration, which is commonly observed in commercially operated fluidized-bed combustors, a uniform coating is presented on the surface of the bed material grains. Along with coating thickness and/or temperature increase, a neck formation may occur between coatings of the individual grains; such formation initiates agglomeration [20]. After the first neck formation, defluidization of the bed particle results in a localized high-temperature zone that favors melt formation and promotes agglomeration. Similarly, Liu et al. [30] pointed out that the formation of agglomeration is caused by “melt-induced” agglomeration mechanisms (ash particle size approaching 30 μm) and “coating-induced” agglomeration mechanisms (ash particle size approaching 10 μm); large ash particles ($>10 \mu\text{m}$) and small ash particles ($<10 \mu\text{m}$) are responsible for the formation of melt and coating, respectively.

Ohman et al. [19] further detailed the formation process of agglomeration, especially concerning the formation of coating layer, as shown in Fig. 15. Firstly, ash deposition occurs on the bed material by a combination of: (a) attachment of small particles to the

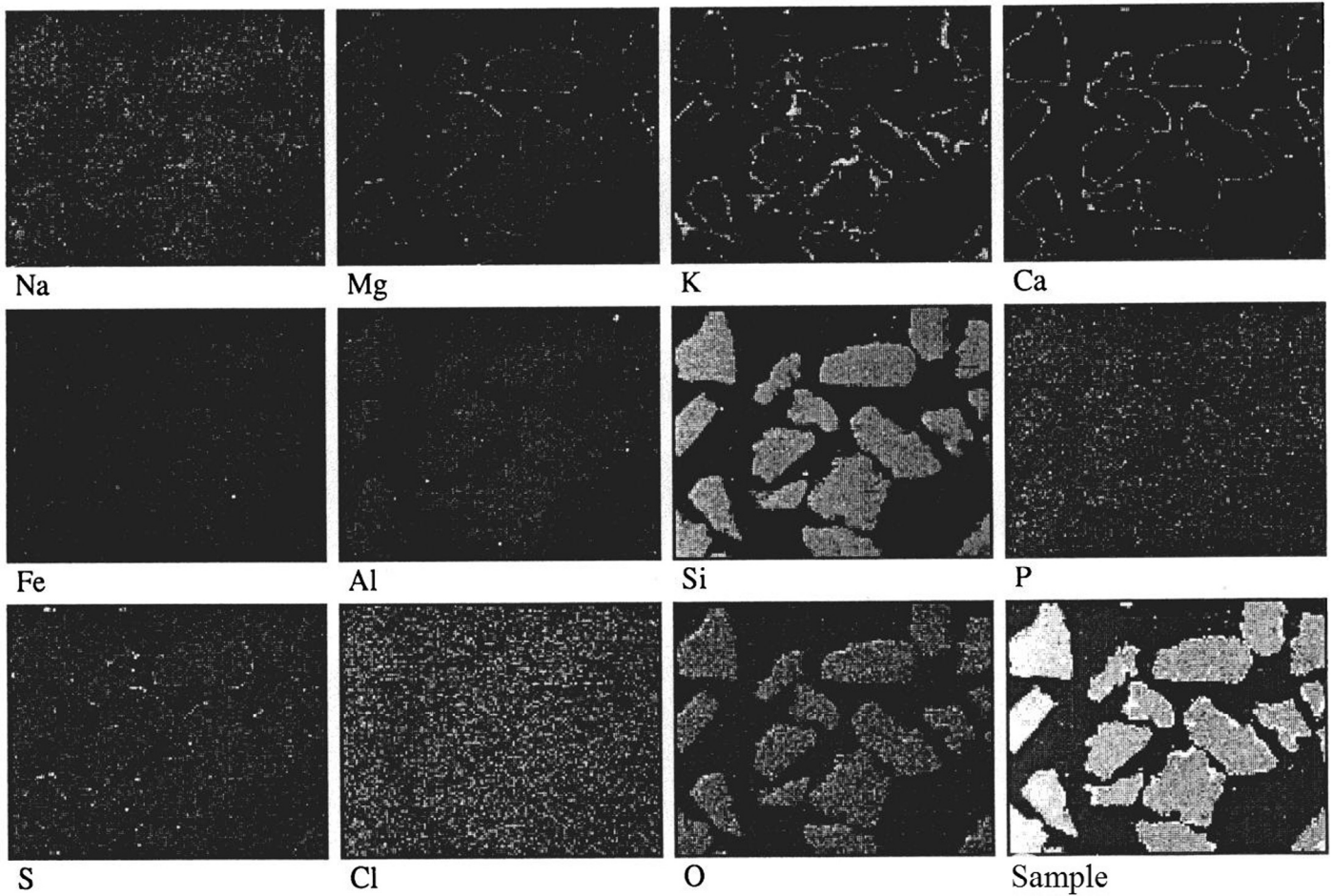


Fig. 13. Example of SEM-EDS elemental mapping for bed sample from the bench-scale test of wood combustion (adapted from reference 19).

bed particle surfaces, (b) condensation of gaseous alkali species (KCl , KOH , K_2SO_4 , K) on bed particles, and (c) chemical reaction of gaseous alkali on the surface. Secondly, accompanied by continuous deposition on the bed particles, the inner layer of the coating is probably homogenized and strengthened via sintering. Thirdly, the melting behavior of the homogeneous silicate layer controls the adhesive force, which is responsible for the final temperature-controlled agglomeration process and defluidization.

Meanwhile, Brus et al. [64] and Grimm et al. [65] classified agglomeration mechanisms into three categories according to fuel properties: (a) bed layer formation initiated by potassium silicate melt (formed on the bed particle surfaces by a reaction with gaseous or liquid K compounds) accompanied by diffusion/dissolution of Ca into the melt, viscous flow sintering, and agglomeration (behavior typical for woody fuels containing Ca , K , and relatively low amounts of Si); (b) direct reaction of gaseous or aerosolized K compounds with the bed particle surface, thereby forming a low-melting K -silicate layer with the subsequent development of a viscous flow sintering and agglomeration (behavior typical for fuels with high alkali and relatively low silicon content); and (c) direct adhesion of bed particles by partly molten ash-derived potassium silicate particles/droplets (typical for fuels with high potassium and organically bound Si in biomass, and low content of other ash-forming elements) and K - Ca / Mg -phosphates particles/droplets (typical for biomass rich in P , K , and Ca/Mg). Generally, the bed material plays an active role in the agglomeration processes dominated by mechanisms (a) and (b) but a much less obvious role in (c) because of the limited interaction between the ash-forming com-

pounds and the bed material. For mechanism (c), the cause of agglomeration is more dependent on the compositions of the fuel ash [17]. These findings were further verified by Grimm et al. [65], who studied the coating compositions of logging residues, bark, willow, wheat straw, and corresponding mixtures by adding P -rich fuels or phosphoric acid in a 5 kW bubbling FB by SEM-EDS and XRD. They pointed out that for combustion of P -rich fuels and fuel mixtures, melting is heavily dependent on the content of alkaline earth metals in the fuel.

2.3.3. Coating forming mechanisms

Coating-induced agglomeration, which results in a uniform coating on the surface of bed material grains, is commonly observed in commercially operated FB combustors. The formation of the coating layer is a result of an interaction between the ash-forming elements in the fuel and the bed particles [17]. Based on experimental data, Visser [20] proposed a coating growth model (Fig. 16). According to experimental research, the coating can be classified as a two-layer (left illustration) or three-layer (right illustration) model. In the two-layer model, the major components in the inner layer are Si and Ca , and the outer layer mainly contains Ca , Si , P , K , and S . In the three-layer model, the major elements in the innermost layer are Si , K , and Ca , and the intermediate layer mainly contains Si and Ca , which have concentrations comparable to those of the inner layer of the two-layer model. In common with the two-layer model, the major elements in the outmost layer are Ca , Si , P , K , and S . The coating layer consists of two or three layers depending on K . The two-layer model with a Ca -silicate layer as the inner

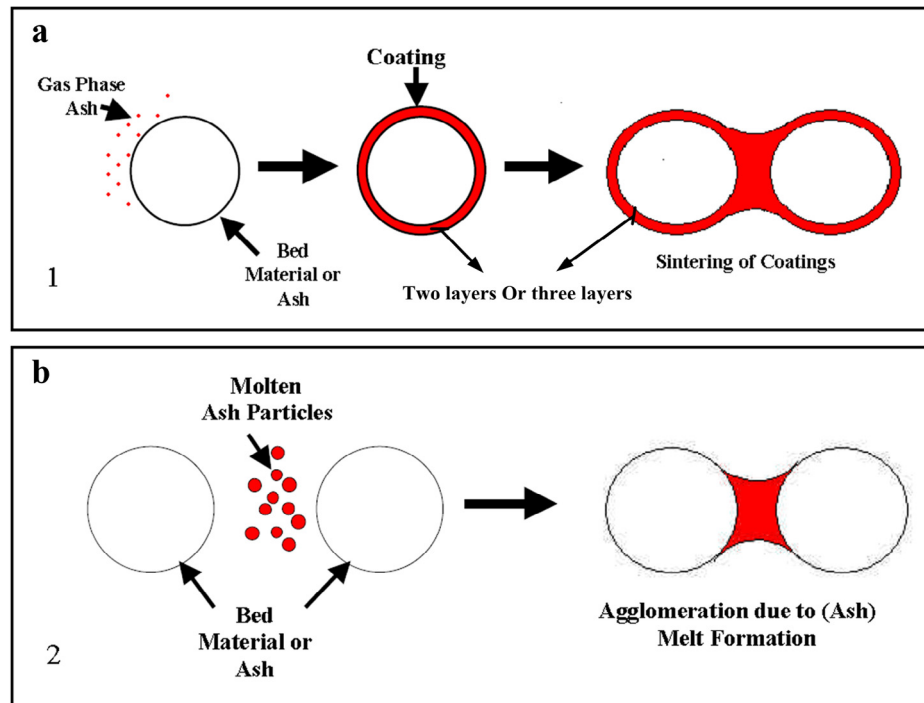


Fig. 14. Agglomeration of bed materials after the melt formation of ash components (a) and coating formation from the gas phase (b) (adapted from references 20,105).

layer is preferable when K is not present. However, when surplus K is present, it is more likely that a K-silicate layer will form first. As residence time increases, K and Ca in the inner or the innermost layer increase, in part, because of the diffusion/dissolution of K and Ca into the quartz grains. In the outer or outermost layer, only K and S gradually increase with time. For thicker coating, K input becomes faster than its diffusion, resulting in some K in the outer layer. The presence of S in the outer coating may be attributed to the reaction of K in the outer coating gas phase S. Excluding the in-

creases in K, Ca, and S, the changes in the concentrations of other elements can be ignored.

Similar coating structures were reported by Nuutinen et al. [91]. They found that 1–3 superimposed coating layers exist on different bed particles. The innermost layer is K-rich and mainly contains alkali-silicates; the outmost layer is Ca- or Mg-rich depending on the composition of both the fuel and bed. Coating layers that contain potassium or sodium may be adhesive and cause the formation of agglomerates by reaction with SiO₂. Hence, quartz and natural sand

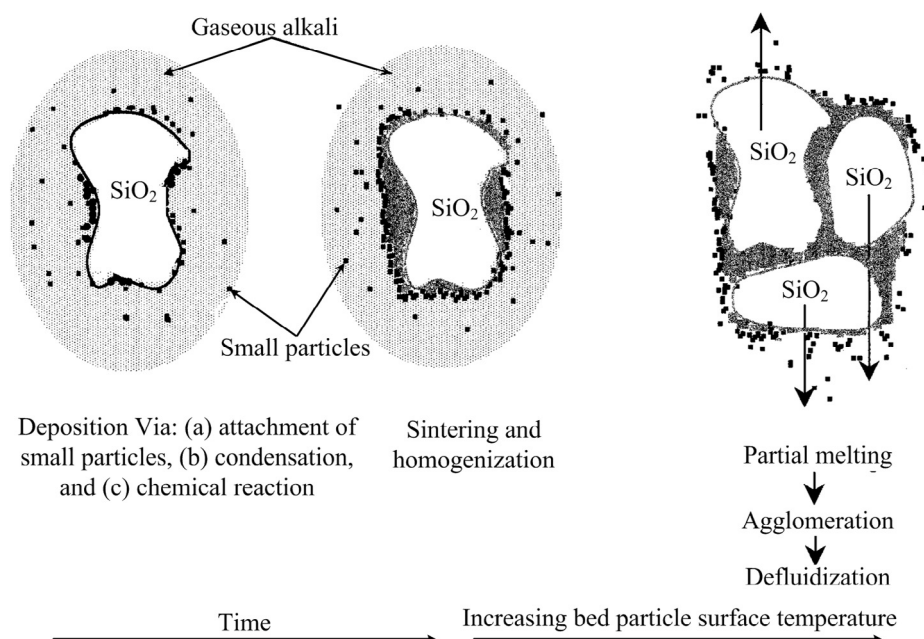


Fig. 15. Important chemical sub-processes of the bed agglomeration mechanism (adapted from reference 19).

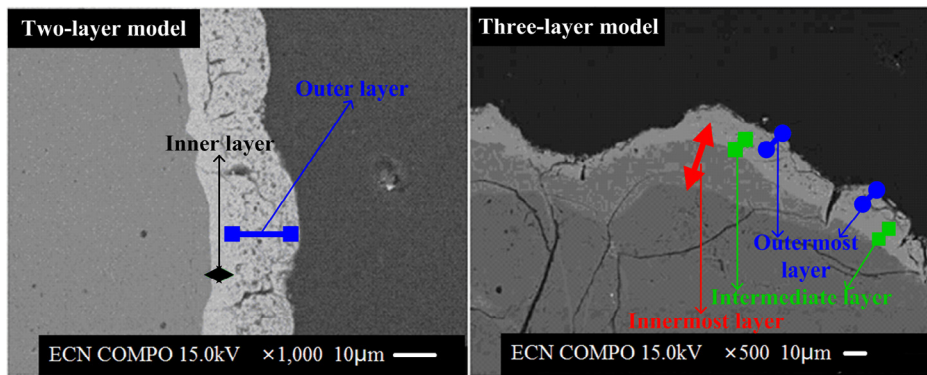


Fig. 16. Coating growth model proposed by Visser (adapted from reference 20).

Upper-right SEM image shows a two-layer coating section of a quartz grain from lab-scale CFB;
Upper-left SEM image shows a three-layer coating section on a quartz grain from commercial CFB

bed materials are problematic when fuel with high alkali metal content is combusted. Owing to the magnesium-containing coating layers on the ground blast-furnace slag granule particles, it can serve as bed material and overcome the problems caused by the absence of SiO_2 in the bed material.

Ohman et al. [19] attempted to determine the formation mechanisms for the coating and proposed that their formation is dominated by a combination of the attachment of submicron-sized particles and the condensation and chemical reaction of gaseous alkali-metal species such as KCl , KOH , or K_2SO_4 on the bed particles surfaces; consequently, the sintering and melting behaviors of the homogeneous silicate layer improve agglomeration. Latva-Somppi et al. [106] further detailed the mechanisms of reaction between fuel-K and SiO_2 : (1) diffusion of vapor to the surface of the bed particle, followed by a surface reaction; (2) deposition of submicrometer-sized K_2SO_4 particles on the bed material and release of sulfur from the reaction between K_2SO_4 and SiO_2 as SO_2 ; and (3) deposition of supermicron particles on the bed material followed by a reaction between SiO_2 and K that originates from the submicron particles.

2.3.4. Agglomeration indicator

Evaluation indexes as an effective tool to predict the changing tendency of targets has been widely applied in various fields. The most comparable evaluation indices, e.g., basic/acid ratio, Si/Al ratio, and fouling index [107], are used with success to predict coal slagging and fouling. They are also used for biomass slagging evaluation [83,84]. To predict the tendency for bed agglomeration, Visser [20] proposed three agglomeration indicators (Exp 2–Exp 4) based on certain simplifications and hypotheses. The first indicator predicts the formation of alkali-silicates on the bed material, the second predicts the formation of a refractory outer coating, and the third predicts the agglomeration potential induced by an alkali-silicate melt phase.

$$I1 = (\text{Na} + \text{K})/(2\text{S} + \text{Cl})$$

Exp 2

$$I2 = (\text{Na} + \text{K} + \text{Si})/(\text{Mg} + \text{P} + \text{Ca})$$

Exp 3

I3:

$$\left. \begin{array}{l} \text{K/Si} > 1 \\ \text{IF } \text{K} > 3 \text{ g/kg fuel}; \text{Si} > 2 \text{ g/kg fuel} \\ \text{K}_2\text{O} + \text{SiO}_2 > 50 \text{ wt.\% fuel ash} \end{array} \right\}$$

Exp 4

THEN Occuring melt-induced sintering in quartz bed.

The first agglomeration indicator, $I1$, reflects the probability that an excess of alkali metals over sulfur and chloride leads to the formation of alkali metal silicates. It is based on the general observation

that the initial gas phase alkali concentration can be attributable to their concentration in the fuel, the bed temperature, and the presence of S and Cl. The latter leads to gas-phase release and binding in relatively volatile compounds at temperature over 800 °C. This estimation assumes that all the S and Cl present in the fuel react with the fuel alkali species and ignore both the release of S and Cl in the forms of HCl and SO_2 and their combination with other cations.

The second agglomeration indicator, $I2$, describes the probability of the formation of a refractory outer coating. This is based on the fact that the coating build-up around SiO_2 grains often develops an inner alkali-silicate reaction rim and a refractory outer rim relatively rich in Ca, P, and Mg. The outer rim has a much higher melting temperature, and hence, a lower potential to lead to agglomeration. A fuel with a ratio in which $(\text{Ca} + \text{P} + \text{Mg})$ is larger than $(\text{K} + \text{Na} + \text{Si})$ is believed to form such a non-sticky outer layer.

Contrary to the two indicators above involved in “coating-induced” agglomeration, the third agglomeration indicator, $I3$, indicates the probability of “melt-induced” agglomeration in a quartz bed.

However, the successful application of the above indicators must consider the following points. Firstly, agglomeration indicators $I1$ and $I2$ are applied consecutively because of the faster gas phase reaction of alkali-halides and sulfates formation than the reaction of K with Si in the bed material; however, if $I1$ is larger than 1.0, $I2$ is considered. Secondly, the consecutive use of $I1$ and $I2$ would suggest that the concentration of alkalis equivalent to the total concentration of $(\text{Cl} + 2\text{S})$ would be subtracted from the total concentration in the fuel before the ratio of $I2$ is calculated. The subtracted concentration represents the fraction being expelled to the gas phase and unavailable for alkali-silicate formation in the bed. Third, the ash components of the mixture are thoroughly mixed on an elemental scale; therefore, elements of both fuels can be added up in the calculation of $I1$ and $I2$.

Using agglomeration indicator $I2$, Piispanen et al. [18] successfully predicted the bed agglomeration propensity of a mixed fuel (containing 60% peat, 20% woodchip and sawdust, and 20% forest residue) burned in a 315 MW CFB boiler. They developed the indicator $I2$ in a quasi-ternary diagram as $(\text{Na} + \text{K} + \text{Si}) - (\text{Mg} + \text{P} + \text{Ca}) - (\text{Al} + \text{S} + \text{Cl} + \text{Ti} + \text{Fe})$. Several other quasi-ternary diagrams have been proposed according to the coating composition and with respect to the melting properties, such as $(\text{Si} + \text{Al}) - (\text{Ca} + \text{Fe}) - (\text{Na} + \text{Mg} + \text{K} + \text{Ti})$ [91], $\text{K}_2\text{O}-\text{CaO}-\text{SiO}_2$ [92], $\text{CaO}-\text{MgO}-\text{SiO}_2$ [93], $\text{K}-\text{Mg}-\text{P}$ [102], and $\text{Ca}-\text{P}$ [102].

In the $\text{K}_2\text{O}-\text{CaO}-\text{SiO}_2$ ash system, increasing Ca content results in high melting temperatures, whereas increasing K concentration moves the composition toward regions with low eutectic temperature [92]. Fuels with low Ca/K ratio result in a high degree

of agglomeration. Mg-K-P and Ca-K-P phase diagrams indicate that the ash composition close to the binary K₂O–P₂O₅ region exhibits eutectic temperatures as low as 590 °C, whereas an increase in either Ca or Mg content strongly shifts the melting temperatures to over 1000 °C. Mg-K-phosphates generally have a lower melting temperatures and result in a higher degree of agglomeration compared with Ca-K-phosphates [102]. In the CaO–MgO–SiO₂ ash system, no melts are found below 1320 °C [93]; thus, no agglomeration problems should occur when both Ca and Mg content in the quartz bed is high. Several other agglomeration indexes exist; for example, BAI that is equal to the ratio of Fe₂O₃ to (K₂O + Na₂O). Bed agglomeration occurs when the BAI value is lower than 0.15 [108]. Nevertheless, the solution to agglomeration requires further study, especially to investigate the most effective combinations of fuel and bed material as well as practical and available agglomeration indicators.

2.4. Countermeasures for the main ash-related issues: additives

As mentioned previously, KOH, KCl, and K₂SO₄ are the dominant alkali metal species generated during combustion. In particular, KCl and K₂SO₄ are the primary components of the sub-micrometer particulate matter in the flue gas produced from biomass combustion [48,80]. Meanwhile, KCl and K₂SO₄ have low melting temperatures of approximately 770 and 850 °C, respectively, and binary systems containing these two potassium salts may melt at lower temperatures of around 550 °C [63]. Therefore, as the principal causative agents for ash-related problems during biomass combustion, KCl and K₂SO₄ content must be reduced. There are various countermeasures for this, including the use of additives [41,109,110], co-firing [87,111], and leaching [99,112,113]. Leaching removes K directly from the source, and additives and co-firing aim to change the ash composition and further reduce the existence of volatile alkali species [110].

2.4.1. Effects of single oxide or element additives

The inorganic content in biomass mainly comprises Si, Al, Ca, Mg, K, Na, Fe, P, S, and Cl. Most of these elements act as nutrients and have essential biological functions for living plants, except for Al, which has no known biological function and is considered to have originated from external mineral matter such as feldspars and clay mineral. Bostrom et al. [48] simplified the classification of the main ash-formation elements as Si, Al, Ca, Mg, K, Na, P, S, and Cl after considering the most important ash transformation reactions responsible for ash-related problems during biomass combustion. Fe and other elements such as Mn are excluded because they are often found individual oxides with limited interactions with the other ash-forming elements.

As listed in Table 5, Bostrom et al. [48] further divided the ash-forming compounds into two categories: basic and acidic. Roughly, the compounds are arranged according to their reactivity from highest to the lowest. Using K as an example, if P₂O₅(g) is consumed, K will react with SO₂(g)/SO₃(g), and then SiO₂(s) and HCl(g) in turn. That is, K-phosphates will be the first species to form, followed by K-sulfate, K-silicate, K-chloride, K-carbonate, and

K-hydroxide according to their thermodynamic stability [109]. However, the order is solely based on thermodynamic considerations, i.e., reflecting a system at equilibrium. In a real system, further reactions will occur and generate K-Ca- and K-Mg-phosphates and -silicates because of the lower formation energies of these phases. For example, along with the burnout of the fuel particle, the molten K-silicate particles with eutectic temperatures as low as 600 °C will aggregate, and form large droplets that initiate slagging and agglomeration; then alkali earth metals may also react with or dissolve into the melt K-silicates [48].

In addition, SiO₂, Al₂O₃, CaO, MgO, P₂O₅, K₂O, and Na₂O have a statistically significant effect on silicate melt-induced slagging and AFC. For example, Al₂O₃ shows a positive effect on IDT increase [67], an increase in the Al₂O₃ content significantly increases AFT, which is at its highest when the Al₂O₃ concentration is at its maximum level [89].

2.4.1.1. Alkali metals: potassium and sodium. Potassium (K) is the alkali metal present in the greatest concentration in biomass, and its volatilization during firing is directly linked to the formation of intransigent surface deposits, agglomeration, and corrosion. The more alkali metals and chlorides the fuel contains, the lower its ash melting point is and the more easily slag appears [84]. K is the root cause of slagging, bed agglomeration, and corrosion in biomass combustion and is mostly present in a soluble form. However, a small amount exists in the form of insoluble silicate contamination of the fuel (i.e., clay and others).

Soluble K, which can be present either in an ionic form in salts or as directly organically bound K ions (e.g., as counterions to carboxylic groups), is released as K(g), KOH(g), KCl(g), and other species during combustion and is thus readily available for further reactions with other compounds of the flue gas. When no chlorine is present in the furnace gas, the dominant vapor contains K(g), K₂CO₃(g), and KOH(g). In contrast, when Cl is available, KCl(g) is the dominant K-containing vapor. The vapor undergoes several subsequent reactions (described as Rs 1–15) in the flue gases depending on the presence of other elements. Using S as an example, when no sulfur is available, K(g) and KOH(g) may condense as a carbonate aerosol (melting point: ~890 °C) by reaction with CO₂, and KCl(g) will condense as KCl aerosol particles or onto the existing fly ash. The condensed KCl(s, l) becomes molten again at furnace operating temperatures (melting point: 770 °C). Moreover, KCl reduces the first melting temperature of the fly ash, thus making the ash sticky at low temperatures and increasing slagging. When S is present, the alkali metal chemistry changes dramatically. According to the kinetic model proposed by Glarborg and Marshall for the sulfation of alkali species in combustion, SO₃ reacts with KCl or KOH and transforms into KHSO₄ or KSO₃Cl, which may then be converted to K₂SO₄ [51]. The reactions lead to Cl-free fly ash and a significant decrease in slagging of the superheater. Several techniques, such as the addition of elemental sulfur and ammonium sulfate in a controlled manner to the fuel or introducing them into the upper furnace, have been developed to promote this reaction [79,111].

Alkali metals also react with silica in the residual ash and are transformed into silicates with very low melting points (<800 °C) [114]. Furthermore, a sticky coating is generated on the surface of inert particles, enhancing their tendency to stick together by forming large clusters, which leads to subsequent bed agglomeration and defluidization. Potassium is one of the main elements in the coating layers on bed particles as well as in the adhesive material of agglomerates [30].

The authors [15] conducted the research on AFC of biomass incinerated at temperatures from 400 to 1400 °C and found that IDT decreases with increasing K concentration. Eldabbagh et al. [115] conducted comparative research on particle-metal interactions at a continuous temperature range of 1000–1400–1000 K

Table 5

Categories of different compounds (reprinted from reference 48, with permission of American Chemical Society).

Basic compounds	Acidic compounds
KOH(l,g) (K ₂ O)	P ₂ O ₅ (g)
NaOH(l,g) (Na ₂ O)	SO ₂ (g)/SO ₃ (g)
CaO(s)	SiO ₂ (s)
MgO(s)	HCl(s)(Cl ₂)
H ₂ O(g)	CO ₂ (g)
	H ₂ O(g)

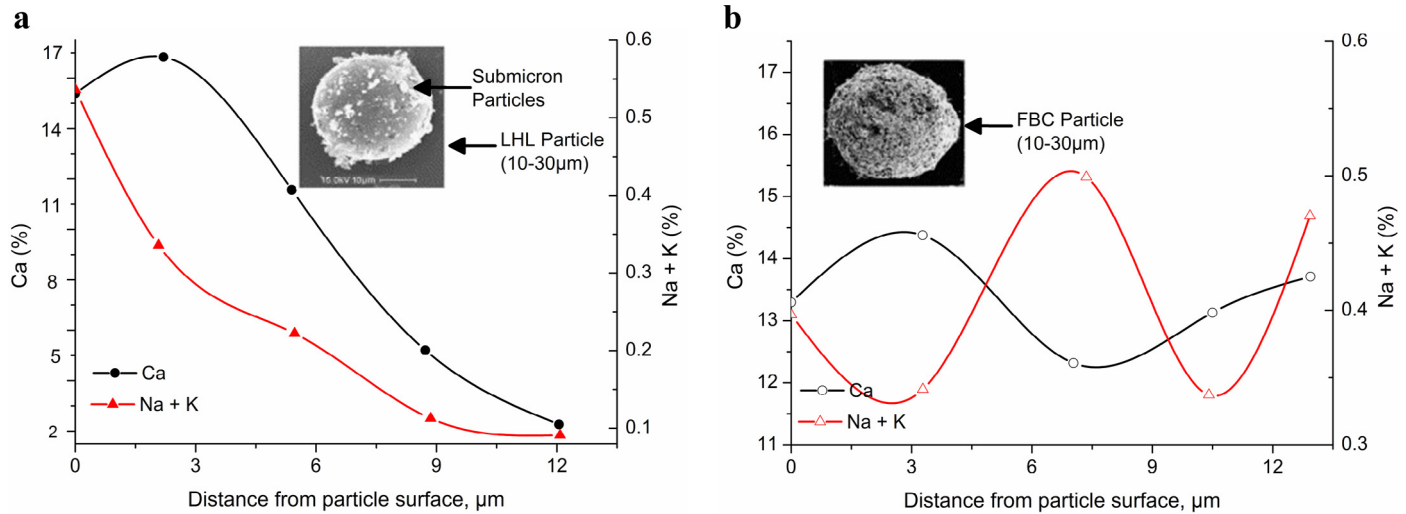


Fig. 17. Radial profiles of Ca and $\text{Na} + \text{K}$ concentrations in the biomass ash particles generated during LHL and FBC combustion, and the corresponding ash particle structure (adapted from reference 115).

- a. LHL case
- b. FBC case

(Low-High-Low temperature, or LHL) and isolated 930 K (classical FBC combustion mode). They found that in the LHL case (Fig. 17a), the concentrations of $\text{Na} + \text{K}$ and Ca are the highest in the region nearest the surface, contrary to irregular distribution in the FBC particle (Fig. 17b). Meanwhile, because of high combustion temperature in the LHL case, the surface dominated by the alkali metals is where the bonding of the submicron particulates occurs. Na and K act as links between supermicron and submicron particles. The continuous temperatures of 1000–1400–1000 K (or the LHL case) means that the fuel was initially fed into the low-temperature region (<1000 K) of the pilot-scale multimode combustion facility and then subjected to high-temperature treatment (~1400 K), followed by quenching in the second low-temperature zone (<<1000 K).

For the purposes of analysis, sodium in biomass can be approximated by potassium in biomass because the concentration of sodium in biomass is generally lower than that of potassium and their functions and roles in the ash transformation reactions are similar [48]. Moreover, the effect of potassium is more considerable than that of sodium; for example, the diffusion coefficients of potassium ($53 \pm 14 \times 10^{-9} \text{ cm}^2/\text{s}$) is approximately four times that of sodium ($2 \pm 6 \times 10^{-9} \text{ cm}^2/\text{s}$) at 1300 °C [98]. Generally, the above descriptions of potassium are valid for sodium, and sodium is treated as simply potassium in some conditions.

2.4.1.2. Alkaline earth metals: calcium and magnesium. Alkaline earth metals, typically calcium (Ca) and magnesium (Mg) in biomass, have low mobility and vapor pressures and cause fewer deposition problems. Generally, as Ca and Mg content increases, the melting temperatures increase and slagging decreases [48,99]. Alkaline earth metals also contribute to the formation of high-temperature melting calcium potassium phosphates and silicates [116], and thus inhibit the occurrence of silicate melt-induced slagging and bed agglomeration. However, calcium sulfate deposits are frequently observed on the surface of the cold reactor. Moreover, calcium is typically a major constituent of the alkali silicates that form on combustion [114].

Ca, the element present in the highest concentration in woody biomass, can be divided into three forms: organically bound, acid-soluble, and acid-insoluble. Generally, acid-insoluble Ca, most of which is in the form of Ca-silicates, is inert under combustion conditions and does not influence the flue gas chemistry. Organically

bound and acid-soluble Ca transfer into CaO during thermochemical conversion and exists as small micrometer-sized particles participating in further reactions in the furnace and flue gases. On the one hand, CaO can react with SO_2 and further influence the sulfation of alkali chlorides that worsens slagging; on the other hand, the recarbonation of CaO may cause sintering at 600 °C to 800 °C.

Mg is chemically similar to Ca but exists at much lower concentrations. The combustion chemistry of Mg is less reactive than that of Ca. Reactions that involve Ca also occur with Mg, but, in most cases, MgO can be regarded as an inert compound during combustion [117].

2.4.1.3. Phosphorus. Phosphorus (P) may be present in biomass fuels either as soluble phosphate salts such as K_3PO_4 or as organic molecules containing phosphorus. In woody biomass, the ratio of inorganic and organic P is around 3, and in several annual plants, the organic P content may be very high (up to 0.2 wt.%) [117]. During combustion, phosphates of both alkali metals and calcium may form. The former may melt at low temperatures (eutectics) and cause bed sintering or agglomeration. However, calcium phosphates do not appear to cause sintering problems. Thus, the Ca/K ratio in the fuel or fuel mix appears to control undesirable deposit formation when P is present. Potassium silicates and phosphates with low Ca(Mg)/K ratio with low melting points may result in severe ash sintering and agglomeration during combustion [110,118]. K-rich phosphates have melting temperatures as low as 700 °C [116].

Moreover, P dominates over Si in the competition for base cations (K^+ , Mg^{2+} , and Ca^{2+}). Consequently, K-Mg-Ca-phosphates form prior to the corresponding silicates [109]. The effect of P on ash-related problems is confusing and requires further study. Grimm et al. [65] suggested that phosphorus is the controlling element in the ash transformation reactions during biomass combustion in fluidized quartz beds because of the high stability of phosphate compounds; however, Steenari et al. [110] pointed out that the presence of phosphorus in biomass ash increases the risk for troublesome ash sintering or melting behavior.

2.4.1.4. Sulfur. S is present in biomass both in the form of inorganic SO_4^{2-} and organic S. Organic S is fully released during combustion as SO_2 , and most inorganic SO_4^{2-} may also be released as SO_2 because of the decomposition reaction of the alkali sulfates [16]. In summary,

most of the S in the fuels is released during combustion and ultimately yields SO₂. The only significant exception is CaSO₄, which may be present in some fuels.

After release, SO₂ affects the alkali metals by sulfation of KCl and KOH, as described in R 1, R 2, and R 15. Alkali sulfates are the dominant alkali species that induce ash-related problems in high-temperature zones. Both experimentation and thermo-chemical calculations show that the transformation of SO₂ into SO₃ is the limiting step that influences the sulfation of alkali species [78,79]. This influence is discussed in Section 2.4.2.4).

2.4.1.5. Chlorine. Chlorine acts as a shuttle in reactions that facilitate the transfer of potassium in the gas phase. Alkali chlorides may either participate in further reactions or be deposited on cold surfaces where chlorine may be substituted by sulfur by sulfation reaction or by reaction with the protective oxide layer of the metal surface, thereby initiating corrosion [114,117]. A common consensus is that chloride evaporates easily and acts as a high-temperature transport medium for potassium [70]. Generally, the higher the amount of chlorine is, the more severe the ash-related problems are.

Cl, most forms of which are water soluble, is present in biomass fuels as chloride compounds that vaporize during combustion as alkali chlorides (KCl(g) and NaCl(g)) [48]. Volatilization increases with temperature and the Cl/Me molar ratio. At 1100 °C, Na volatilizes at molar ratios (Na/Cl) ≤ 0.07, whereas K does so at a molar ratio (K/Cl) ≤ 0.5. The effect of chlorine is therefore more significant for K than Na [119]. Similarly, these primary Cl compounds may undergo a number of further reactions with other ash-forming compounds; for example, the metal chlorides may react with SO₂ into sulfates and release HCl.

2.4.1.6. Silicon. Si, being the major insoluble inorganic species in selective leaching, is generally present as silica (SiO₂) or as various silicate minerals in the residual fraction. Under FB conditions, most silicate remains in a crystalline form and does not cause slagging, fusion, or corrosion because of their high melting points.

However, silica, together with potassium present in large concentrations, is directly linked to the formation of tenacious surface deposits on firesides and heating surfaces [120]. SiO₂-K₂O eutectics have melting temperatures as low as 550 °C [121]. Generally, silicon and potassium concentrations are low in stem wood (dead tissue) with less ash-related problems. However, their concentrations are high in the bark, foliage, living tissues, and most annual growth plant materials. Contamination from sand and/or soil (either naturally or artificially) is preferentially present in bark, foliage, and agricultural residues [34]. For agricultural residues such as straw, which contain high and almost equal concentrations of Si and K that are finely distributed throughout the fuel organic matrix, low-melting K-silicates cause severe ash-related problems during combustion [117]. A relatively good correlation exists between silicon content in fuel ash and the fraction of fuel ash that forms slag consisting of a large number of different particles held together by a sticky K-silicate melt [13]. However, research indicates that ashes with less than 47 wt.% SiO₂ show significant alkali metal losses, and ashes with high contents of SiO₂ retain alkalis in the melt and crystalline structures [120].

Lindstrom et al. [34] conducted combustion research on five woody biomass pellets in an underfed pellet burner (20 kW) and reported that the slagging tendency of silicon rich forestry biomass assortments is greater than that of the silicon poor assortments. Contamination by sand and/or soil results in enhanced silicon content in the residual ash, which promotes slagging. To reduce the risk of slagging, there are several recommended remedies such as delimiting or defoliation of forestry rejects, avoiding unnecessary contamina-

tion of sand and soil during harvesting, transport, and storage of fuel, and debarking of logs prior to upgrading.

Silica and its silicates can affect the chemistry of other ash-forming elements, especially K, Na, and Ca, through secondary reactions and thus indirectly affect the deposition and corrosion properties of fly ash. The most important secondary reaction is the conversion of alkali vapors (e.g., KOH(g), KCl(g), K₂SO₄(g)) into corresponding alkali silicates.

2.4.1.7. Aluminum. Al is present in many forms in biomass fuels and wastes. Organically bound Al or precipitated Al-salts are found in the acid-soluble leaching fraction. During furnace processes, they all form alumina (Al₂O₃), which is a solid nonreactive compound that does not appear to participate significantly in the ash chemistry of fluidized bed systems. In some biomass fuels, Al may be present in the form of silicates when clay or other impurities are present; moreover, they may react with alkali vapors, thus affecting the alkali chemistry in flue gas. In addition, metallic aluminum, Al(s), which may be present in certain waste-derived fuels, has a tendency to oxidize into Al₂O₃ during combustion.

In summary, Al compounds are usually nonreactive compounds that do not participate significantly in the ash chemistry of fluidized bed systems. An exception is the capability of aluminosilicates to capture alkali [117] and increase AFT [89].

2.4.2. Effects of mineral additives

The minerals in biomass can be classified into internal and extraneous. Internal minerals such as whewellite (calcium oxalate hydrate), phytolith (amorphous silica), or phytate (phosphate) are probably significantly much more reactive in comparison with extraneous minerals such as quartz, feldspars, and clays. Therefore, several extraneous minerals such as lime, calcite, kaolin, and feldspars are utilized as additives and are expected to improve ash-related problems during biomass combustion.

When blended with fuels or added into combustion systems, the additives can (1) enhance ash melting temperatures by altering or diluting the ash composition with refractory elements (i.e., Si, Al, and Ca); (2) bind and convert low-melting species into less troublesome compounds with high melting temperatures; and (3) reduce concentrations of problematic ash species (i.e., KCl) in the combustion system by means of physical adsorption [121].

2.4.2.1. Lime or calcite. The addition of lime (CaO and Ca(OH)₂) or calcite (CaCO₃) significantly reduces slag formation during biomass combustion [9,110,122]. For P-rich fuels such as cereal grains (barley, rye, and wheat), the addition of lime or calcite benefits the formation of more high-melting-temperature calcium potassium phosphates in the ash residues [122]; similarly, for Si-rich fuel such as agro/forestry residues, the addition of lime or calcite contributes to the formation of high-melting-point calcium magnesium silicates, which in turn reduces slagging [9].

Xiong et al. [9] conducted research on the slagging characteristics of corn stover with and without added calcite and kaolin during combustion and found that both additives can increase melting temperatures by 100 °C to 200 °C. Also, calcite is more effective than kaolin in reducing molten slagging, which decreases by two-thirds and one-half, respectively. The corresponding morphologies of molten slagging are shown in Fig. 18. The samples containing additive calcite have the smallest and most fragile particles, followed by those containing kaolin and, lastly, those with no additives. Similar results were reported by Steenari et al. [110], and the best anti-sludging effect is achieved when both additives (lime and kaolin) are used; however, lime alone provides almost the same effect.

Bostrom et al. [109] conducted research on the small-scale combustion of oat in a horizontal burner and reported that calcite as an additive increases molten slagging and is accompanied by an

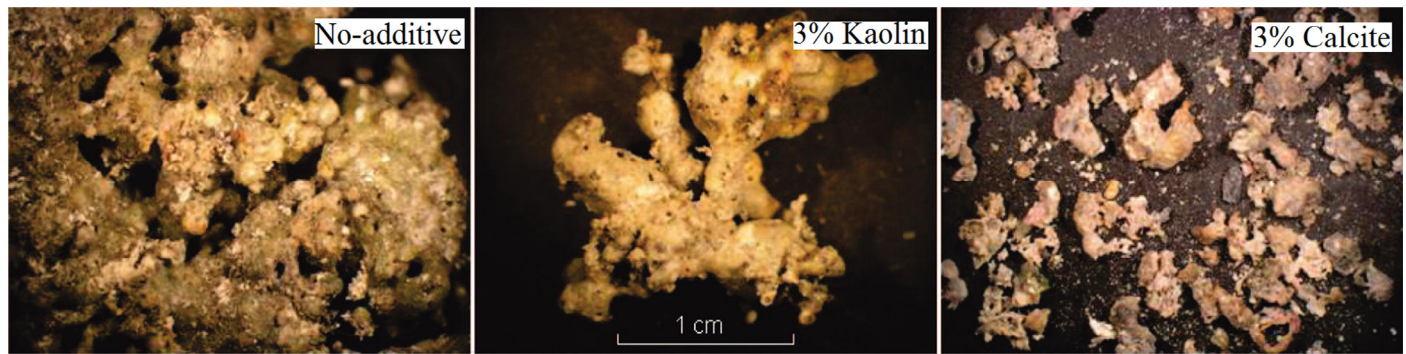
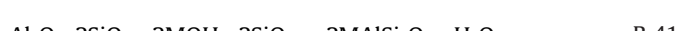
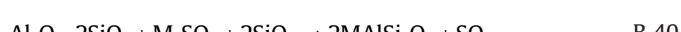
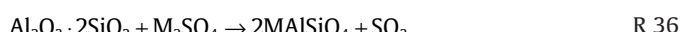


Fig. 18. SEM images of the morphology of the slag formed when combusting corn stover pellets with and without additives (adapted from reference 9).

increasing concentration of K-sulfate and KCl in flue gas and decreasing concentration of both HCl and SO₂. These observations are inconsistent with the common view that calcite prevents slagging formation. The abovementioned distinct results are more likely caused by the different fuel properties or fuel ash compositions. Therefore, the effect of lime or calcite on slagging requires further comprehensive study in consideration of the variation in ash or fuel compositions.

2.4.2.2. Kaolin. Kaolin, which mainly contains kaolinite ($\text{Al}_2\text{Si}_2\text{O}_5(\text{OH})_4$), has been identified as an efficient sorbent for the sequestration of potassium. It decomposes at temperatures between 450 °C and 600 °C by releasing water and forming an amorphous mixture of alumina and silica called meta-kaolinite. The meta-kaolinite suppresses the release of potassium from the biomass and removes gaseous potassium species by reacting with potassium compounds into potassium aluminum silicates with high melting temperatures. The binding of potassium compounds from biomass fuels by kaolin can be described by R 34-R 42 [109,110,121].



The two main products from the above reactions, KAISiO₄ (kalsilite) and KAISi₂O₆ (leucite), which have melting temperatures of greater than 1600 °C and 1500 °C, respectively, and have also been identified in biomass ash and deposits, have been widely investigated [9,15,41,110,121]. Kaolin reduces the concentrations of troublesome alkali chlorides and sulfates in flue gas and ashes, and thus reduces alkali-induced slagging and coating-induced agglomeration; it also forms refractory alkali aluminum silicates and eliminates both melt-induced slagging and melt-induced agglomeration.

However, the temperature has an impact on the capacity of kaolin to react with KCl; the amount of gaseous potassium captured by

kaolin decreases with increasing temperature [123]. Firstly, the porosity of kaolin particles decreases at high temperatures, thereby limiting the pore diffusion of gaseous alkali chlorides and sulfates into the kaolin particles and their corresponding capturing capacity [124]. Secondly, the reduction in the active surface areas of the kaolin particles with increased temperature restricts the chemical reaction intensity and rates between kaolin and potassium chlorides/sulfates [123]. Thirdly, as the temperature rises above 950 °C, meta-kaolinite dissociates into amorphous silica and alumina-silica spinel, which transfer converts to pseudomullite at 1000 °C [123]. Both alumina-silica spinel and pseudomullite have low potential to react with KCl in comparison with meta-kaolinite [121]. Thus, kaolin appears to be a good choice to solve ash-related problems in CFBs or at CFB combustion temperature. For grate and pulverize furnaces, the effect of kaolin requires further investigation. Although kaolin can be utilized as an additive to solve ash-related problems, the high costs involved limit its application and require further assessment [9].

Alternatively, the presence of a soil component in wood fuel can be advantageous in reducing high-temperature alkali losses and may help reduce alkali-induced slagging and agglomeration because the admixed soil increases viscosity and the opposite effect of viscosity on agglomeration. However, these possible benefits are offset by the negative effects of soil addition, namely, reduction of the melting temperature and increase in the probability of melt-induced slagging formation, increased required load, and increased cost for ash-handling facilities and ash disposal [120].

2.4.2.3. Zeolites. Zeolites, which are members of the aluminum silicate family similar to kaolin, have drawn much interest for their capacity to capture alkali during biomass combustion. One of the most important applications of zeolites is to act as water softeners to increase detergent performance during washing and laundering. As a core component of detergents, a large amount of detergent zeolites is carried in the wastewater and subsequently enters the municipal sewage systems, finally being deposited in sewage sludge after wastewater processing. Therefore, sewage sludge is rich in zeolites, which remain as aluminum silicates and carry various cations (i.e., Ca⁺ and Na⁺) [27]. Aluminum silicates (mainly zeolites) in sewage sludge are the main compounds that bond gaseous KCl from the fuel and alleviate ash deposition consequently [27,73].

Wang et al. [121] studied the sintering and melting behaviors of wheat straw and barley husk with kaolin and zeolite additions and reported that even when heated at 1000 °C, no significant melting is observed from the mixtures of kaolin/KCl and zeolite 24A (containing mainly $(\text{Na}_2\text{O})(\text{Al}_2\text{O}_3)(\text{SiO}_2)_2 \cdot 2\text{H}_2\text{O}/\text{KCl}$). However, the mixture of zeolite Y (containing mainly $(12(\text{SiO}_2) \cdot (\text{Al}_2\text{O}_3))/\text{KCl}$) sinters severely into hard aggregates and is blocked at heating

temperatures above 800 °C. The elimination of ash melting by the addition of kaolin and zeolite 2A is attributed to the reaction with KCl to form high-melting potassium aluminum silicates [121] such as KAlSiO_4 . Zeolite Y worsens aggregates, which may be caused by the high Si/Al ratio that decreases IDT [7,67] and improves the formation of low-melting potassium silicates. Therefore, zeolite composed of high Al/Si is favorable for the reduction of slagging and agglomeration. However, zeolite that possesses high Si/Al requires further discussion.

2.4.2.4. Sulfur. K released from fuel during combustion predominantly exists as chlorides and hydroxides. Once released, it is easily available for chemical reaction with other components. Sulfur reduces the formation of KCl in the flue gas by sulfation. During combustion, elemental sulfur or other sulfur/sulfate-containing additives can be utilized for the sulfation of alkali chlorides and converting them into alkali sulfates via both homogeneous (gas phase) and heterogeneous (liquid or solid phase) mechanisms, which have been proposed for the formation of alkali sulfates from alkali chlorides identified in deposits or ash particles [79,111,125].

Fig. 19 shows the principal migration and transformation pathways of KCl in biomass combustion. During combustion, KCl(g) , either formed directly or from the reaction between KOH(g) and HCl(g) (1), may be captured in the combustion chamber by means of reactions with ash minerals that originated either from the fuel or additives (2), and sand particles in the CFB (3); it may also be sulfated (4) in the combustion chamber. The remaining KCl(g) that is not captured/sulfated in the chamber flows into the flue gas and

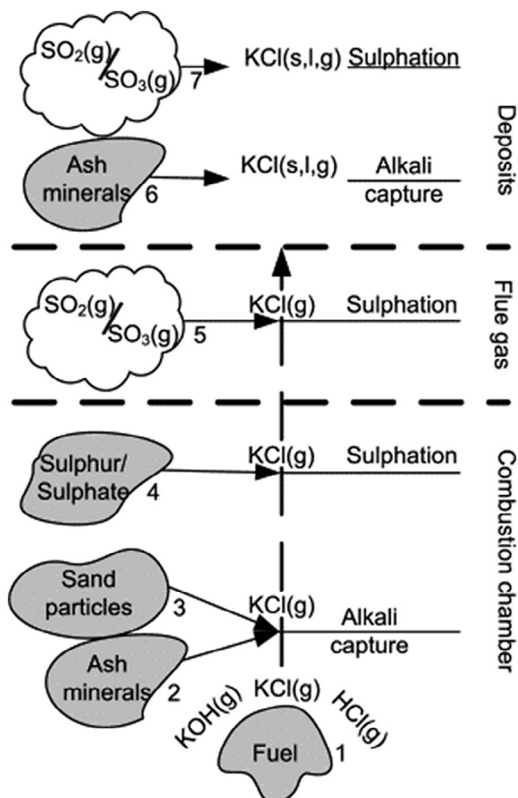


Fig. 19. Principal migration and transformation pathways of KCl in biomass combustion (reprinted from references 111,125, with permission of Elsevier).

1. Release of KOH , KCl , and HCl from a fuel particle; 2. Alkali capture by ash minerals (combustion chamber); 3. Alkali capture by reactions with sand particles (combustion chamber); 4. Sulfation of KCl (combustion chamber); 5. Sulfation of gaseous KCl in the flue gas; 6. Alkali capture by ash minerals in deposits; 7. Sulfation of KCl (s, l) in deposits by SO_2/SO_3 .

may be further sulfated by $\text{SO}_2(\text{g})/\text{SO}_3(\text{g})$ (5). Along with a reduced flue gas temperature, KCl(g) condenses into KCl (s, l) as deposits, which are then silicated, aluminosilicated, and sulfated by heterogeneous reactions.

The presence of gaseous SO_3 is of greater importance than that of SO_2 for the sulfation of gaseous KCl ; this was confirmed by Kassman et al. who used elemental sulfur (S), ammonium sulfate ($(\text{NH}_4)_2\text{SO}_4$, and peat in their experiments [79,111]. They reported that the sulfation of gaseous KCl is more efficient with $(\text{NH}_4)_2\text{SO}_4$ even when the S/Cl molar ratio is around half of that of elemental sulfur and peat. For example, KCl is reduced from 30 ppm to 5 ppm at an S/Cl molar ratio of 2.1 when using $(\text{NH}_4)_2\text{SO}_4$, but only to 10 ppm at an S/Cl molar ratio of 6.4 when using sulfur. These results can be clearly identified from the SEM-EDX maps of the deposits in the 12MW CFB, as shown in Fig. 20, where the lighter parts represent the presence of a specific element in the particles [79]. The deposit mainly consists of potassium and chlorine in the reference case, and the distribution of these elements is highly correlated (Fig. 20a). At a low S/Cl molar ratio achieved by the addition of elemental sulfur (Fig. 20b), the deposits consist of mainly potassium and chlorine. However, with an increased S/Cl molar ratio achieved by the addition of elemental sulfur (Fig. 20c), the deposits instead mainly consist of potassium and sulfur, and these elements have corresponding distributions. However, the effect is incomparable with the addition of $(\text{NH}_4)_2\text{SO}_4$ (Fig. 20d), which converts KCl into K_2SO_4 completely.

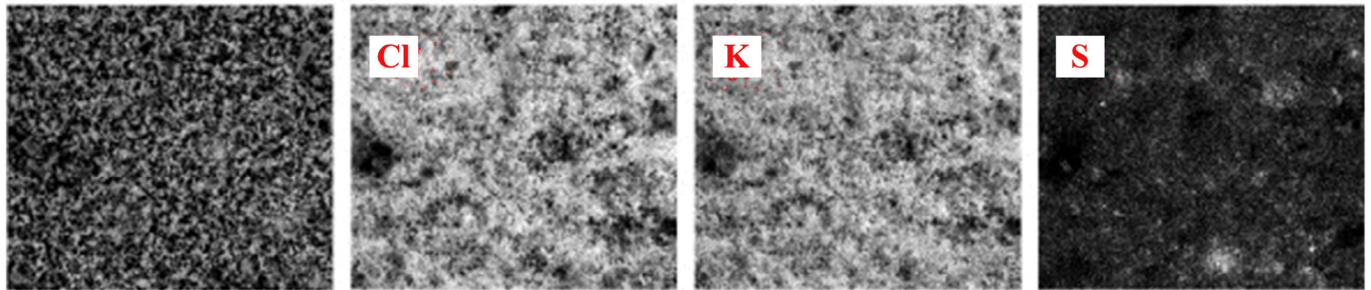
Aside from the homogeneous sulfation reactions of KCl by SO_2/SO_3 , a heterogeneous sulfation reaction by ash components also exists. The heterogeneous sulfation reaction should be valued even though it is less significant than the homogeneous reaction. Fig. 21 shows a comparison of the results of elemental S and peat with high S content during the sulfation of KCl . In comparison with elemental sulfur, although the addition of peat possesses lower S/Cl, it better reduces the amount of KCl in flue gas and Cl in the deposits. Thus, chlorine in the deposits is reduced by K-capture of ash minerals in parallel to sulfation during co-combustion with peat.

Although $(\text{NH}_4)_2\text{SO}_4$ can effectively convert KCl into K_2SO_4 and therefore reduce corrosion induced by the Cl present in deposits, it results in a higher rate of deposit formation and serious deposits, as shown in Fig. 22 where the deposit formation rate of biomass with the addition of $(\text{NH}_4)_2\text{SO}_4$ is significantly higher than that of the pure biomass without any additives. Meanwhile, chlorine and sulfur accelerate the formation of ash deposits, whereas peat as co-firing fuel can not only reduce the Cl content of the deposits and minimize corrosion but can also eliminate ash deposition. Material containing sulfur can be utilized as additive, but the other protective elements (e.g., aluminum and silica), which function as the main alkali sequestration path by the formation of alkali alumina silicates, are more important than sulfur and its associated sulfation reactions [126,127]. Consequently, whether the aluminum and silica are sufficient for KCl capture or not, the effect of corrosion and deposit should be balanced when sulfur or sulfur-containing fuels and additives are required.

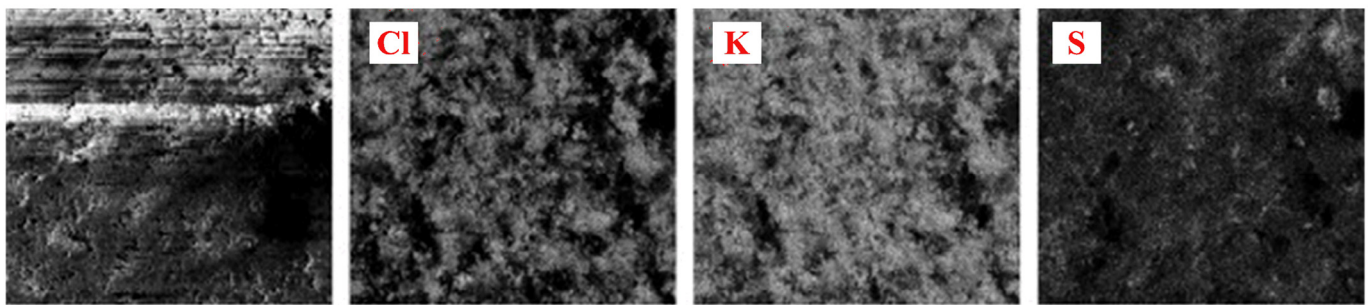
In summary, the effects of the additives on ash-related problems during biomass combustion require further investigation with respect to the following points.

- (1) To clarify the dependence or applicability of additives in biomass species. For example, the effects of calcium discussed in the section titled "Lime or calcite" may be effective for certain biomass, but ineffective, or even have the opposite effect, for other types of biomass and conditions;
- (2) To reveal the effects of temperature and other factors on reactivity. For example, the declining K sequestration effectiveness of kaolin discussed in the section titled "Kaolin" is essential for the selection of additive under different combustion conditions.

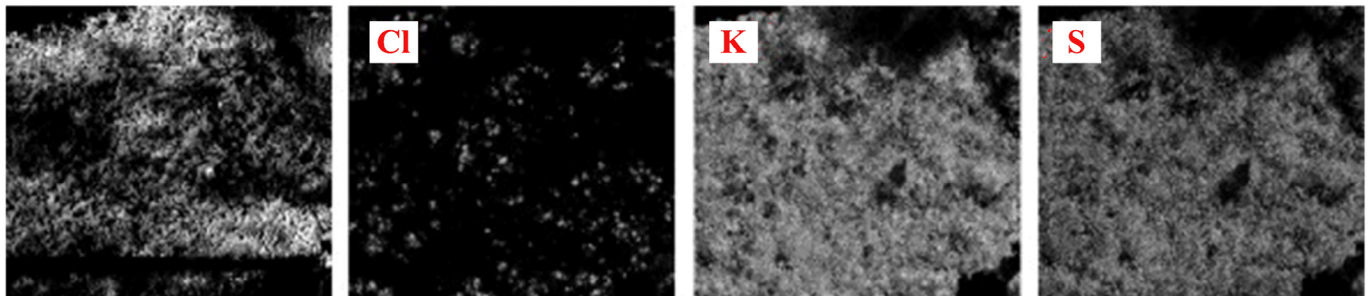
a. Reference case (80 cal% wood+20 cal% straw)



b. Reference case by the addition of elemental sulphur (S/Cl molar ratio:2.1)



c. Reference case by the addition of elemental sulphur (S/Cl molar ratio:6.4)



d. Reference case by the addition of $(\text{NH}_4)_2\text{SO}_4$ (S/Cl molar ratio:2.1)

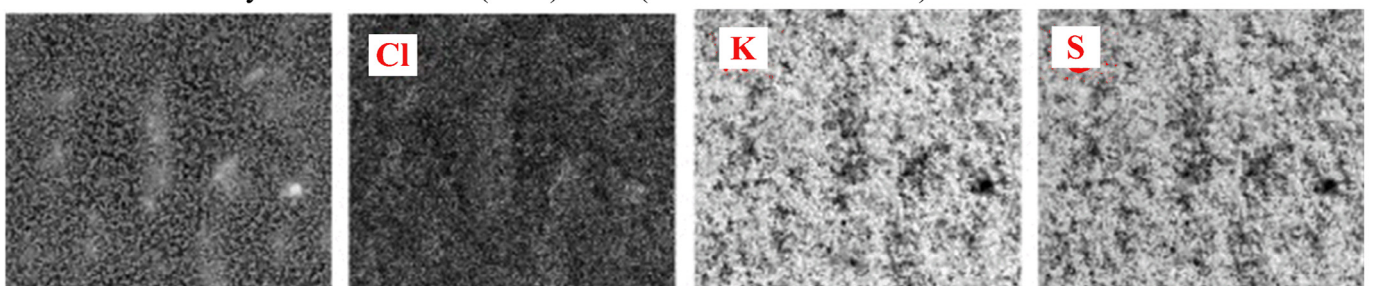


Fig. 20. SEM-EDX maps of the deposits collected during the combustion of biomass by addition of S from different sources (adapted from reference 79).

- (3) Differences between similar additives. For example, kaolin, zeolite 24A, and zeolite Y discussed in the section titled “Zeolite”.
- (4) Balancing the comprehensive influences on various ash-related problems such as how to balance the effects of S on corrosion and slagging, as discussed in the section titled “Sulfur”. Meanwhile, synthesizing consider alkali-induced slagging, silicate melt-induced slagging (ash fusion), and agglomeration that may occur concurrently rather than separately.

- (5) Unifying the economic and technical indicators or evaluation indexes through further study.

2.5. Countermeasures for main ash-related issues: co-firing

2.5.1. Co-firing benefits and classifications

Co-firing in existing coal-fired boilers is a promising biomass utilization approach and is widely used in Europe and the USA [128]. Most of the newly built coal power plants in Europe have a requirement of 10–20 cal% co-firing capability [129]. Biomass co-firing can

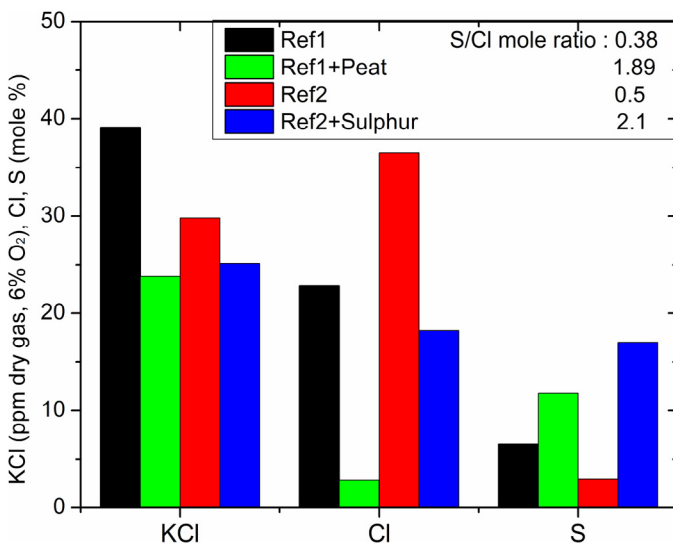


Fig. 21. Concentration of gaseous KCl, and Cl and S in the deposits collected during the combustion of biomass by addition of S from different sources (adapted from reference 111).

not only eliminate or reduce various ash-related issues that inevitably occur in dedicated biomass-fired furnaces [6,129–132], but can also utilize and exploit renewable energy. Moreover, co-firing has the following advantages:

- (1) Increased boiler efficiency [5,26,42]. The equivalent coal consumption of co-firing in large PC furnaces (~330 g/kWh with a modest co-firing ratio) is basically half of that in dedicated biomass firing furnaces (for example, ~630 g/kWh in grate furnace) with a thermal efficiency of approximately 50% [133]. According to the assessment of National Renewable Energy Laboratory (NREL, DOE, U.S.) [134], the power generation efficiency of biomass co-firing remains either unchanged or slightly decreases, and their efficiency can be maintained at 33%–37% even with an elevated co-firing ratio of 15 cal %. Therefore, co-firing can utilize the high boiler efficiency of large PC furnaces.

- (2) Reduced emissions of NO_x, SO₂, and CO₂ [26,42,135]. Biomass, particularly plants with a short growth cycle, is a “neutral” renewable energy, that is, the next generation of biomass can effectively reabsorb the CO₂ released by the combustion of the previous generation. The ash of biomass contains large quantities of alkali metals [15,16] such as KCl, which can capture sulfur during combustion and reduce SO₂ emissions [73,136]. A high concentration of the volatile hydrocarbon of biomass can react with NO_x [137,138]. Thus, co-firing favors lower NO_x, SO₂, and CO₂ emissions. However, the emission of HCl/Cl₂ may be enhanced because of the high chlorine content in biomass.
- (3) Reduced fuel costs and investment [42]. Generally, biomass purchase prices are lower than those of coal; for example, agricultural residues are usually discarded or incinerated in the field. Thus, biomass co-firing has lower fuel costs than traditional fuels.

Currently, biomass co-firing technologies mainly involve co-firing in FB and PC furnaces [139,140]. In comparison with the relatively simple FB co-firing, the co-firing technologies for PC furnaces can be classified into injection co-firing, co-milling co-firing, pre-gasification co-firing, and parallel co-firing [139], as shown in Fig. 23 [26]. Co-milling co-firing, which uses a single boiler to burn biomass together with coal, is the most extensive approach. This method entails the least investment and is favorable when a small proportion of biomass is co-fired. However, mill capacity limits co-firing ratio [141]. Injection co-firing, which also uses a single boiler to burn biomass together with coal, needs to be coupled with dedicated biomass combustion and logistics systems that result in large investment. However, the co-firing ratio can be improved. Pre-gasification and parallel co-firing increase biomass co-firing ratio significantly, even with 100% biomass, but both methods require the construction of two systems (combustion and gasification) and are expensive [142]. Pre-gasification co-firing requires an extra gasifier to convert solid biomass into a gaseous fuel, which is then burned together with the coal in the boiler. Parallel co-firing employs a separate boiler for biomass combustion, and the steam generated from the biomass-fired boiler is then mixed with steam from the coal-fired boiler. Thus, currently, both co-milling co-firing and injection co-firing are the most widely used.

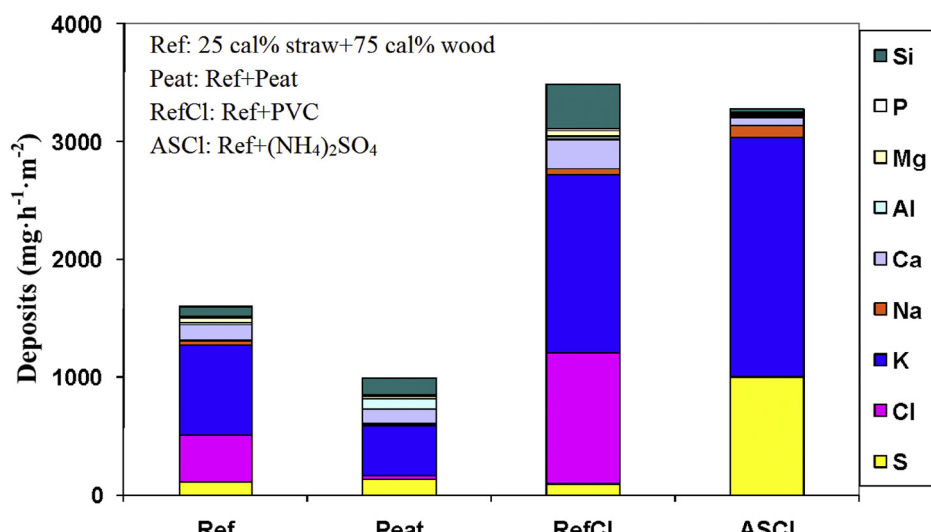


Fig. 22. Comparisons of deposition formation rate and deposition components given as elements in the combustion of biomass with different additives (adapted from reference 111).

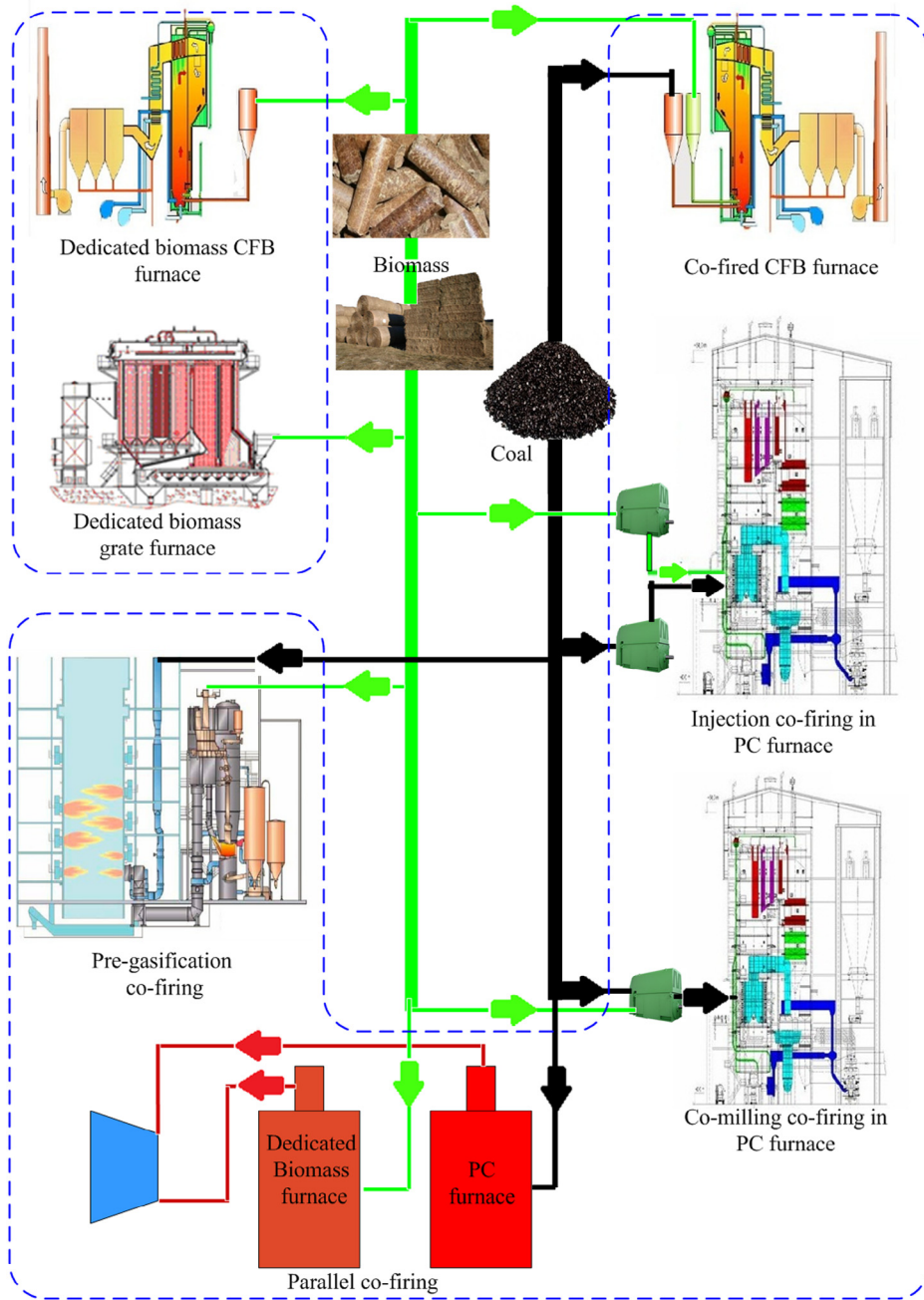


Fig. 23. Schematic of biomass firing and co-firing technologies (reprinted from reference 26, with permission of MDPI).

2.5.2. Co-firing in CFB

Fluidized bed combustion technology has been successfully demonstrated at a large scale. Also, it has been shown to meet the technical requirements necessary for the co-firing processes because of its inherent advantages over conventional systems, e.g., simple design, fuel flexibility, high efficiency, and low pollutant emission [5]. The relatively low and uniform temperature and the good mixing of bed material disfavor slagging; however, bed agglomeration easily occurs [135].

Fig. 24 shows a typical commercial CFB boiler built at Chalmers University of Technology; it has been widely utilized to study the effects of additives and co-firing on deposits [27,111]. Kassman et al. [111] conducted research on gaseous KCl and chlorine in deposits by means of IACM (on-line measurements of gaseous KCl), deposit probe measurements, and ash analysis in the co-firing testing of peat

and a mixture of wood and straw pellets. They reported that the chlorine content of the deposits is reduced remarkably because of the capture of potassium by the reactive components of peat ash (Al, Fe, Ca, and Si) and the sulfation of KCl during co-combustion. Elled et al. [27] further pointed out that the formation of alkali chlorides in the flue gas and deposits can be controlled by the addition of municipal sewage sludge. Despite the fact that the fuel is highly contaminated with chlorine, it can be used because of the relatively high content of sulfur and other reactive ash components (Si, Al, Ca, Fe, and P) in the sludge. Similarly, Nordin [135] conducted research on co-combustion of high sulfur coal and lucerne in a 5 kW pilot-scale CFB and found that agglomeration, which occurred when lucerne was burned alone because of the formation of K-rich silicates from the bed and ash particles and K from the grass, did not occur. Among the reactive ash components, Ca presents the highest

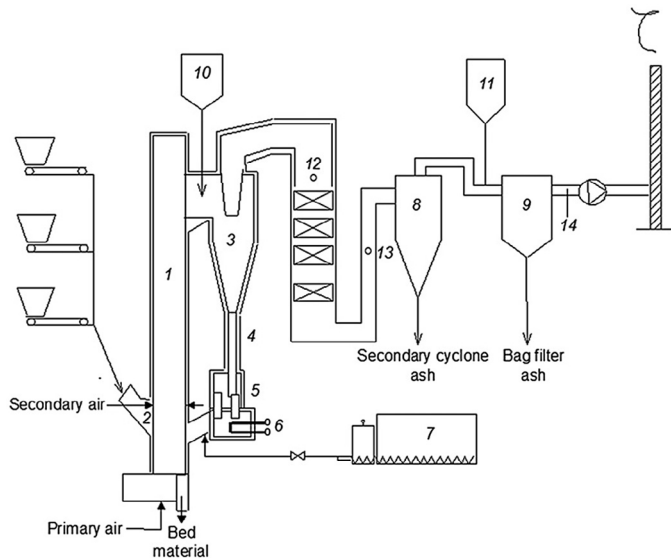


Fig. 24. Schematic of a 12 MWth CFB boiler (reprinted from references 27,111, with permission of Elsevier).

1.furnace; 2.fuel chute; 3.primary cyclone; 4.cyclone leg; 5.particle seal; 6.external heat exchanger; 7.cement pump for co-fired fuel and additives entering; 8.secondary cyclone; 9.bag filter; 10.cyclone inlet for additive injection; 11.upstream of bag filter for hydrated lime injection; 12-14. measurement points

effectiveness in anti-slagging. This finding was confirmed by Wang et al. [87], who studied the effects of sewage sludge mainly containing Si, Al, Ca, P, and Fe and marble sludge composed of 95.12 wt.% CaO and 2.99 wt.% MgO on the slagging characteristics during combustion of wood waste pellets in a 1.2 MWth STEPFIRE boiler. When 4% and 8% of marble sludge was added, only 1.5% and 2.5% of the ingoing ash formed slagging. The addition of 4 wt.% of sewage sludge reduced the slagging formation fraction from 34% to 26%, but increased it to 38wt.% with 8% addition fraction. Meanwhile, in comparison with sewage sludge, the slagging was fragile and could be pressed into power using fingers after the addition of marble sludge. The aforementioned research indicated that co-firing in CFB can reduce slagging and agglomeration. However, the degree of decrease is highly dependent on the co-firing fuel and the co-firing ratio.

2.5.3. Co-milling co-firing in PC furnace

As illustrated in Fig. 23, in co-milling co-firing where coal and biomass blends are co-milled in the existing coal mills, biomass is blended with the coal either on-site or off-site. Therefore, additional dedicated biomass mills are not required. In the UK, all power stations that perform biomass co-milling co-firing employ on-site blending to satisfy Ofgem's audit requirements [142].

Fig. 25 shows an on-site fuel blending system utilized in co-milling co-firing technology. Conventionally, coal is transferred by a belt conveyor and biomass is discharged into the coal evenly and



Fig. 25. On-site fuel blending system utilized in co-milling co-firing mode (adapted from reference 143).

continuously by a blanking hopper. The mixture is then transported into the coal mills for pulverization. This is the preferred approach in many stations embarking on co-firing for the first time because it requires only minimal retrofitting and low investment for the boiler system. Basically, a biomass co-firing ratio up to 5–10 cal% is permitted; at higher co-firing ratios, the capability of the coal mills to co-mill biomass becomes the barrier [143].

Savolainen [130] implemented co-milling co-firing testing with varied sawdust/coal ratios in a 315 MW PC furnace. The results showed that co-firing does not cause slagging and can reduce SO₂ emissions. However, when the co-firing ratio is increased to 2.5 cal%, milling deteriorates and results in increased unburned carbon in fly ash and decreased boiler efficiency. Fortunately, with torrefied biomass or bio-char, the co-firing ratio can be increased [143].

2.5.4. Injection co-firing in PC furnace

As illustrated in Fig. 23, injection co-firing involves a completely separate feed line for the biomass fuel with separate handling, drying, milling, and burners/injectors. Although this is more expensive to install, it allows for greater flexibility in handling and processing biomass, with a low potential for adversely affecting the primary coal stream. The milling properties of biomass are typically different from those of coal. Biomass also has a significantly greater content of volatile matter (around 80%) than coal (45% for bituminous coals and 10% for anthracite). Separate handling streams for biomass and coal can allow co-firing to occur in plants with strict limits on the volatile content of fuels used [144].

As shown in Fig. 26, existing injection co-firing modes were classified into four basic modes by Livingston [143]; all injection co-

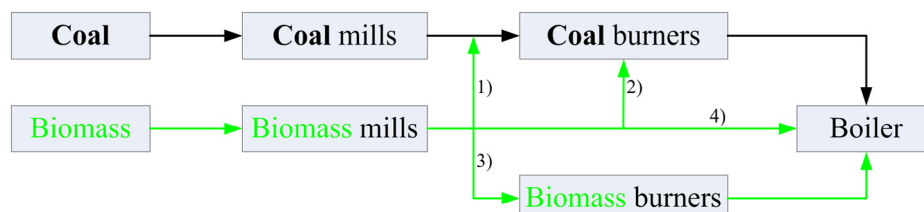


Fig. 26. Direct injection co-firing mode (adapted from reference 143).

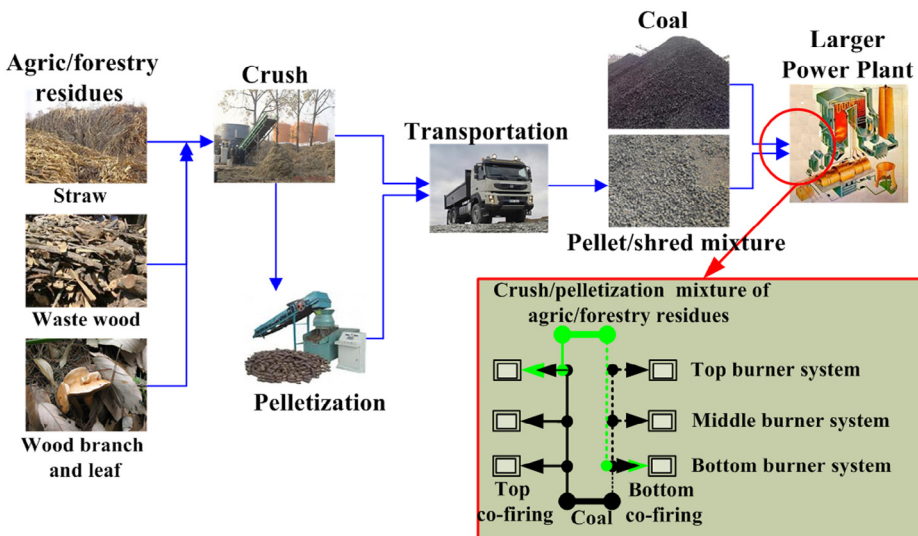


Fig. 27. Proposed co-firing mode of agricultural/forestry residues and coal (reprinted from reference 26, with permission of MDPI).

firing systems involve the pneumatic conveying of the pre-milled biomass from the fuel reception and handling facility to the boiler chamber. The processes are as follows: 1) direct injection of pre-milled biomass into the pulverized coal pipework, 2) direct injection of pre-milled biomass into modified coal burners, 3) direct injection of the pre-milled biomass through dedicated biomass burners, and 4) injection of the pre-milled biomass directly into the furnace.

Biomass has a high moisture and fibers content, which is unfavorable for milling; as a result, the mill, pipework, and burners may become blocked. Furthermore, the high volatility and low ignition temperature negatively affect the operation of the unadapted coal mill. In addition, without a burner, i.e., without an air supply system for the biomass, the biomass cannot ignite timely and burn completely. Therefore, considering the cumbersome maintenance and low investment of co-milling co-firing and the high co-firing ratio of injection co-firing, a new co-firing mode was proposed and demonstrated in a previous study [26].

As illustrated in Fig. 27, the proposed co-firing mode is more dependent on injection co-firing combined with co-milling co-firing. Firstly, various agricultural/forestry residues are collected and pretreated by a crusher and a molding machine; Secondly, the crush and pellet mixtures are transported to power plants; Thirdly, blends of coal and the pellet/shred of agricultural/forestry residues are injected into a specific burner system (top or bottom burner system) after co-milling, and the other burner systems are fed with pure coal. The agricultural/forestry residues are injected into only one burner system similar to injection co-firing and are mixed and co-milled with coal before injection similar to co-milling co-firing. Hence, the co-firing mode is a combination of injection co-firing and co-milling co-firing. In an injection co-firing furnace, pure biomass is injected into the specific burner system after milling, whereas in a co-milling co-firing furnace, biomass and coal mixture are injected into each burner system after co-milling. The advantages of this new proposed co-firing mode are as follows.

- (1) Compared with dedicated biomass firing, the proposed co-firing mode entails lower investment with immediate benefits, lower pollution emissions, lower coal consumption, and higher boiler efficiency. The proposed co-firing mode also eliminates slagging and reduces the dependence on seasonal biomass, such as that on the agricultural/forestry residues.
- (2) Unlike injection co-firing, there is no need to construct a specific logistics system; hence, saving is made.

- (3) Compared with co-milling co-firing, agricultural/forestry residues are only injected into one burner system rather than into all burner systems; this condition reduces the shutdown probability caused by the blockage of the mills, which results from the uneasy milling property of agricultural/forestry residues.
- (4) Co-firing by the top or bottom burner system provides increased boiler efficiency in comparison with dedicated PC combustion. Generally, several layers of burner systems exist in boiler units. Thus, the injection location of the biomass, which influences the boiler efficiency and polluting emissions, make plant operator more difficult [143]. The authors [26] conducted co-firing testing based on the proposed co-firing mode in a 300 MW PC furnace that contains six layers of burner from bottom to top; detailed description are available in reference 138. The results showed that the boiler efficiency of co-firing is 0.05% to 0.31% higher than that of dedicated PC combustion when the co-firing ratio is below 5 wt.%. The boiler efficiencies are approximately 0.2% higher with agricultural/forestry residue co-firing in the bottom and top burner systems than that in the middle burner system; however, a high co-firing ratio (>10 wt.%) results in reduced boiler efficiency [145]. These results were partly confirmed by Wang et al. [138], who also performed co-firing testing in the same units and found that boiler efficiency decreases by between 0.19% and 0.52% with a co-firing ratio from 9.68 wt.% (6.53 cal%) to 22.7 wt.% (16.1 cal%). Hughes and Tillman [145] also reported that the boiler efficiency decreases slightly with a co-firing ratio of 9.7 wt.% to 13.5 wt.% in Plant Hammond, Georgia, USA. Notably, a low biomass co-firing ratio (<5 wt.%) increases boiler efficiency, particularly the biomass injected into the bottom and top burner systems. By contrast, a high biomass co-firing ratio decreases boiler efficiency.

However, research on ash-related issues conducted in large PC furnaces is scarce and requires more practical demonstrations, particularly concerning the co-firing ratio.

2.6. Countermeasures for main ash-related issues: leaching

Although the inherent chlorine and alkali species extracted from soil during growth are notorious for ash-related issues during biomass combustion, the Cl and alkali content of certain grasses and straws can be reduced by using Cl-free fertilizers [146] and

restricting the use of inorganic fertilizers such as potassium fertilization, which may have undesirable consequences for crop yield and farm revenue [113]. Simple screening can also remove undesirable components such as adventitious soil that is added during harvesting and handling processes that contributes to fouling and slagging [32,113]. Also, leaves with higher alkali content than the trunk and larger branches can be removed [112]. However, most undesirable constituents are inherent to the biomass and dispersed throughout the entire fuel. Thus, power plant operators currently rely on the selection of fuel that contains low amounts of ash, chlorine, and alkali metals; consequently, many fuels that may be available at lower cost are excluded [113].

Leaching is an effective pretreatment strategy to remove inherent inorganic species, particularly alkalis, sulfur, and chlorine in biomass to mitigate ash-related issues [14,33,147]. During combustion, alkali metals are relatively volatile; they form hydroxides, chlorides, and sulfates, which produce molten salt mixtures on accessible surfaces, and result in slagging and fouling. Chlorine is a facilitator of alkali evaporation. It leads to the condensation of alkali chlorides on heating surfaces in the boiler and promotes corrosion of these surfaces [99]. Leaching can remove these key ions and reduce the formation of their corresponding salts.

The inorganic species in biomass can be classified into three categories [31,148]: water-soluble portion (i.e., salts readily soluble in water, including alkali chlorides, sulfates, carbonates, and alkali earth chlorides), dilute-acid leachable portion (i.e., organically bound inorganic species and minerals that are water-insoluble but acid soluble, including alkali earth carbonates, sulfates, and sulfides), and residual (other acid insoluble minerals, including silicates and elements that are bound to the organic matrix with a covalent bond). According to the above categories, leaching strategies can also be classified into water, acetate, and acid leaching. Approximately 100% of Cl and 90% of alkali metals are water soluble; thus, much attention has been devoted to water leaching [99,112,113].

Compared with natural water leaching (rain and snow) that is weather dependent, technical leaching can address the problems of the unpredictability of weather and rainfall-induced biomass losses. Overall, it constitutes a more reliable measure of quality optimization of biomass; nevertheless, leaching by natural precipitation remains an alternative [14,113,147].

2.6.1. Technical water leaching (batch leaching)

When water leaching is mentioned, most people will recall batch leaching. In batch leaching, the targeted materials are immersed in a water container under controlled conditions, and the targeted materials not only come into contact with the leaching solution but are also in continuous contact with the leachate.

Vamvuka and Zografos [99] reported that batch water leaching can result in a significant reduction in ash (up to 40%) and problematic elements such as K (up to 93%), Na (up to 96%), P (up to 85%), and Cl (up to 97%); it can also improve fusibility behavior [83]. Both Dayton et al. [113] and Bakker et al. [149] reported similar results. Dayton et al. [113] conducted batch water leaching experiments on rice straw, wheat straw, switchgrass, mixed wood fuel, banana grass, and sugarcane bagasse, and reported that K was depleted by an average of 82%, Cl by an average of 95%, both Na and S by an average of over 50%, and P by an average of 43%. As a result, the alkali index decreased by 81%. Bakker et al. [149] conducted research on untreated and leached rich straw as well as untreated and leached rice straw blended with commercial wood fuel in a lab-scale FB combustor. They discovered that K, Cl, P, and S in leached straw ash are significantly lower than that in untreated straw. The combustion of unblended leached straw was stable and without agglomeration, whereas the combustion of untreated rice straw under similar conditions resulted in extensive bed agglomeration, rapid defluidization, and unstable combustion temperatures. The com-

bustion of a wood-based fuel blend containing 25% untreated rice straw also resulted in rapid bed agglomeration, whereas the combustion of similar fuel blends containing leached rice straw did not result in any difficulties in controlling combustion temperatures and bed fluidization. Ash deposition on the heat exchanger declined when 25% leached rice straw was blended into the commercial wood fuel relative to firing commercial wood fuel along with no leached straw.

Thus, ash-related problems originating from high Cl and alkali metals in biomass, including bed agglomeration, slagging, and corrosion, can be mitigated by batch water leaching [113,147].

2.6.2. Technical semi-continuous leaching

Although batch leaching has been widely applied because of its simple operation, it over-leaches the water-soluble inorganic species because of the extensive and lengthy contact between the acidic leachate and biomass sample [148,150,151].

Liaw and Wu [148] revealed that under conventional batch leaching conditions, the leachate is acidic because of the extraction of several organic acids from the biomass sample such as acetate, formate, and oxalate; the cation/anion ratios ($\text{Na} + \text{K} + 2\text{Mg} + 2\text{Ca}$) / ($\text{Cl} + 2\text{S} + 3\text{P}$) of the leachate are 2.5 and 3.3 for wood and leaf, respectively. This suggests that at least some of the alkali and alkaline earth metals leached from the biomass samples do not exist in the biomass samples as water-soluble salts. Therefore, under batch water leaching conditions, the organic acids leached from biomass samples remain in the leachate system. Some of the acid soluble (but water-insoluble) alkali and alkaline earth metals are leached because of the extensive and lengthy contact between the acidic leachate and the biomass sample. Conventional batch water washing of biomass overestimates the contents of water-soluble inorganic species in biomass samples. Similar reports were presented by Wu et al. in another reference [150] and also by Ho et al. [151].

Aiming to eliminate the overestimation of the contents of water-soluble inorganic species in biomass samples through conventional batch water leaching, Liaw and Wu [148] proposed the semi-continuous leaching method. Unlike in a batch leaching reactor where various amounts of water-insoluble inorganic species (but soluble in the acidic leachates) are leached out because of the extensive and lengthy contact between the acidic leachate and the biomass sample, the leaching products in semi-continuous leaching method are rapidly separated from the biomass particles. The process ensures that it is the fresh water (rather than the acidic leachate) that continues to perform the leaching action in the biomass sample.

Fig. 28 shows a comparison of batch leaching and semi-continuous leaching; it clearly shows that batch leaching over-leaches alkali and alkaline earth species. Furthermore, **Fig. 29** shows a comparison of the various inorganic species leached by the continuous leaching process (water leaching + dilute acid leaching ($\text{HCl}/\text{H}_2\text{SO}_4$)) of mallee wood under batch and semi-continuous leaching. All of the alkali and alkaline earth species over-leached by batch water leaching are acid soluble, and the leachate of batch water leaching contains some acid. The majority of Na and K compounds are water-soluble, but a large proportion of Mg and Ca compounds are only acid soluble. The water insoluble but acid-leachable Mg and Ca might bond with the organic structure of the biomass and become leachable through ion exchange with hydrogen ions from the diluted acid or form water insoluble salt such as calcium/magnesium oxalate and/or calcium/magnesium carbonate [148].

The effects of water and acid leaching on straw ash components and structures are illustrated in **Fig. 30**. Comprehensive analysis of the ash components and structures shows that unleached straw ash is coated with molten material (mainly alkali silicates) with a high concentration of alkali and alkaline earth metals. Water leaching can reduce the concentration of K and Na in the ash.

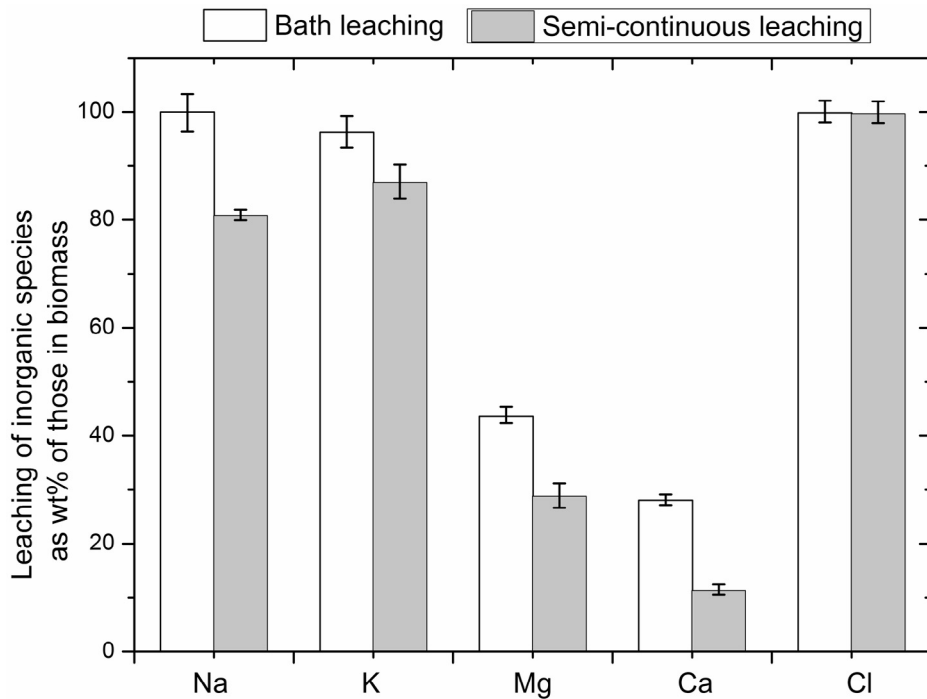


Fig. 28. Percentages of various inorganic species leached from water washing of mallee wood under batch and semi-continuous leaching conditions (adapted from reference 148).

Consequently, the formation of low-melting alkali silicates is reduced. With increased acid concentration, K and Na contents in the ash and the outmost molten material of the ash particle are reduced [152]. Compared with the internal part of the ash particle (point b), the external part of the ash particle (point a) contains fewer alkali and alkaline earth species because of sufficient contact with the leaching solute.

Although semi-continuous leaching is more precise in quantifying the water-soluble concentration of alkali and alkaline earth species, conventional batch leaching is a better choice in industrial applications because of its simple operation and water conservation. Moreover, the ion-exchangeable alkali and alkaline earth species that are partially over-leached out during batch

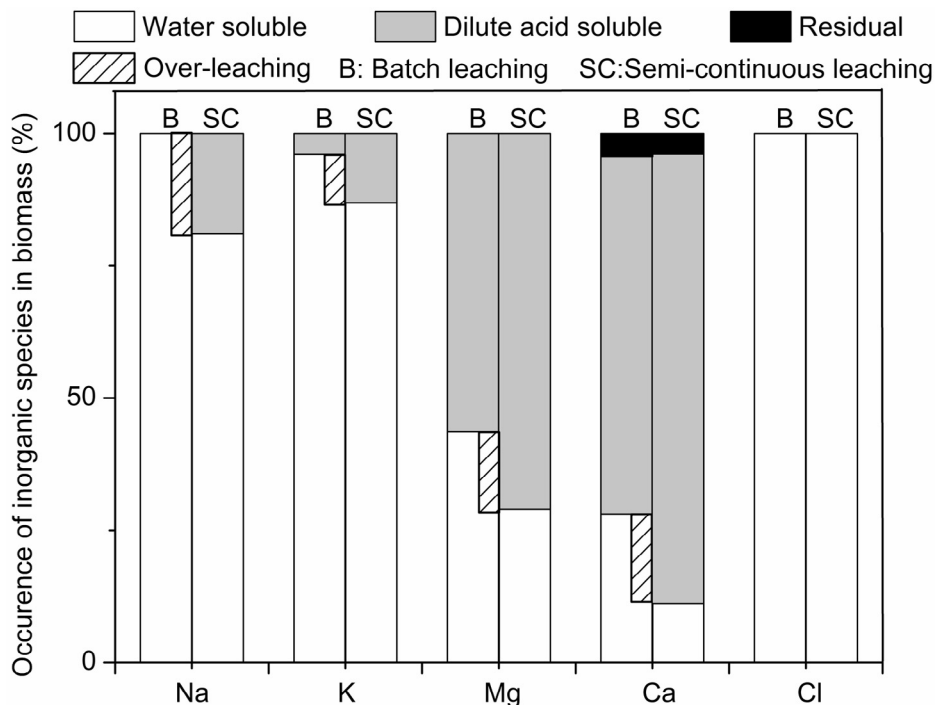


Fig. 29. Occurrence of inorganic species in mallee wood via continuous water and dilute acid leaching under batch and semi-continuous leaching conditions (adapted from reference 148).

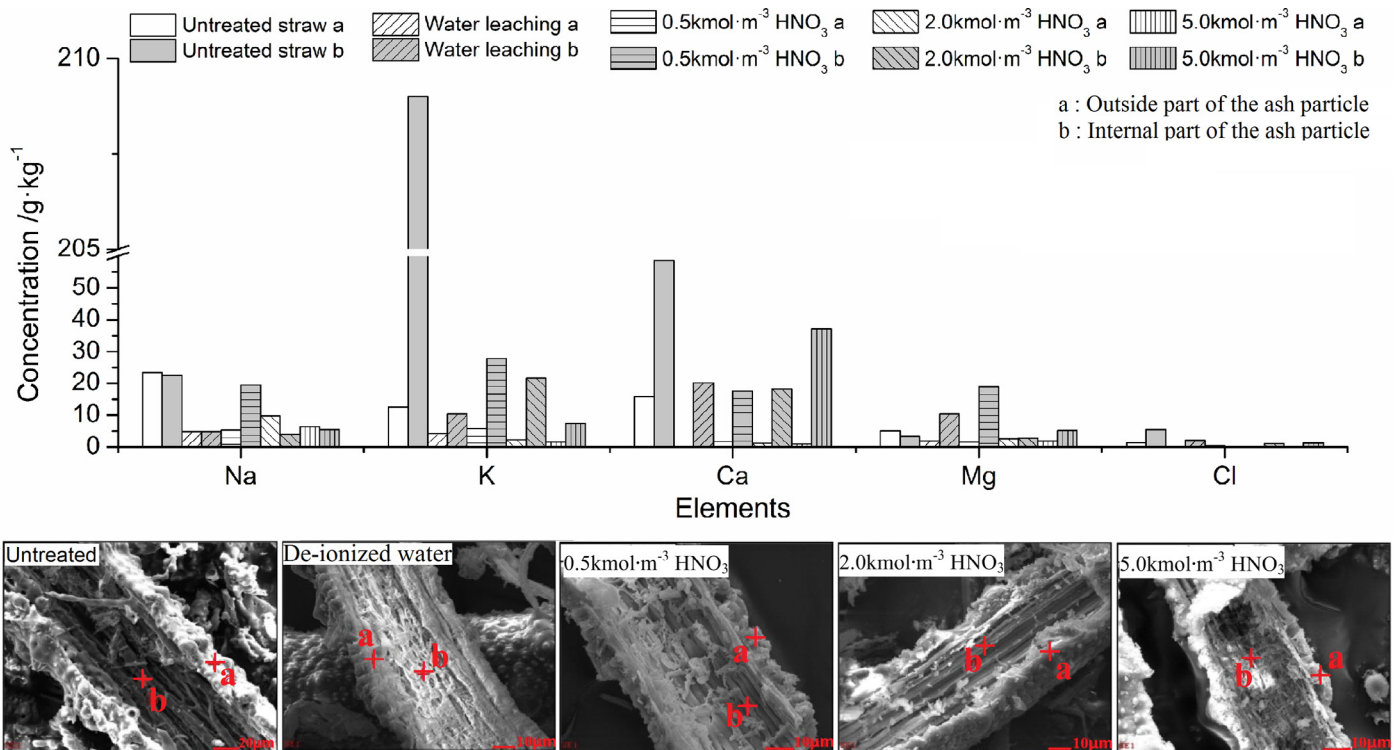


Fig. 30. SEM-EDS analysis on a straw ash sample (adapted from reference 152).

leaching are also responsible for slagging, agglomeration, and corrosion. Therefore, extraction can mitigate ash-related issues.

2.6.3. Natural water leaching by rain and snow

Although technical leaching can extract Cl, S, alkali, and alkaline earth metals in biomass and further reduce slagging, bed agglomeration, and corrosion [113,147], batch leaching and semi-continuous leaching require the consumption of large quantities of water and energy and entail the need to construct a leaching field. Natural leaching can overcome these problems.

The reduction in unwanted elements by leaching from rainfall has been recommended as a post-harvest quality optimization process even though leaching by natural precipitation is highly dependent on suitable weather conditions [147]. High precipitation during a short period is an ideal condition; for example, thunderstorms during warm weather periods. However, natural leaching is dependent on the weather, and no certainty exists as to whether suitable weather will occur at the right time in any given year. Meanwhile, natural precipitation during the field period always results in biomass losses such as leaf loss [147].

Compared with technical leaching strategies, leaching by natural precipitation is more weather dependent and reduces unwanted elements less; however, it has some advantages that technical leaching lacks, such as lower costs, little or no need for additional energy input, and independence from external facilities [147]. Although natural precipitation always results in leaf losses, incorporating the leaf back into the soil benefits the recycling of key inorganic nutrients [148]. It can also reduce the content of high-risk alkali species in the entire woody biomass and further alleviate ash-related problems because the leaf has a higher alkali content than the other parts of the plant [112]. Therefore, reducing the concentrations of Cl, S, and alkali metals in biomass by rain and snow during the field drying period should be encouraged as an option in bio-fuel quality optimization [33,113,147].

2.6.4. Effect of leaching intensity: amount of water and/or time

In batch leaching, semi-continuous leaching, and natural leaching, the amount of water or leaching time has significant effects on the removal of Cl, S, alkali metals, etc. For example, Smith and Brown [153] reported that, for the same quantity of water, low leaching efficiency is more associated with a water application rate of 40 mm h⁻¹ than with 20 mm h⁻¹. By simulating natural rain leaching by means of a lawn sprinkler and plastic lined with fine mesh, Tonn et al. [147] revealed that the concentrations of Cl, S, K, and ash in dry herbage decrease with increased duration of simulated rain.

Fig. 31 shows the changes in Cl, K, and ash concentrations in grassland garbage under three leaching methods: simulated rain (i.e., natural rain leaching), high-intensity irrigation (i.e., approximate semi-continuous leaching), and laboratory batch leaching. With increased amount of water application during simulated rain and high-intensity irrigation leaching and increased duration of leaching time during laboratory batch leaching, the concentrations of Cl, K, and ash decrease, i.e., the leaching efficiency increase. For batch leaching, the extraction of Cl, K, and ash occurs mainly at the initial stage and prolonging the duration of leaching has a slight effect. For both simulated rain and high-intensity irrigation, the leaching efficiencies increase with either increased amount of water application or leaching time. In theory, a critical point exists after which the concentrations of Cl, K, and ash will change only slightly, even though both the amount of water application and leaching time increase continuously.

Similar results were reported by B. Tonn et al. in another paper [33]. Fig. 32 shows the effects of initial contents of K (Fig. 32a) and Cl (Fig. 32b) on leaching efficiencies for different leaching times. As shown in the figure, for both Cl and K, the leaching efficiencies increase with time. The elemental contents before and after leaching show a strong linear relationship; that is, for the same leaching time, the greater is the initial content, the greater is the residual content.

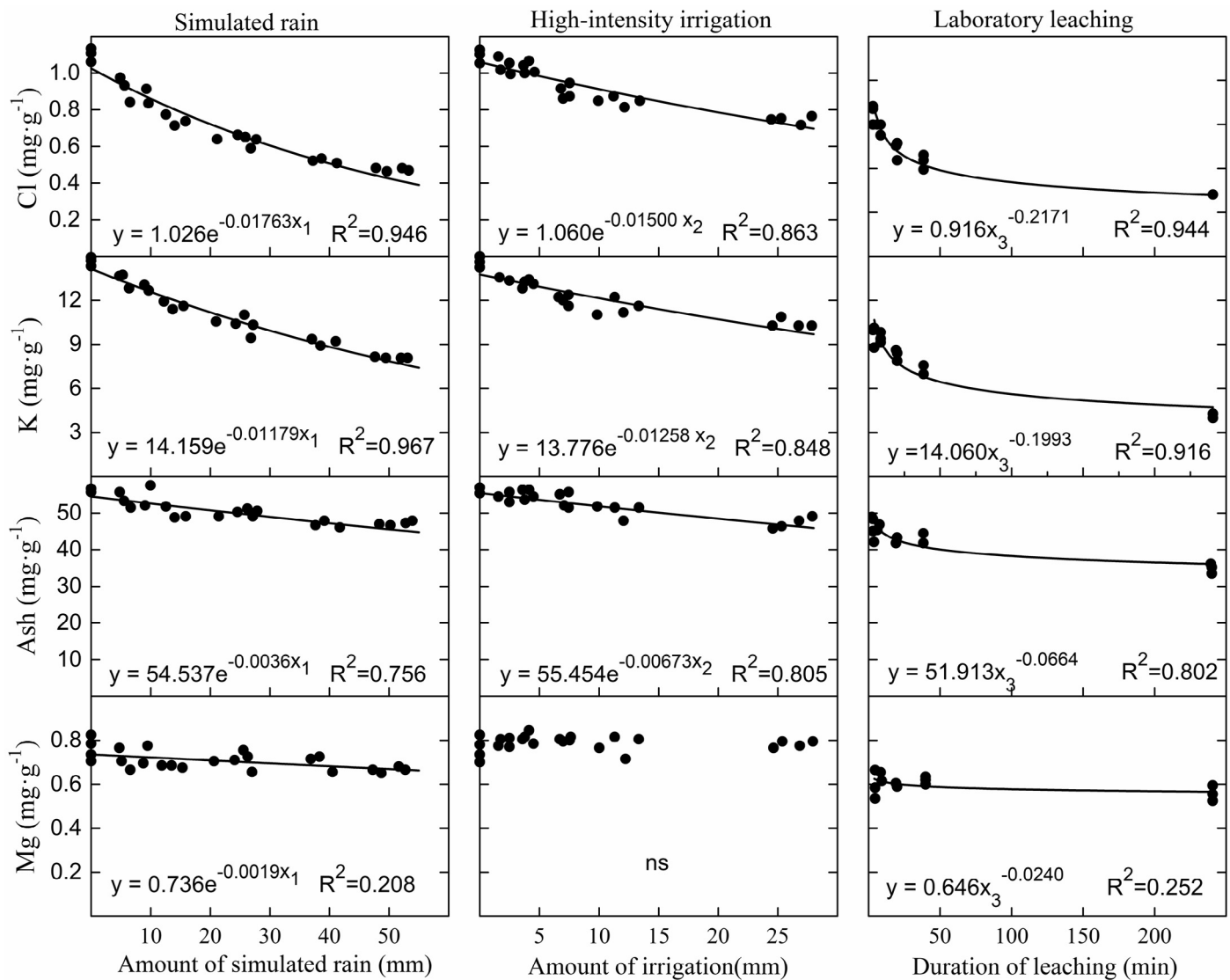


Fig. 31. Changes in Cl, K, and ash concentrations in grassland herbage in response to three different leaching methods (reprinted from reference 147, with permission of John Wiley and Sons).

x_1 is the amount of water applied as simulated rain (mm), x_2 is the amount of water applied as high-intensity irrigation(mm), and x_3 is the duration of laboratory leaching (min)

Furthermore, Tonn et al. [147] determined the relationship between the amount of water required by simulated rain and that required by high-intensity irrigation on the leaching efficiencies for Cl, K, and ash, as shown in Fig. 33. A close linear relationship exists between the effects of simulated rain and high-intensity irrigation on the concentrations of Cl and K. For K, the slope is close to 1.0, indicating that in spite of the large difference in water application rates, the change in K concentration per mm of water applied is nearly identical. In the case of Cl, the leaching efficiency per millimeter of water is low at a high water application rate. For ash, the leaching efficiency per mm of water is very high at a high water application rate. These different relationships may be attributed to the synthetic effects of diffusion and the mechanical processes [147]. If the diffusion of leachable components from the interior of the biomass particle to the surface plays a considerable role, the diffusion time may be the limiting factor in the leaching process at high rates of water application. Alternatively, mechanical processes such as the washing-off of surface dust or the movement of water through the plant cell walls may also affect the leaching process. If mechanical processes are dominant, then high leaching

efficiencies will be obtained at a high rate of water application. High rates tend to be associated with large raindrop sizes and velocities, similar to batch leaching (complete immersion), and the mechanical action imposed by the shaker in laboratory leaching. Therefore, diffusion processes appear to play a dominant role for Cl; ash is more dependent on mechanical processes, and both diffusion and mechanical processes influence K.

These comprehensive analyses indicate that, for industrial applications, batch leaching is a better choice than semi-continuous leaching because of its easy operation and extra extraction of acid-soluble alkali and alkaline earth metals, especially alkali metals that are responsible for intractable ash-related problems. In contrast to batch leaching, which overestimates the water-soluble inorganic species because of the extensive and lengthy contact between the acidic leachate and the biomass sample, and thus, leads to the extra extraction of water-insoluble (acid-soluble) ions, semi-continuous leaching, which can exactly extract water-soluble alkali and alkaline species, is more suitable for experimental determination. To eliminate the problematical chlorine, alkali, and alkaline earth species, natural leaching is a more economical technology, but

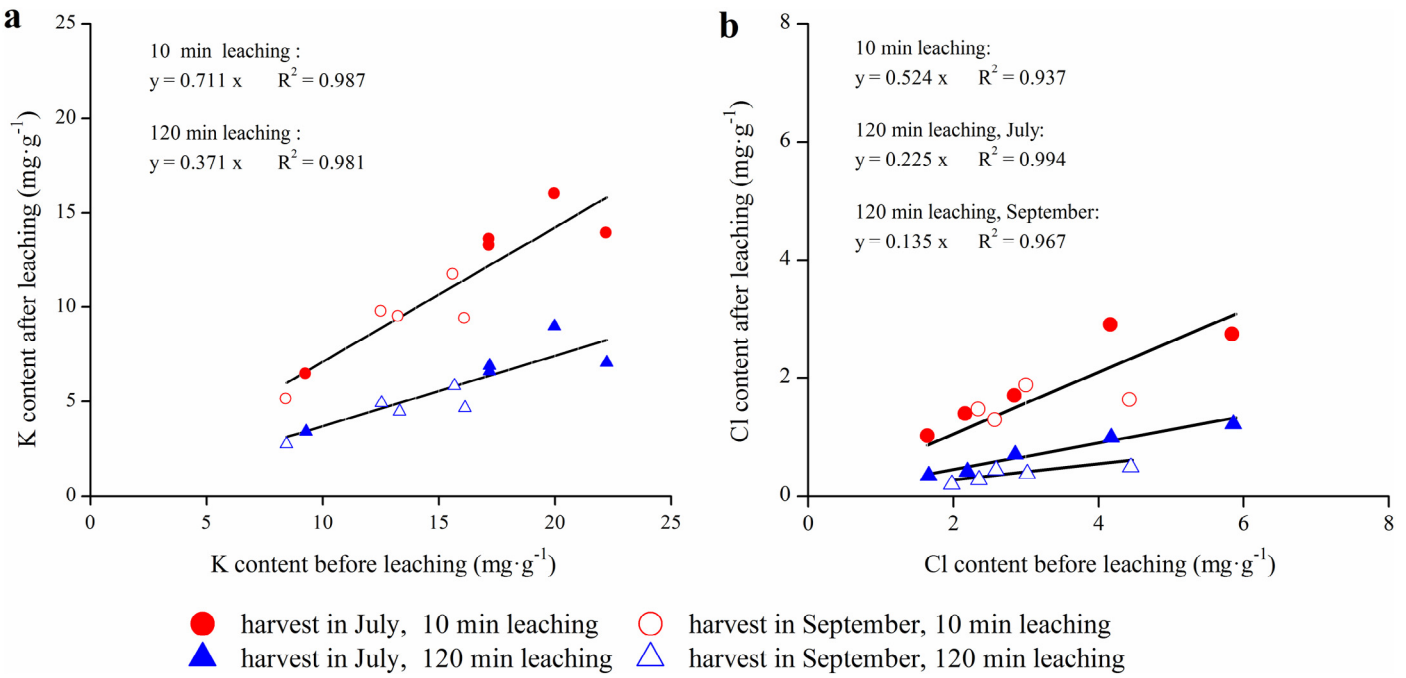


Fig. 32. Relation of (a) K and (b) Cl contents before and after leaching for grassland biomass harvested either in July or September (reprinted from reference 33, with permission of Elsevier).

considerable attention must be paid to the harvest season [33]. In addition, the leaching effect presents a certain dependence on biomass species; for example, leaching can prevent the formation of deposits and agglomerates of olive residues burned in bubbling FBs, whereas the effect on Danish wheat straw is minimal [114].

In sum, in either technical leaching or natural leaching, leaching intensity (including the amount of leaching water, leaching duration or time, water application rate, and others) should be considered. For low-ash biomass, such as stem wood, the diffusion of leachable components from the interior of the biomass particle to

the surface plays an important role, and long leaching duration and low water application rate are preferable. For high-ash biomass, such as bark and straw that are easily contaminated by clay and dust, strong leaching (high water application rate and big liquid particle size) should be applied.

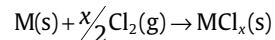
3. Part II. Corrosion

3.1. Corrosion mechanisms

During combustion, the flue gas containing $\text{Cl}_2(\text{g})$, $\text{HCl}(\text{g})$, $\text{NaCl}(\text{aerosol})$, $\text{KCl}(\text{aerosol})$, and others species may cause direct corrosion by accelerating the oxidation of the metal alloys. It may also influence the corrosion caused by other mechanisms such as the corrosion of superheater tubes by molten alkali salts. Alkali chlorides deposited on superheater tubes are well known to cause corrosion in boilers burning biofuels and waste, and they are also the main factor that limits the final steam temperature, and consequently, the efficiency of biofuel and waste boilers [117,154]. A detailed classification and discussion of corrosion mechanisms based on its various possible origins are provided below.

3.1.1. Corrosion associated with Cl_2

3.1.1.1. Oxidation atmosphere. In oxidation atmosphere, metal gradually oxidizes and forms a smooth and dense oxide scale adjacent to the metal. The oxide scale provides a barrier for further diffusion of oxygen and most other gaseous species to the metal and, as a result, oxidation corrosion is limited. Regular oxidation corrosion of metal presents a parabolic trend [155]. However, chlorine can penetrate the protective oxide layer through the pores and cracks and reacts with the metal alloys to form metal chlorides at the scale-metal surface via R 43 [156,157].



where M represents Fe, Cr, and Ni. At the scale-metal surface, the volatile metal chlorides such as FeCl_2 and CrCl_2 are

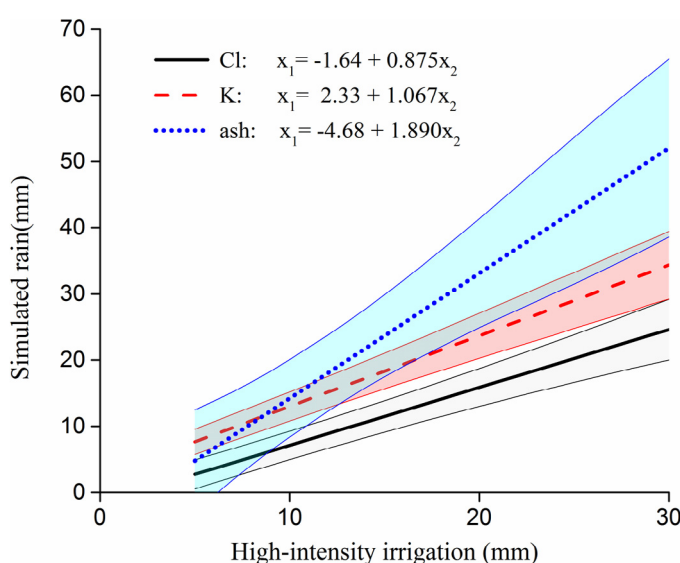


Fig. 33. Comparison of the effects of simulated rain and high-intensity irrigation on grassland herbage chemical composition (reprinted from reference 147, with permission of John Wiley and Sons).

Solid line: Cl; dashed line: K; dotted line: ash. x_1 : amount of water applied as simulated rain (mm); x_2 : amount of water applied as high-intensity irrigation (mm)

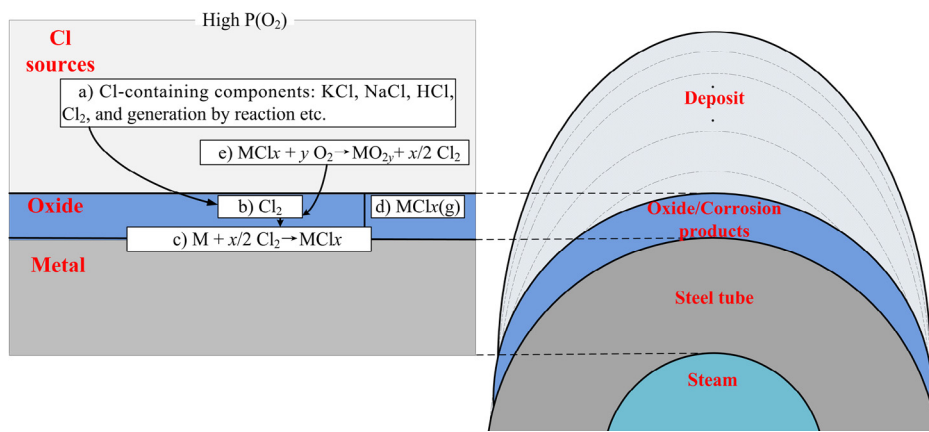
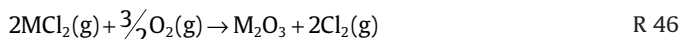
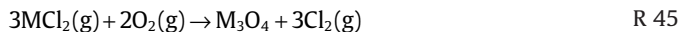


Fig. 34. Schematic of the active oxidation process, based on reference (adapted from reference 47).

thermodynamically stable because of the very low concentration of oxygen (O_2 is consumed to produce the metal oxide scale, which hinders the inward diffusion of oxygen). However, metal chlorides have high vapor pressures at the metal-scale interface, and continuous evaporation takes place via R 44.



The volatile metal chlorides diffuse outward to the scale surface, and oxygen concentration increases with increasing distance from the metal surface, leading to the oxidation of the volatile metal chlorides to solid metal oxides by R 45 and R 46 [156,157].



The resulting oxides form a very loose metal oxide layer that provides no protection against further attack [157]. Through R 45 and R 46, the released chlorine diffuses either to the bulk gas or back to the metal surface; thus, a cycle that, with little net consumption of chlorine, provides a continuous transport of metals away from the metal surface toward regions with higher oxygen partial pressure is formed [22,156]. The net result is that the metals are oxidized into oxides according to R 47 [22].



The above process is called active oxidation corrosion [21,22,156–158], as shown in Fig. 34. The process can be summarized in five steps [47,159]: a) release of Cl-containing compounds; b) transport of Cl_2 through the scale; c) chlorination of iron, chromium, etc.; d) volatilization of MCl_2 (outward transport to the inner oxide layer and to the outer oxide layer) accompanied by the cracking of the oxide layer; and e) oxidation of the metal chlorides and release of chlorine.

Although there are arguments about the corrosion rate (i.e., whether it depends on the outward diffusion of volatile metal chlorides through the porous scale or inward diffusion of Cl_2), the common belief is that active oxidation begins with little incubation time after chlorine is introduced [160]. More attention should be paid to the effects of temperature [154,156,157,161], atmosphere [157,162], potassium compounds present [157,163], alloying elements including concentrations [21,23,159] and species (such as Cr, Ni, Si and Al) [23,155,159,162,164], and the formation mechanisms on the layered corrosion structure [23,156,161].

Ma et al. [23] studied the high-temperature corrosion of pure Fe, Cr, and Fe-Cr binary alloys in O_2 containing trace KCl vapor at

750 °C and the detailed formation process of the multilayer oxide structure (shown in Fig. 35a). In the initial corrosion stage, Cr_2O_3 is formed prior to oxidation, and an enriched zone of Fe is formed near the surface of the substrate. In the presence of KCl vapor, Cr_2O_3 reacts with KCl and releases Cl_2 , which induces active oxidation. Cl_2 diffuses inward and reacts with the substrate, and the reaction products, $FeCl_2$ and $CrCl_2$, diffuse outward. In addition, $FeCl_2$ is prone to form because of the enrichment of Fe near the substrate; then $FeCl_2$ diffuses outward through the Cr_2O_3 layer because of high vapor pressure and is further oxidized on the Cr_2O_3 surface (as shown by the arrow in Fig. 35b(a)). During active oxidation, the formation of chlorides and the transformation from chloride to oxide result not only in the detachment of scales from the substrate but also in the formation of a pore structure in the scales. O_2 and Cl_2 penetrate into and react with the substrate, an internal layer of Cr_2O_3 is formed and Fe-enriched zone near the surface generated again (Fig. 35b(b)). The above corrosion process is a cycle, and multilayer oxide scales are generated (Fig. 35b(c)).

3.1.2. Reducing atmosphere. In a reducing atmosphere where oxygen is absent or insufficient, metal chlorides form directly on the metal surface through R 43. Therefore, the volatilization of metal chloride, which is strongly dependent on temperature, governs the rate of corrosion [22]. The entire process (illustrated in Fig. 36) can also be divided into five steps [47]: a) release of Cl-containing compounds; b) transport of Cl_2 through the scale; c) chlorination of iron, chromium, etc.; d) volatilization of MCl_2 (outward transport to the inner oxide layer and to the outer oxide layer) accompanied by the cracking of the oxide layer; and e) escape of chlorides from scales by evaporation.

In a reducing atmosphere, metal chlorides may evaporate straight into the atmosphere and result in the depletion of chlorine, which may be recycled back into the scale in an oxidizing atmosphere. In molten corrosion, along with the depletion of chlorine, the corrosion process slows with time. The first melting temperature of the deposit increases as the chloride content of the deposit decreases [47]. Even though some H_2S may exist under a reducing atmosphere and a corrosive environment can be created by sulfate deposits, corrosion is much slower than that in the presence of chloride-containing melt [47].

3.1.2. Corrosion associated with gaseous alkali chlorides

To inhibit high-temperature corrosion, various alloying materials, such as chromium, have been added in Fe- and Ni-based alloys. Metallic chromium forms protective oxide layers that mainly contain Cr_2O_3 , which can prevent chlorine corrosion effectively. However,

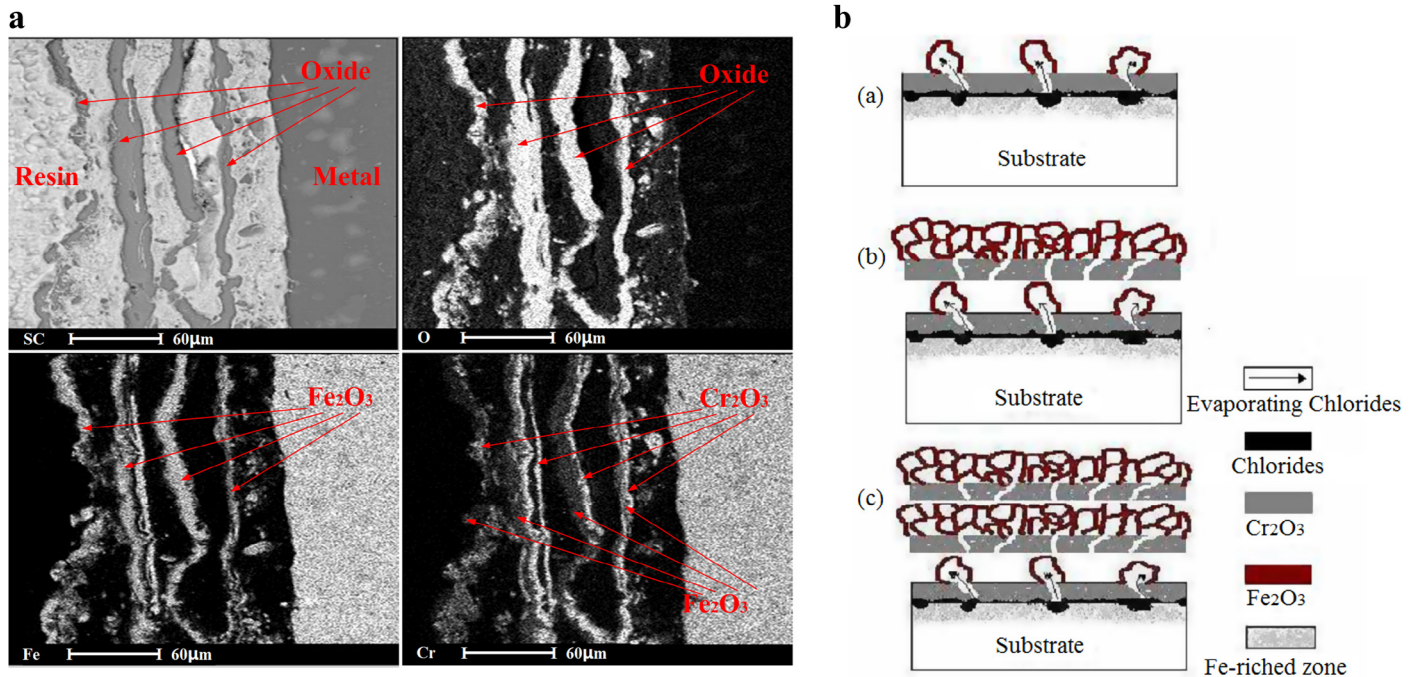
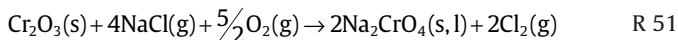
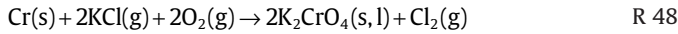


Fig. 35. Illustrations and schematic of the accelerated corrosion mechanism of Fe–Cr alloys in the presence of trace KCl vapor at high-temperature oxidizing atmosphere (adapted for illustration a, and reprinted for illustration b from reference 23, with permission of Elsevier).

- multilayer oxide scale formed for Fe-40Cr alloy
- schematic diagram of the formation process

these layers are easily broken by a reaction with gaseous KCl/NaCl into $(K, Na)_2CrO_4$ by R 48–R 51 [164].



Once the chromium oxide and chromium are transformed into potassium chromate, the protectiveness of the oxide scale is destroyed, and iron oxides grow rapidly. However, the corrosion

associated with gaseous alkali chlorides is highly dependent on the supply rate of gaseous alkali chlorides, which depends on the distance from the sample surface to the salt source at constant temperature [164].

The chlorine released by R 48–R 51 can further react with the alloy to form iron, nickel, and chromium chlorides and accelerate corrosion through the mechanism described in Section II.1.1.

3.1.3. Corrosion associated with solid/deposited alkali chlorides

Biomass combustion is associated with severe slagging containing high concentrations of alkali chlorides and sulfates. The innermost layer of deposits is generally composed of KCl and K_2SO_4 [6]. The presence of KCl and K_2SO_4 in the deposit can cause a very high corrosion rate, even at temperatures below the melting point of pure

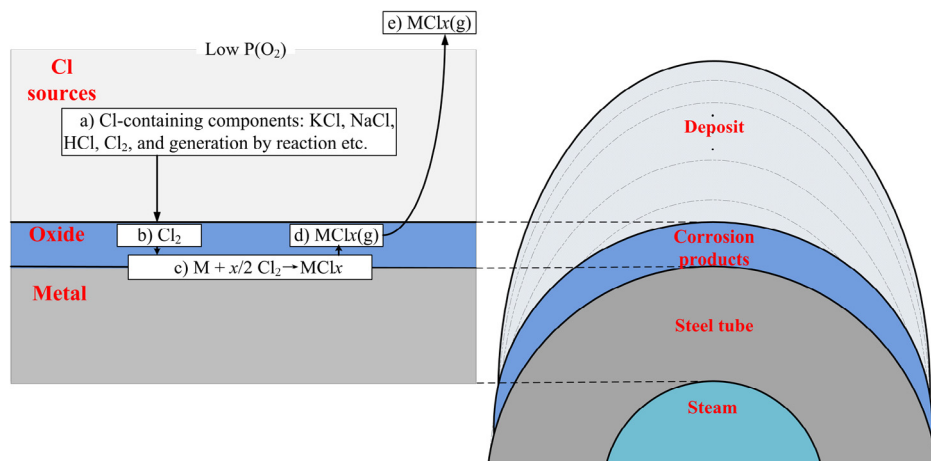
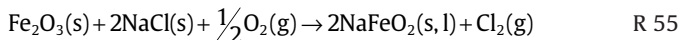
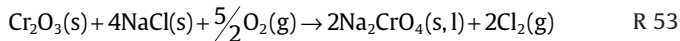


Fig. 36. Schematic of the reaction of Cl in reducing atmosphere, based on reference (adapted from reference 47).

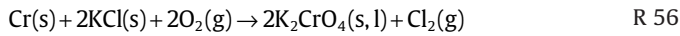
salts. Concerning these two species, KCl is more worthy of concern. Also, NaCl has a similar corrosive behavior to KCl [46].

High partial pressures of chlorinated species generated in the deposit close to the metal surface can lead to a corrosion mechanism similar to the gaseous phase corrosion attack described in Section II.1.2. The potential reactions are listed below:



The reaction products, $(\text{K}, \text{Na})_2\text{CrO}_4$ and $(\text{K}, \text{Na})\text{FeO}_2$, have been observed in corrosion testing. Compared with $(\text{K}, \text{Na})\text{FeO}_2$, $(\text{K}, \text{Na})_2\text{CrO}_4$ is more stable and can exist in the presence of higher Cl content. When a much high partial pressure of Cl is obtained from R 52 and R 53, R 54 and R 55 move to the left side where iron oxide coexists with chloride salt [164].

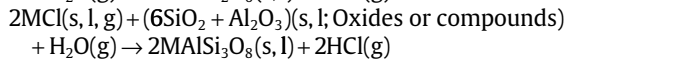
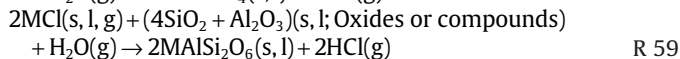
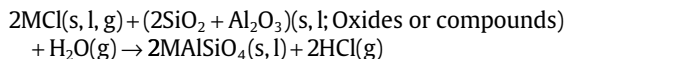
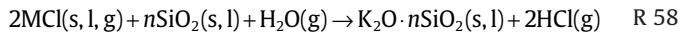
Several other reactions corresponding to the transformation of KCl into Cl_2 may occur in the deposits.



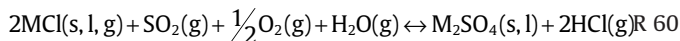
Both R 56 and R 57 are much faster than R 52 and R 53 [46]. In short, R 52–R 57, which generate Cl_2 , indirectly induce the corrosion described in Section II.1.1.

3.1.4. Corrosion associated with sulfation/silication of alkali chlorides

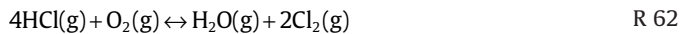
As discussed in Section I.1.1, alkali chlorides can be transformed into silicates and alumina-silicates through silication (R 58) and alumina-silication (R 59), respectively, and they are also easily sulfated in the presence of SO_2 (R 60). HCl generated through R 58–R 60 is responsible for corrosion. Even in the absence of water vapor, alkali chlorides can also be sulfated by the release of Cl_2 (R 61) instead of HCl.



.....

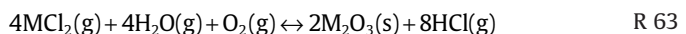


The released HCl and Cl_2 diffuse toward the metal surface to form volatile metal chlorides, such as FeCl_2 and CrCl_2 . Alternatively, HCl can be oxidized into Cl_2 through the metal-oxide catalyzed R 62 [156].



Some metal chlorides diffuse out through the deposit to areas with a high partial pressure of O_2 . There, the metal

chlorides are oxidized into metal oxides through R 45, R 46, and R 63. Alternatively, the metal chlorides may also evaporate straight into the atmosphere under reducing atmosphere.



The Cl_2 and HCl released by the reactions can also diffuse toward the metal surface again. Thus, the net reaction leads to the continuous transport of metal from the metal-scale interface to high oxygen-scale in the bulk gas. After sulfation or silication, the corrosion mechanisms are similar to those described in Section II.1.1 for gas-phase Cl attack.

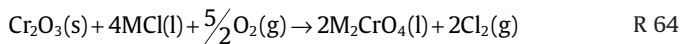
3.1.5. Corrosion associated with molten alkali chlorides

Pure NaCl, KCl and K_2SO_4 have melting points of 801, 774, and 1069 °C, respectively. However, together they can form low-temperature eutectics. Using NaCl/KCl and KCl/ K_2SO_4 as examples, NaCl-KCl and KCl- K_2SO_4 can melt at temperatures as low as 657 °C [46,165] and 694 °C [22], respectively. Fig. 37 shows the binary phase melting diagrams for NaCl-KCl [165] and KCl- K_2SO_4 [22] eutectic mixtures. The melting trend line has a "V" shape with reduced KCl concentration in the binary systems. The eutectic temperature can be as low as 657 °C and 694 °C for the NaCl-KCl and KCl- K_2SO_4 mixtures, respectively.

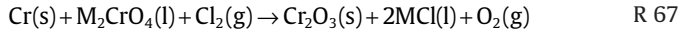
Table 6 shows the melting points and eutectic temperatures of compounds and mixtures that probably exist during the corrosion processes that occur during biomass combustion. When the metal surface temperature becomes sufficiently high for molten phases to form in the deposit, corrosion may increase [22]. The molten phase increases the corrosion rate by three methods: 1) molten deposits may form a flux with the protective oxide layer [47], 2) chemical reactions may be faster than solid-solid reactions in the liquid phase [21,46,47], and 3) a liquid phase provides an electrolyte or a pathway for ionic charge transfer for electrochemical attack [22,47].

Aside from the high solvencies and diffusivities of oxygen and chlorine in the molten phase which accelerate the corrosion kinetics [21,46], the corrosion mechanisms that occur in the molten phase should be similar with those presented for solid/deposited alkali chlorides described in Section II.1.3.

However, Li et al. [46] studied the corrosion behavior of various model alloys with NaCl-KCl coatings at 670 °C in air and found that a breakdown of the protective oxide readily occurs by dissolution into the melt; the degradation rate can be especially fast if the oxide has a high solubility. The corrosion resistance is reduced as the Cr component dissolves in the molten chlorides under an oxidizing atmosphere. Cr_2O_3 , which is corrosion resistant in other cases, acts as chromate in NaCl-KCl melt. The corresponding reactions contain R 64–66.



M denotes K and Na. The chromates and chlorine act as oxidants and cause further oxidation of Cr by R 67 [46,164].



As indicated by R 64–R 67, a self-sustaining corrosion process exists in the molten system without alkali chloride consumption. Meanwhile, the high reactivity of Cr_2O_3 in the molten alkali chlorides makes the protective chromic scale disappear or become more porous, which further deteriorates corrosion [164].

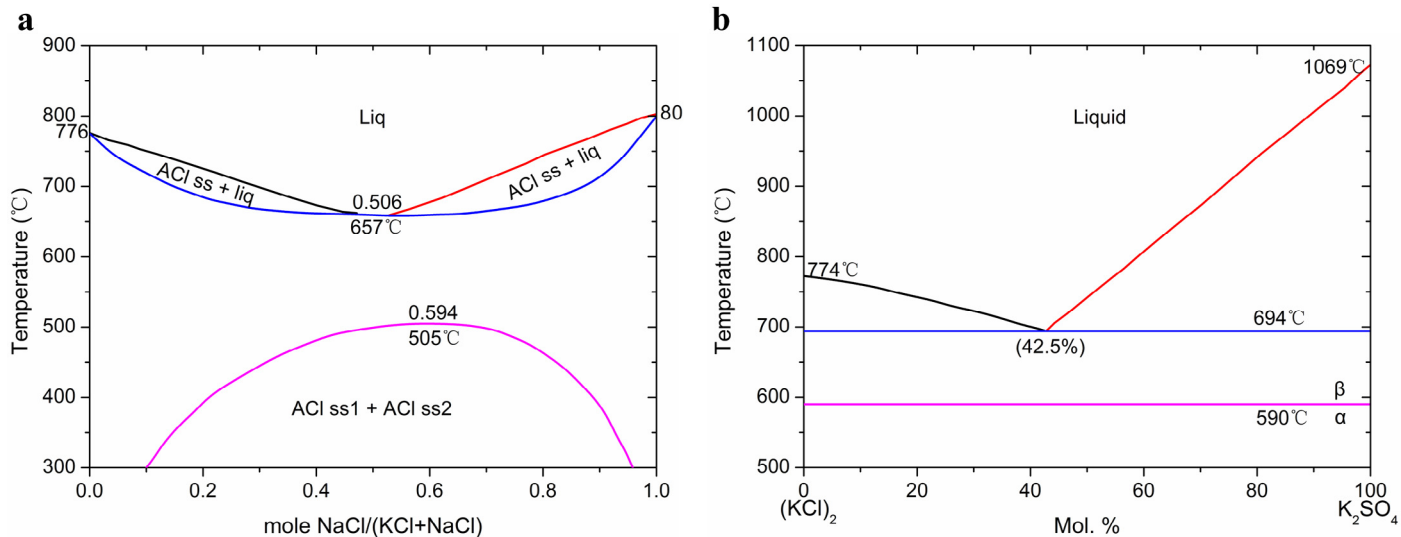


Fig. 37. Binary phase melting diagrams of NaCl-KCl (reprinted from reference 165, with permission of Elsevier) and KCl-K₂SO₄ (reprinted from reference 22, with permission of Elsevier).

a. NaCl-KCl b. KCl-K₂SO₄

"Liq" is a molten solution, "ACI ss" is a solid solution, and "ACI ss1 and ACI ss2" are two compositionally different solid solutions.

3.1.6. Corrosion associated with molten alkali sulfates

The most common form of accelerated corrosion in superheater tubes in a coal-fired conventional boiler is caused by the presence of molten alkali-metal-trisulfates. In a biomass-fired furnace, deposits with a white layer rich in alkali sulfates are widely reported. The deposited alkali sulfates cause corrosion by reacting with SO₂ and iron oxide to form liquid alkali-iron-trisulfate (R 68 and R 69).

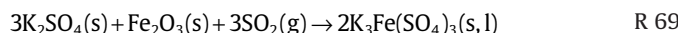
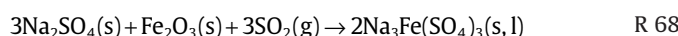


Table 6

Melting and eutectic temperatures of different pure species and binary mixture existing in corrosion products during biomass combustion (adapted from references 22 and 63).

Species	Melting/eutectic Temperature (°C)	Composition at eutectic point (mol% alkali)
NaCl	801	-
KCl	772	-
FeCl ₂	677	-
FeCl ₃	300	-
NaCl-FeCl ₂	370–374	~56
NaCl-FeCl ₃	151	45.3
KCl-FeCl ₂	340–393	45.8–91.8
KCl-FeCl ₃	202–202	24–47
CrCl ₂	845	-
CrCl ₃	947	-
NaCl-CrCl ₂	437	53.7
NaCl-CrCl ₃	544–593	68–95
KCl-CrCl ₂	262–475	36–70
KCl-CrCl ₃	700–795	54–89
Na ₂ CrO ₄	792	-
K ₂ CrO ₄	980	-
NaCl-Na ₂ CrO ₄	557	-
KCl-K ₂ CrO ₄	650	68.4
Na ₂ Cr ₂ O ₇	356.7	-
K ₂ Cr ₂ O ₇	398	-
NaCl-Na ₂ Cr ₂ O ₇ (1)	592	30
KCl-K ₂ Cr ₂ O ₇	366–368	25–27.5
K ₂ SO ₄	1069	-
KCl + K ₂ SO ₄	550	-

Below 550 °C, the ash deposit is a porous layer that allows relatively free gas diffusion between the tube surface and the bulk flue gas; the corrosion rate increases with increasing temperature, which improves gas diffusion [166]. However, the corrosion rate, which is highest when the deposit forms a molten layer of alkali-metal-trisulfates next to the tube surface, decreases along with a further increase in temperature because of the disappearance of pores.

During biomass combustion, the presence of chloride accelerates the corrosion of molten alkali sulfates. Firstly, chlorides may cause the breakdown of the normally protective scale, through which SO₂ and SO₃ cannot diffuse. Once the protective scale is destroyed, SO₂ and SO₃ can penetrate the oxide layer through the ruptures in the scale and result in further corrosion. Secondly, the presence of chlorides in alkali sulfate can form eutectics and decrease the melting temperature of the salt mixture, thus accelerating corrosion. Fig. 38 shows the effects of the coating of NaCl-Na₂SO₄ on steel corrosion. The Na₂SO₄ coating on the steel surface exacerbates corrosion, and the corrosion rate significantly increases even when as little as 1 wt.% NaCl is blended into Na₂SO₄.

Generally, corrosion in molten salts can be characterized in two steps: oxidation of the metal and basic or acidic dissolution of oxide scales. For oxidation, oxygen provided by dissolution from the gas phase or by dissolution of oxygen-bearing molecules in the molten salt has to diffuse through the melt layer to the metal surface. The corrosive oxygen species in molten sulfates are formed by the dissociation of the sulfate ion in the melt.



The SO₄²⁻ or O²⁻ generated by R 70–R 72 is the oxidizing species for the metal and results in an increase in the oxide ion activity at the oxide/melt interface. With increased activity of O²⁻ at the oxide/melt interface, the oxidation of the metal surface is enhanced.

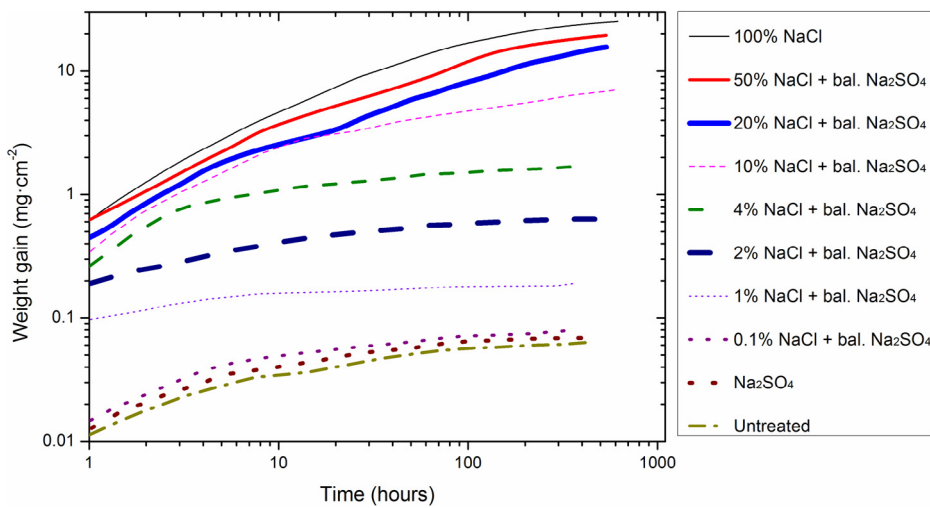


Fig. 38. Effects of coatings of sodium salts ($\text{NaCl}-\text{Na}_2\text{SO}_4$) on the corrosion of 18Cr-12Ni-1Nb steel at 650°C (reprinted from reference 22, with permission of Elsevier).

metal interface, basic dissolution of the oxide scale occurs through R 74 or R 75.



A concentration gradient of O^{2-} - and dissolved species is established during the corrosion process. As the concentration of O^{2-} decreases throughout the melt, the solubility of dissolved species decreases and precipitation occurs [167]. Therefore, a gradient of O_2^{2-} and a solubility gradient exist for dissolved species in the melt, and basic fluxing becomes possible, as illustrated in Fig. 39. As a result, the dissolved species re-precipitate in regions with a low concentration of O^{2-} and a high concentration of O_2 , and voluminous and porous scales are formed.

The re-precipitation of oxide according to R 75 leads to the suppression of SO_3 evaporation from the melt. The high-solubility SO_3 in the sulfate melt dissolves by chemical reaction with the melt as a pyrosulfate.

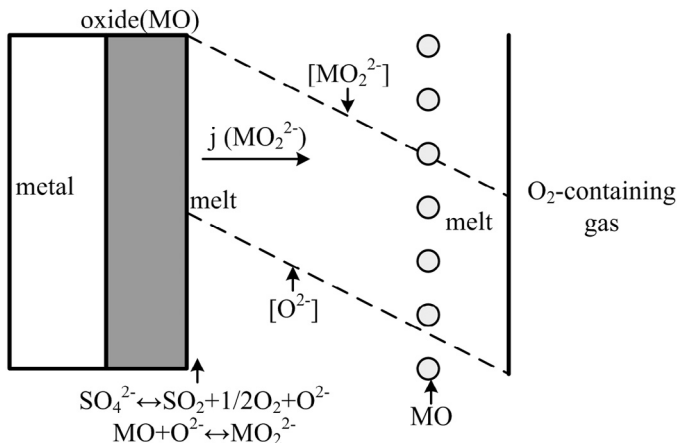


Fig. 39. Schematic of the basic fluxing process in sulfate melts that is responsible for corrosion caused by molten alkali sulfates (reprinted from reference 167, with permission of Elsevier).

The pyrosulfate ion causes acidic fluxing of oxide scales according to R 77.



3.1.7. Corrosion associated with molten alkali carbonates

Compared with sulfate melts, the chemistry of carbonate melts, and therefore, their corrosion mechanisms, are quite different. The formation of O_2 by the decomposition of the carbonate ion, given by equilibrium reactions R 78–R 80, is unlikely because of the highly positive values of the Gibbs free energy for R 79 (being 198–224 kJ/mol in the temperature range of 400–700 °C). The Gibbs free energy for R 71 is lower than 35 kJ/mol in the same temperature range.



By conducting electrochemical measurements with Au-electrodes, Nishina et al. [168] proposed two different corrosion oxygen species: superoxide ions (O_2^-) and peroxide ions (O_2^{2-}).

(a) Superoxide ions (O_2^-)

Firstly, on the melt-scale surface, O_2 reacts with CO_3^{2-} to form superoxide ions through R 81.



Then, in contact with the metal, the superoxide ions may be reduced to peroxide and oxide ions by R 82 and R 83, respectively.



(b) Peroxide ions (O_2^{2-})

Firstly, O_2 reacts with CO_3^{2-} to form peroxide ions through R 84.



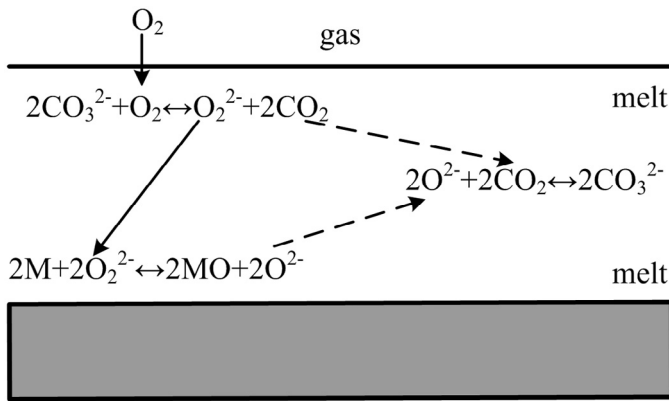


Fig. 40. Schematic of basic dissolution in carbonate melts via O_2^{2-} ions; oxygen is dissolved in the melt by a chemical reaction, and the oxidation of metal produces oxide ions (reprinted from reference 167, with permission of Elsevier).

Then, in contact with the metal, peroxide ions may also be reduced according to R 83.

In the case of corrosion, the electrons necessary for both R 82 and R 83 are delivered by the oxidation of metal M through R 85.



Hence, the overall process possible for the oxidation of metal by O_2^{2-} ions in contact with a carbonate melt is given by



This reaction produces oxide ions; therefore, basic dissolution of oxide scales can occur according to R 86. Compared with the melt/gas interface, a higher concentration of O_2^{2-} ions is established at the oxide/melt phase boundary. Therefore, a solubility gradient of the dissolved species exists throughout the melt, and basic fluxing might be possible as observed in sulfate melts. The reaction sequence, taking place by oxidation (via O_2^{2-} ions), is shown in Fig. 40.

The dissolution of oxide scales may also occur by peroxide ions in carbonate melts according to R 87.



The O_2^{2-} ions, consumed by R 87, are delivered continuously by the reaction of oxygen from the gas phase with the carbonate ion in the melt (R 84). Therefore, the concentration of O_2^{2-} ions is low at the oxide/melt scale and high at the melt/gas interface, as shown in Fig. 41. The figure shows a schematic of the basic dissolution of metal in carbonate melts initiated by O_2^{2-} ions responsible for corrosion caused by molten alkali carbonates. In this case, no fluxing of oxide occurs because no solubility gradient is established in the melt [167]. If the corrosion product is soluble (as in the case of CrO_4^{2-} from Cr_2O_3), the melt will be saturated with chromate without precipitation of Cr_2O_3 . If it is insoluble, stable layers of corrosion products will be formed.

3.2. Corrosion countermeasures or influence factors

3.2.1. Alloying and salts

High-quality alloys are recommended to prevent or reduce corrosion. Alloyed chromium is known to improve steel by forming a protective oxide layer consisting of either a corundum-type solid solution or, if the chromium content of the steel is sufficiently high, even pure Cr_2O_3 .

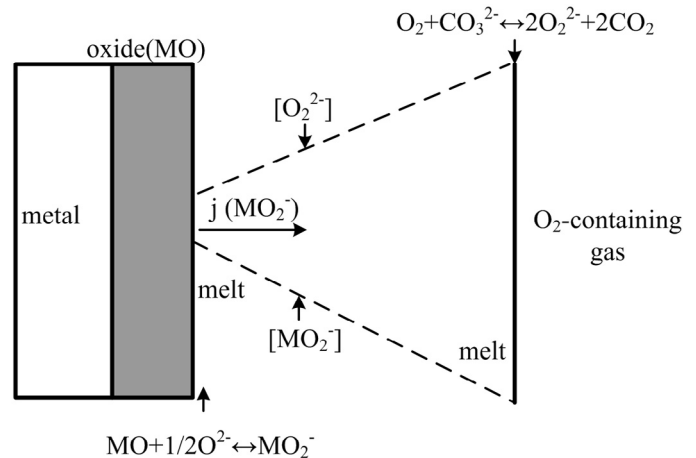
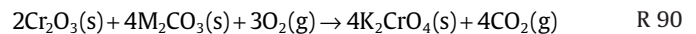
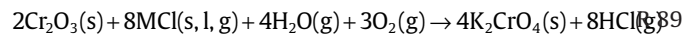
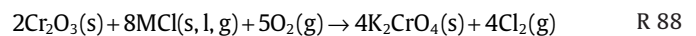


Fig. 41. Schematic of the basic dissolution in carbonate melts via O_2^{2-} ions that is responsible for corrosion caused by molten alkali carbonates (reprinted from reference 167, with permission of Elsevier).

However, the protective chromium oxide may be destroyed by reaction with alkali chlorides and carbonates (R 88–R 90) with alkali chromate as the intermediate.



Ma et al. [23] studied the high-temperature corrosion of pure Fe, Cr, and Fe-Cr binary alloys in O_2 containing trace KCl vapor at 750 °C and reported that the corrosion rate of Fe-Cr alloys is reduced as the concentration of Cr increases (shown in Fig. 42). Meanwhile, a multilayer oxide scale consisting of an outer Fe_2O_3 layer and an inner Cr_2O_3 layer is formed. The corresponding corrosion mechanisms associated with gaseous KCl are clearly described in Section II.1.2. In the presence of KCl vapor, the Cr and/or formed Cr_2O_3 will react with KCl and release Cl_2 . The released Cl_2 induces active oxidation and forms cracks and pores oxide scale. When the protective Cr_2O_3 layer is destroyed, further corrosion of the metal substrate is

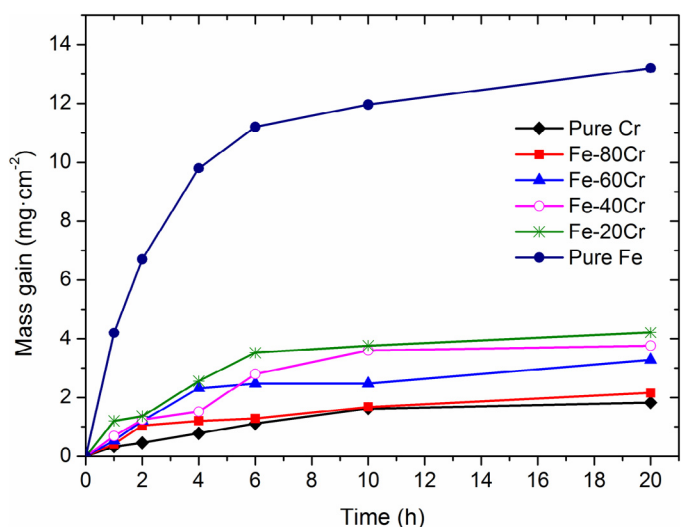


Fig. 42. Corrosion kinetics of Fe-Cr alloys corroded for 20 h in the presence of 298 ppm KCl vapor at 750 °C (reprinted from reference 23, with permission of Elsevier).

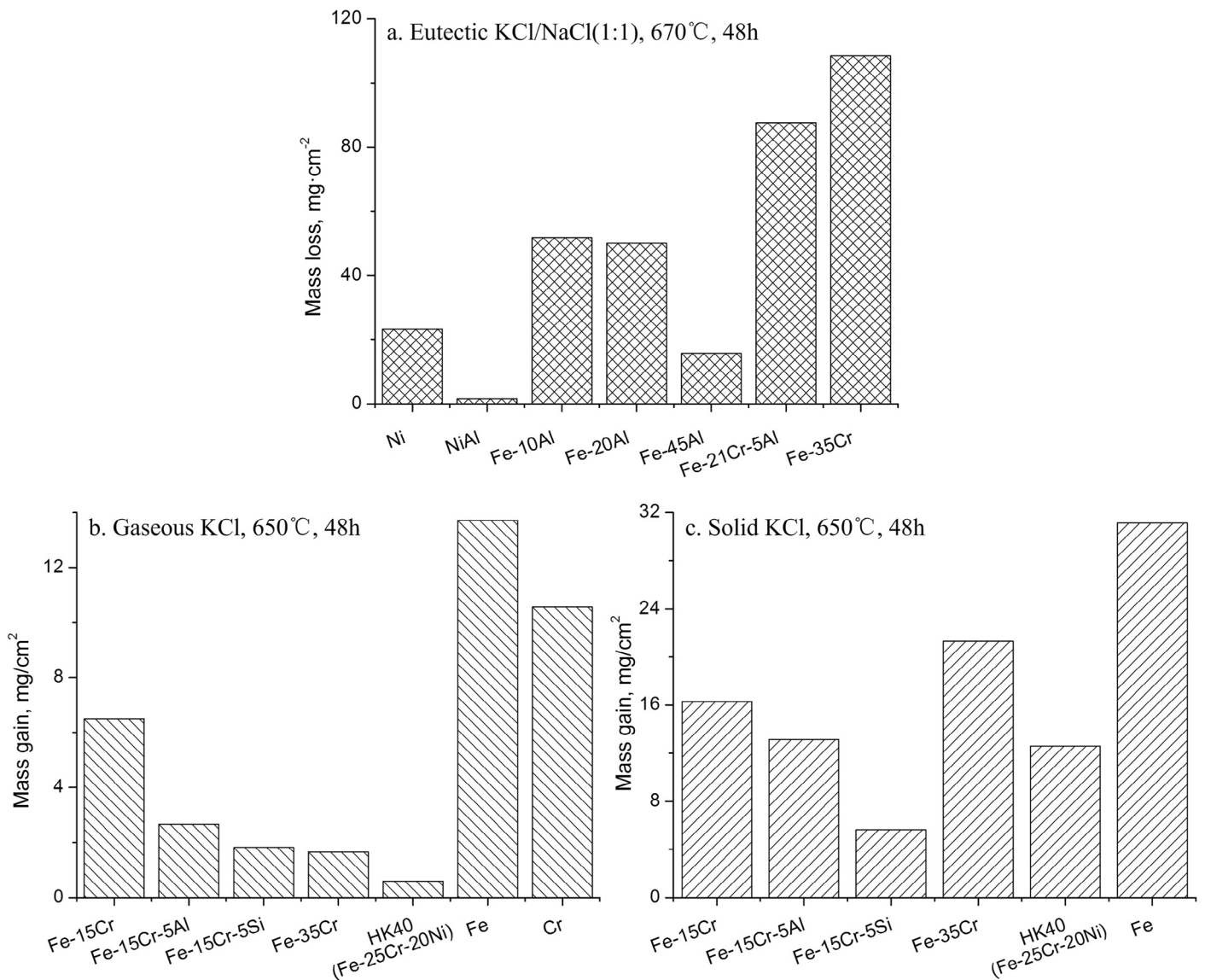


Fig. 43. Summary of the corrosion of Cr, Si, and Al modified Fe- and Ni-based alloys (reprinted from references 46,164, with permission of Elsevier).

accelerated by the reaction of O_2 and Cl_2 that have penetrated into the metal.

Li et al. [46,164] conducted research on gaseous and solid KCl and eutectic KCl/NaCl concerning the corrosion of Cr, Si, and Al modified Fe- and Ni-based alloys, as shown in Fig. 43. Eutectic KCl/NaCl can be regarded as molten or liquid KCl because of the equally corrosive behavior of the individual KCl and NaCl components that has been observed in various Fe-Cr, Fe-Al, and NiAl model alloys, ferrite, austenite, AISI347, and Sanicro 28 [46,154]. Fig. 43 shows that the corrosion strength of KCl (and also applicable to NaCl) is in the order molten state > solid state > gaseous state. This result may be attributed to the different corrosion mechanisms or coexisting multi-corrosion mechanisms between molten and solid KCl and the substance. For example, the breakdown of protective oxide layer occurs by dissolution into the melt, the corrosion rate is fast if the oxide is highly soluble in the melt, and the breakdown facilitates oxide activation [46]. Otherwise, both low melting $K_2Cr_2O_7$ and eutectic KCl- K_2CrO_4 that are attributed to the reaction between Cr_2O_3 and solid KCl can also induce local molten corrosion and accelerate it [46]. However, this phenomenon remains unclear and requires further investigation.

Fig. 43 also indicates that the alloying element Si has the best corrosion resistance followed by Al and Ni. For corrosion associated with gaseous KCl, high chromium content presents good resistance because of the low partial pressure of oxidation, which allows the formation of a protective Cr_2O_3 layer near the substrate. For corrosion associated with both molten and solid KCl, higher chromium content has a detrimental effect because of the high dissolution of Cr_2O_3 in the molten salts [46]. Alloying with aluminum facilitates the formation of a dense aluminum chromium oxide mixture, which restricts further corrosion at the initial stage; however, the chromium from the surface layer is gradually converted into potassium chromate and eventually overgrown by a porous iron oxide. Addition of Si provides a protective support by forming a continuous inner layer of silica that effectively precludes the active oxidation of iron [164].

Lehmusto et al. [157,163] systematically studied the effect of KCl and K_2CO_3 deposits on the corrosion of 10CrMo, 304L, and alloy 625 at 500, 550, and 600 °C, as shown in Fig. 44. The corresponding compositions of the three alloys are listed in Table 7, according to references 21,22,162. The presence of potassium induces initial accelerated oxidation, whereas, the presence of chloride or chlorine

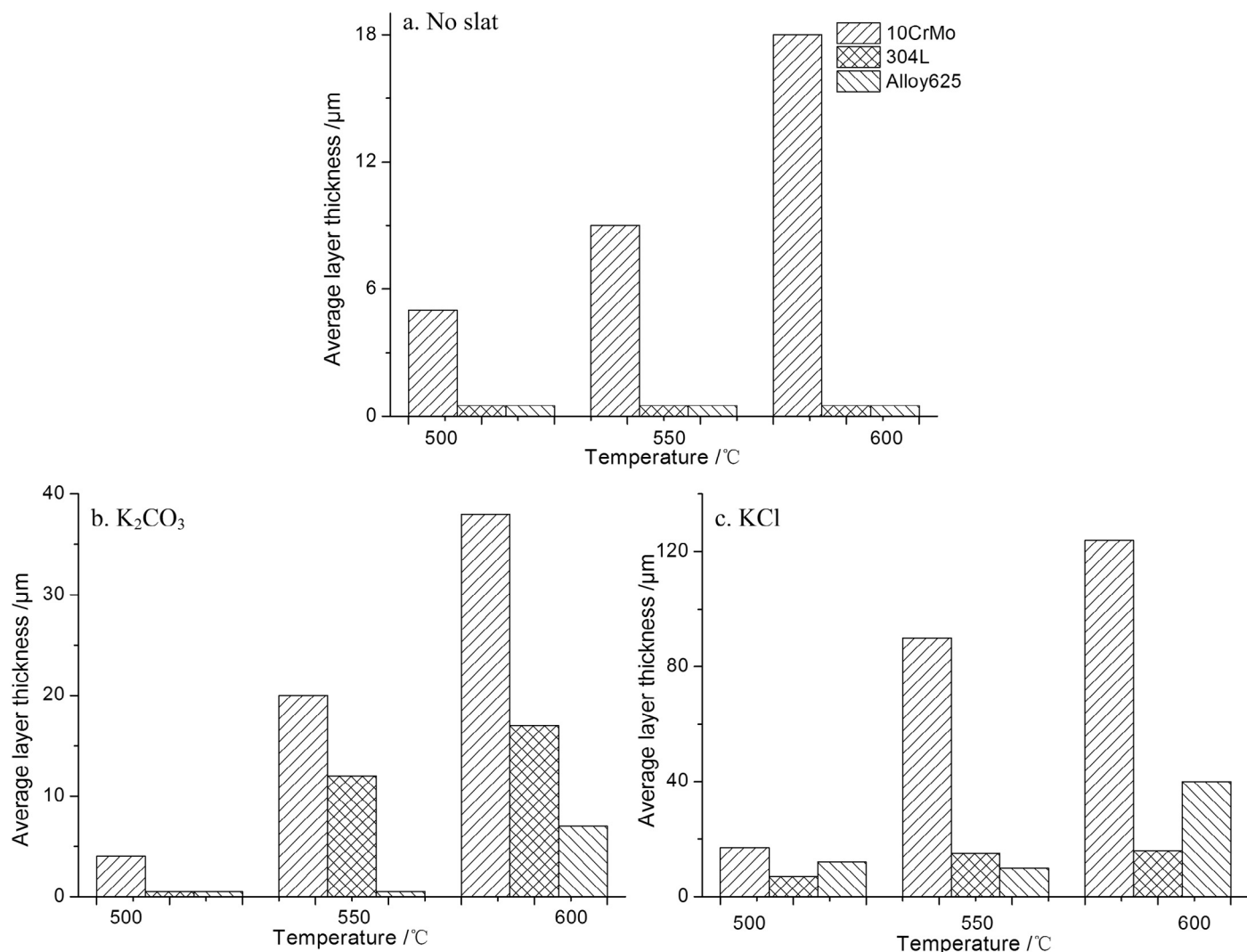


Fig. 44. Comparison of the corrosion behavior of 10CrMo, 304L, and Alloy 625 covered by KCl and K₂CO₃ deposits at 500, 550, and 600 °C (adapted from references 157,163).

is essential for it to continue based on the average corrosion layer thickness shown in Fig. 44 and the structure presented in the paper. The oxides formed in the presence of K₂CO₃ are more homogeneous with well-adhered thin layers, whereas the oxides formed in the presence of KCl are multilayered with poorly adhering layers. The formation mechanisms are explained in Fig. 35. Similar results (corrosion is initiated with potassium and potassium chromate as the intermediate, and the presence of chlorides and chlorine is essential for it to continue) have also been reported elsewhere [161,162]. As shown in Fig. 44, temperature also plays a key role in the corrosion process. Corrosion accelerates with increasing temperature, which improves the diffusion of the gas reactants (Cl₂ and O₂) and gaseous reaction products (KCl and CrCl₂). Meanwhile, a high chromium content inhibits corrosion. Generally, the corrosion behavior of an alloy depends on the relation between chromium loss

by evaporation and the supply of chromium to the oxide by diffusion into the alloy [162]. If chromium loss is rapid in comparison with chromium diffusion, the protective scale becomes severely depleted in chromium, resulting in rapid oxidation, for example, in 10CrMo. By contrast, alloy 625 shows good corrosion resistance. Fe-based alloys with low Cr exhibit rapid corrosion, but highly alloyed steel such as austenitic stainless steel or Ni-based alloys have good resistance to corrosion [159]. 18Cr-8Ni stainless steel is bordering regarding the formation of protective oxide scales [21]. Aside from the use of Cr as an alloying element, Si [164], Al [46,164,169], and Co [155,170] give high corrosion resistance when used as the coating or alloying element.

Low-alloy Fe-based steels suffer from severe corrosion in Cl-containing environments because the partial pressure of iron chloride is high at elevated temperature ($\Delta G = -238 \text{ kJ/mol}$, 550 °C). Ni-based alloys are more resistant than steels because the partial pressure of nickel chloride (1.3×10^{-5} , 550 °C) is significantly lower than the partial pressure of iron chlorides (2.1×10^{-4} , 550 °C), and the Gibbs energy change of NiCl₂ ($\Delta G = -181 \text{ kJ/mol}$, 550 °C) formation is less negative than that of FeCl₂ ($\Delta G = -238 \text{ kJ/mol}$, 550 °C) formation [47]. For CrCl₂, the partial pressure and Gibbs energy change are 2.0×10^{-7} and -292 kJ/mol , respectively [47]. The data above support the conclusion that the corroded oxide scale is

Table 7
Composition of 10CrMo [22], 304L [21,162], and alloy 625 [21], unit: wt. %.

Alloy	Fe	Cr	Ni	Mn	Si	Mo
10CrMo	96.25	2.25	-	0.5	-	1.0
304L	68–71	18–18.5	9.0–10.2	0.8–1.4	0.2–0.6	0.5
Alloy 625	1.0	21.4	68.5	0.4	-	8.5

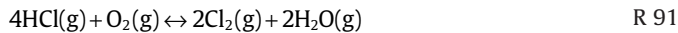
composed of an outermost iron oxide layer followed by an oxide layer containing chromium, iron, and nickel, and then a nickel-rich region before the bulk metal [163].

Therefore, during the combustion of biomass with high alkali chlorides and sulfates that induce various corosions, the corrosion caused by molten alkali chlorides is the most severe and should be avoided first, followed by the corrosion caused by solid/deposited alkali chlorides and gaseous alkali chlorides. For gaseous corrosion, a high Cr content inhibits the process by forming a protective Cr_2O_3 oxide layer because of the higher amount of Cr supply than the amount of Cr loss by evaporation. For molten and solid/deposit corrosion, a high Cr content accelerates corrosion. Therefore, other alloying elements such as Si, Al, and Co, which possess high corrosion resistance, should be investigated. Meanwhile, more attention should be focused on the effects of heavy metals, particularly Zn and Pb. These two metals may form the low-melting-point compounds ZnCl_2 and PbCl_2 , which accelerate the corrosion reactions [161].

3.2.2. Atmosphere and temperature

Accompanying the combustion of biomass, H_2O , SO_2 , Cl_2 , and HCl as reactant gases enter the flue gas and influence the corrosion reactions listed in Section II.1. A study has reported that 0.1 wt.% chlorine in biomass corresponds to approximately 100 ppmv chlorine in the gas phase; commonly, biomass contains around/more than 1 wt.% chlorine [22]. The effects of HCl and Cl_2 on corrosion have been investigated extensively and are believed to be essential for continued corrosion and the formation of a multilayer structure [157,161–163].

Mayer and Manolescu [171] investigated the effect of HCl on the morphology of the protective oxide layer. Without HCl in the synthetic flue gas, a continuous, nonporous scale is formed. At 0.1 vol% HCl , although some blisters occur in the Fe_2O_3 layer, the scale is still continuous. At 0.2 vol% HCl , the layer becomes porous and non-continuous. At 0.8 vol% HCl , the Fe_2O_3 layer becomes completely disintegrated, and the Fe_3O_4 layer becomes irregular and porous. At 2 vol% HCl , the continuity of all the layers is destroyed, and the corrosive gases have free access to the FeO layer and Fe. HCl and Cl_2 can be mutually transformed in oxygen and water vapor atmospheres (R 91), and metal oxides acting as catalysts improve the generation of Cl_2 [22,156].



For H_2O , when the concentration is above 1 ppm, R 89 becomes more probable. At a temperature above 400 °C, water vapor is known to destroy the protective chromium oxide layer even when no other corrosion compounds are present [172]. This condition is due to the formation of Cr(VI) oxide hydroxide vapor (R 92), which converts the protective chromium oxide-rich surface into a poorly protective Fe-rich oxide [162,163].



Fig. 45 shows a comparison of the corrosion results of humid O_2 and dry O_2 . H_2O significantly deteriorates the corrosion of low alloy steels such as 304L, whereas the effect on high alloy steels such as Sanicro 28, is minimal [162].

Lehmusto et al. [157,163] investigated the effects of water vapor on the corrosion of 10CrMo, 304L, and alloy 625 covered with KCl or K_2CO_3 at 500, 550, and 600 °C. Without potassium salts, H_2O deteriorates the corrosion of low alloy steels because of the formation of Cr(VI) oxide hydroxide vapor, which converts the protective chromium oxide-rich surface into a poorly protective Fe-rich oxide. However, for high alloy steels such as alloy 625, the effect is unidentified. The different effects can be attributed to the competitive relationship between chromium loss by evaporation and supply of

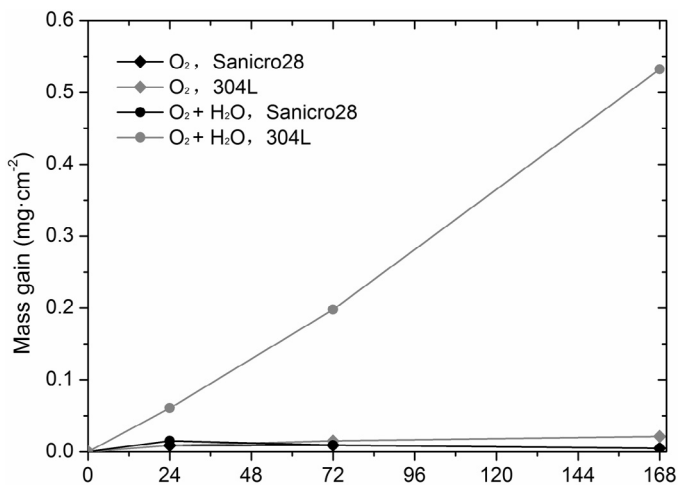


Fig. 45. Mass gain vs. exposure time for 304L and Sanicro 28 exposed at 600 °C in O_2 and $\text{O}_2 + \text{H}_2\text{O}$ (reprinted from reference 162, with permission of Elsevier).

chromium to the oxide by diffusion in the alloy [162]. For low alloy steels such as 10CrMo, chromium supply from the substrate fails its evaporation as Cr(VI) oxide hydroxide vapor, thus H_2O accelerates corrosion, whereas for high alloy steels such as alloy 625 because of the high chromium content in the substrate, chromium diffusion from the substrate is far greater than the evaporation; thus, corrosion is inhibited.

However, when the steel surfaces are covered with potassium salts, the effect of H_2O becomes more complicated. For KCl, H_2O decreases corrosion in two possible ways: (1) in the presence of H_2O , a denser oxide layer might form; and (2) water vapor might inhibit the reaction between the steel and the salt [157]. For K_2CO_3 , the opposite trend is observed. Therefore, the effect of H_2O on corrosion requires further discussion.

The effects of temperature on the corrosion behavior of 10CrMo, 304L, and Alloy625 in dry and wet conditions are illustrated in Fig. 46. With or without coating (K_2CO_3 and KCl), temperature, which accelerates corrosion, has a significant effect. Generally, high temperature means a large amount of corrosion. Grabke et al. [160] studied the corrosion behavior of Cr-Mo steel at different temperatures by adding NaCl, as shown in Fig. 47. Below 450 °C, the effect of temperature is slight; with increased temperature up to 550–600 °C, the corrosion rate presents a parabolic shape with time, and becomes nearly linear at 650 °C. This result may be due to the different corrosion mechanisms or corrosion kinetics, which both require further study.

4. Part III. Ash utilization

With the rapid development of biomass combustion power generation, the large volume of ash by-product has become an intractable problem throughout the world. According to statistics, the worldwide annual output of biomass ash, which is comparable to that of coal ash with an annual production of 780 million tons, is approximately 476 million tons [173]. Therefore, an eco-friendly and economic solution to recycle this by-product is essential.

According to the statistics provided by the American Coal Ash Association (ACAA) from 2000 to 2012 (Fig. 48) [174], the utilization rates of the three major by-products of coal combustion, namely, fly ash (average annual production of 67.6 Mt), bottom ash (average annual production of 17.6 Mt), and boiler slag (average annual production of 2.1 Mt) range from 32% to 45%, 29% to 48%, and 61% to 83%, respectively. Approximately 70%–84% of fly ash are used in construction, including concrete and concrete products, blended

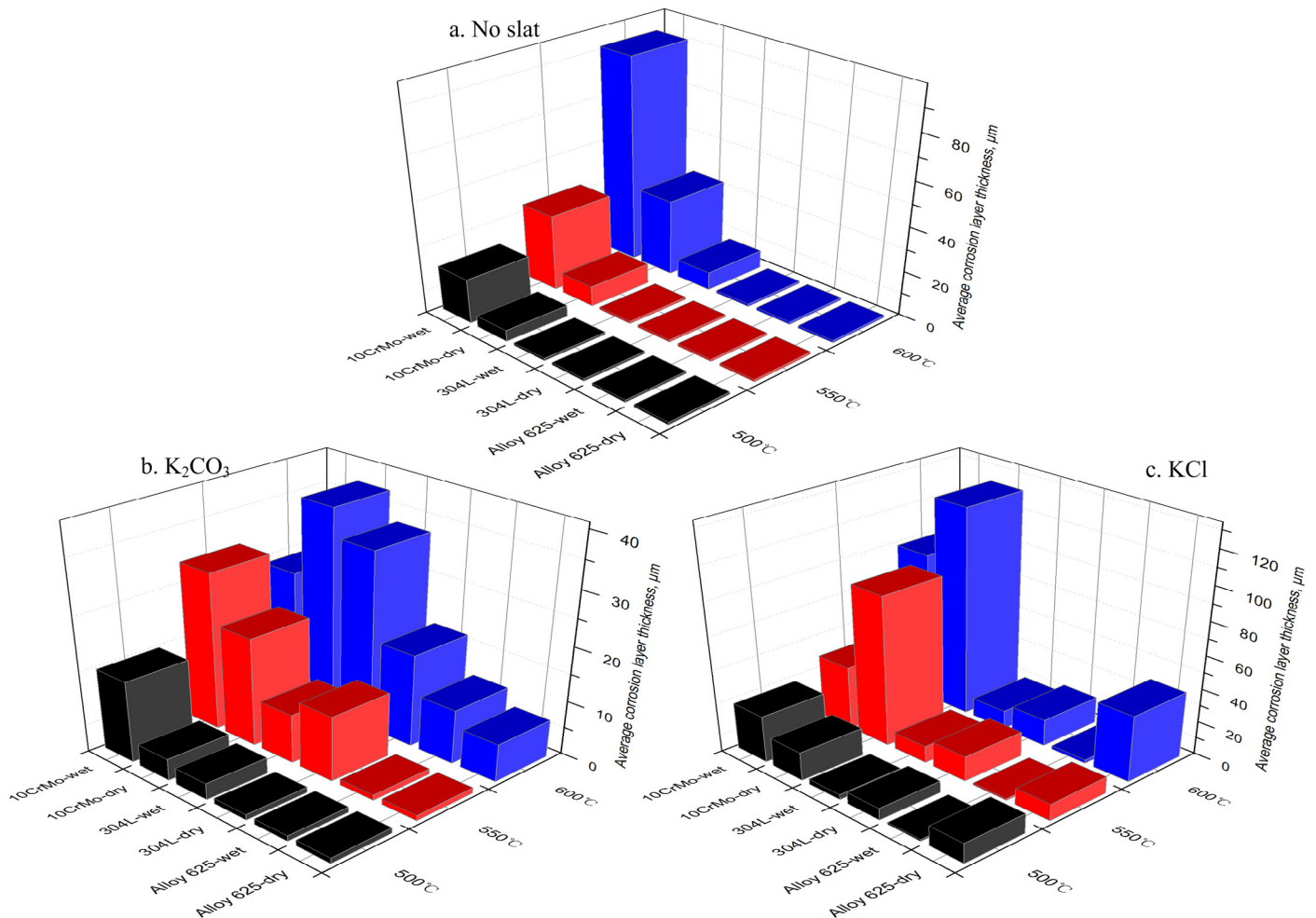


Fig. 46. Comparison of the corrosion behavior of 10CrMo, 304L, and Alloy625 in dry and wet conditions 500, 550, and 600 °C, respectively (adapted from references 157,163).

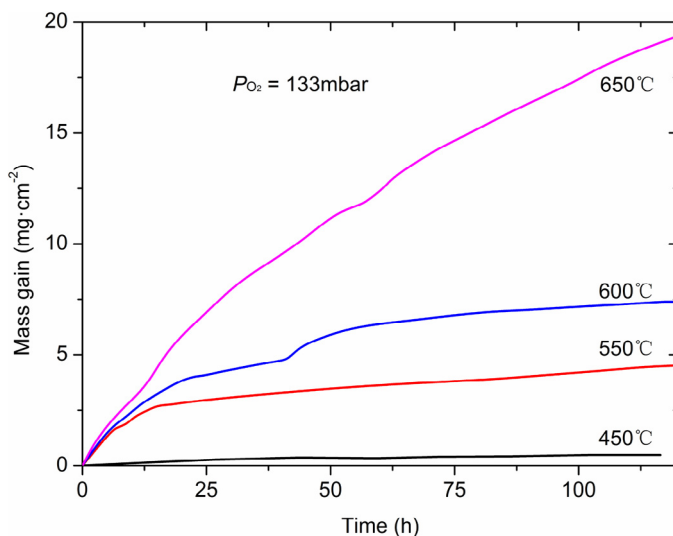
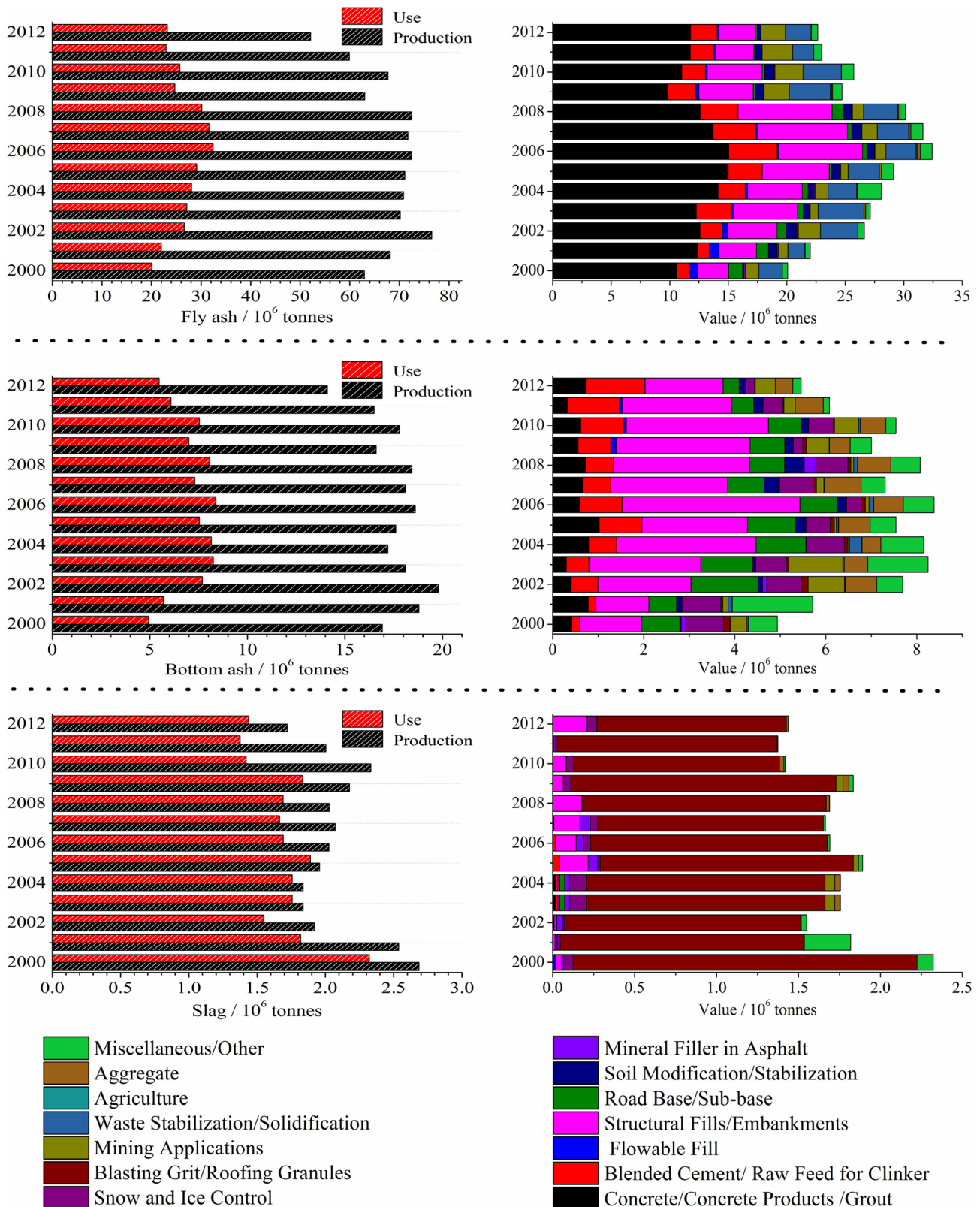


Fig. 47. Mass gain vs. time after preoxidation of Cr-Mo steel by the addition of NaCl at different temperature and oxidation atmospheres (reprinted from reference 160, with permission of Elsevier).

cement/raw feed for clinker, flowable fill, structure fill/embankments, and road base/sub-base. Less than 1% is used in agriculture and soil modification and stabilization. Approximately 48%–75% of bottom ash is used in construction materials, less than 6% is used in agriculture and soil modification and stabilization, and 17%–30% is used for snow and ice control. For boiler slag, 81%–98% are used as blasting grit/roofing granules. These different utilization approaches are mainly related to the respective properties of the three by-products. For example, fly ash and bottom ash have high pozzolanic activity, durability, and abrasion resistance, which allow them to be utilized as cement and concrete replacements. Meanwhile, bottom ash is coarse and porous and can thus be used as a filler. Boiler slag has a low density, so it is widely utilized as roofing granules.

Similar reports were presented by the European Coal Combustion Products Association e.V (ECOBA) as shown in Fig. 49 [175]. In 2003, 2004, 2006, and 2010, the utilization rates of fly ash (average annual production of 40.4 Mt), bottom ash (average annual production of 5.5 Mt), and boiler slag (average annual production of 1.7 Mt) in the EU-15 countries ranged from 44% to 50%, 39% to 51%, and 100%, respectively. The by-products were also mainly used as construction materials and in soil improvement/stabilization. In several countries (e.g. the Netherlands, Italy, and Denmark) with a fly ash production of approximately 2 Mt/y, fly ash is recycled completely. In France (3 Mt/y), Canada (6 Mt/y), Australia (10 Mt/y), the UK (15 Mt/y), and Germany (40 Mt/y), fly ash utilization rates range between 50% and 85%. In India (112 Mt/y), China (100 Mt/y), and the USA (75 Mt/y), which are the top three countries in terms of



Note: Data originated from American Coal Ash Association(ACAA), and accessed on Oct. 29th, 2014
URL: <http://www.acaa-usa.org/Publications/Production-Use-Reports>

Fig. 48. Statistics of the production and use of fly ash, bottom ash, and boiler slag from coal combustion in the USA from 2000 to 2012 (data from American Coal Ash Association [174]).

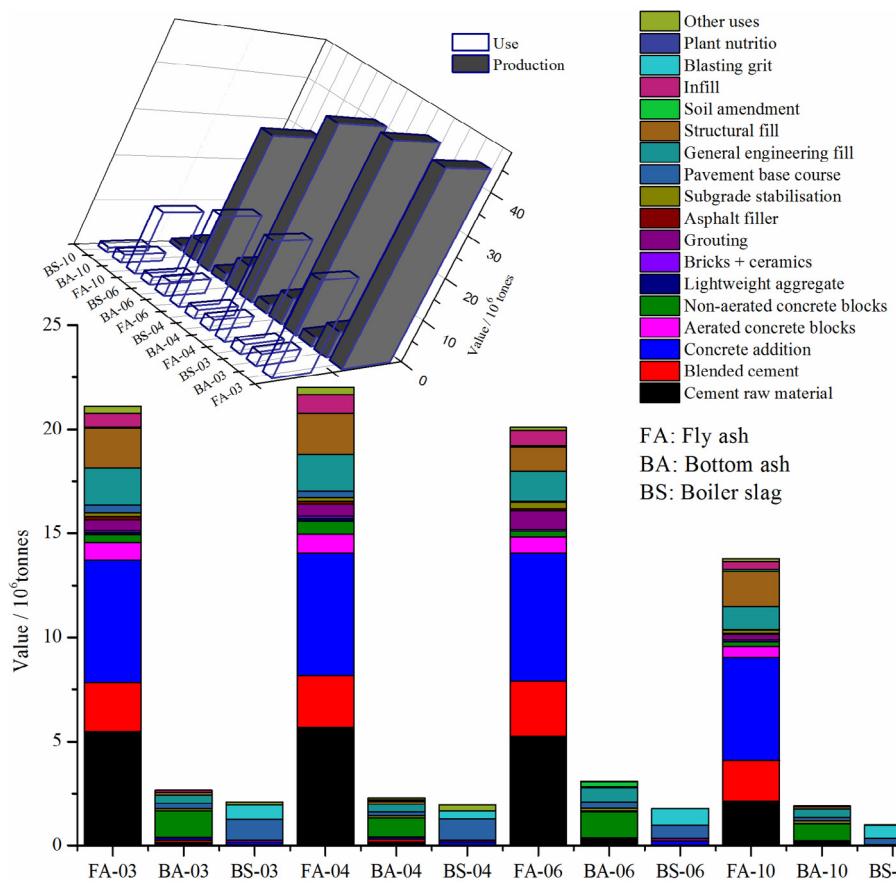


Fig. 49. Statistics of the production and use of fly ash, bottom ash, and boiler slag from coal combustion in the EU-15 in 2003, 2004 and 2006 (data from European Coal Combustion Products Association e.V (ECOBA) [175]).

fly ash production, the utilization rates are low; in particular, the utilization rate for India is only 38% [176].

Many studies on ash as a constituent of cement or construction materials [177–194] and on its use in agriculture/forest fertilization and improvement [176,178,195–197] have been conducted. However, most studies focused on coal ash rather than biomass ash. Research on biomass ash utilization is scarce.

4.1. Physico-chemical properties of biomass ash

Ash produced during biomass combustion mainly consists of fly ash and bottom ash. With reference to the definitions of fly ash [198] and bottom ash [199] during the process of coal combustion, biomass fly ash (BFA) is a fine, powdery substance that “flies up” from the biomass combustion chamber (boiler) and is captured by emission controls such as electrostatic precipitator, fabric filters “baghouses”, and scrubbers [177]. Biomass bottom ash (BBA) comprises angular, porous, agglomerated ash particles formed in biomass furnaces that are too large to be carried with the flue gases and impinge on the furnace walls or fall through open grates to an ash hopper at the bottom of the furnace [177]. In the USA, more than half of the concrete produced today uses coal fly ash at a proportion of 40%–70% as a substitute for traditional cement. Bridges, skyscrapers, roads, dams, massive walls, girders, and foundations are built by using high-performance fly ash concrete mixes to achieve superior strength and longevity [198]. Coal bottom ash can be utilized as a replacement for aggregates, because it is sufficiently well-graded in size and avoids the need for blending with other fine aggregates to meet gradation requirements. Its porous surface structure makes it lighter than conventional aggregates and useful in

lightweight concrete applications; however, it has less durability than conventional aggregates [199].

BFAs are also employed as raw materials in the cement and brick industry in Austria and the Netherlands, as construction materials for landfill in Sweden, and for grouting mines or as asphalt or concrete fillers in several other countries. BBAs, or mixtures of bottom and coarse fly ashes from clean biomass fuels, are commonly utilized as fertilizer on agricultural or forest soils in Finland and Sweden, as an additive for compost production in Austria, and as a liming agent for forest soils in Austria and Germany [25]. However, the properties of biomass ash are diverse because of the variety of biomass fuel sources [15,177,185,186,200]. For example, agricultural residues and bark generate a high ash content (5% to 10% and even up to 30% to 40%), whereas woody biomass generates low ash content (typically less than 2%) [201,202]. The properties of biomass ash also vary depending on the soil type where the biomass was grown [12,200], harvesting seasons [200], combustion technologies [177,185] (fixed beds that burn particles with a size of 1–10 cm typically have a combustion temperature of 1000–1200 °C [186,201,203], FBs that burn particles with a size of 10⁻²–1 cm typically have a combustion temperature of 800–900 °C [186,201,203], and PC furnaces that burn particles with a size of 10⁻⁴–10⁻² cm typically have a combustion temperature above 1200 °C [138,203]), and collection location [201]. Thus, no single application is suitable for all types of ash [202].

Ash utilization as a raw material in cement manufacture is primarily dependent on its chemical composition [200], as expressed in the usual oxide convention in Table 8. Similar to coal ash, the chemical composition of biomass ash exhibits certain similarities to those of cement and soil, such as its oxide content, loss on

Table 9

Heavy metal concentration limits for utilization of biomass ash as a soil conditioner in forests and agriculture; units: mg/kg, dried base.

Element	Austria ^a	Sweden	Denmark	Lithuania	Germany	Finland ^c
	Class A/B					AGR/FOR
As	20/20	30	-	30	40	25/40
Cd	5/8	30	5/15 ^b	30	1.5	2.5/25
Cr	150/250	100	100	100	2	300/300
Cu	200/250	400	-	400	-	600/700
Ni	150/200	70	30/60	70	80	100/150
Pb	100/200	300	120	300	150	100/150
Zn	1200/1500	7000	-	700	-	4500
V	-	70	-	70	-	-
B	-	500	-	500	-	-
Hg	-	3	0.8	3	1	1
References	[210]			[209]	[25]	

^a If the concentrations are below limits according to A, no soil analysis is required.

^b Left values for straw ash; right values for wood ash.

^c Left values for application on agricultural soils (AGR); right values for application on forest soils (FOR).

ignition (LOI), particle density, water-holding capacity, and porosity. These similarities ensure that it can be used as a substitute or used as an additive for cement and as a soil ameliorant. Physical properties (such as LOI, bulk density, water-holding capacity, porosity, specific surface area (SSA), pH, trace and heavy element content, etc.) further dictate special applications, including use as a cement additive/replacement and use in soil/forestry stabilization/fertilization. Heavy metal content such as As, Cd, Cr, Cu, Ni, Pb, Zn, V, B, and Hg are severely restricted. **Table 9** shows a summary of the heavy metal concentration limits for the utilization of biomass ash as a soil conditioner in forests and agriculture. As shown in the table, Austria, Sweden, Denmark, Lithuania, Germany, and Finland have strict standards.

4.2. Utilization for construction materials

4.2.1. Relative standard on ash utilization in cement

According to a report by KEMA [25], shown in **Table 10**, most fly ash and bottom ash from wood firing or low co-firing ratios (up to 20 wt.%) can be utilized as a cement/concrete component. For EN 450-1:2005 + A1:2007 [224], 10% of fly ash, derived from biomass/coal co-firing with a ratio up to 20 wt.%, is currently used as additive for cement provided that it fulfills the above requirements. Additionally, fly ash from biomass/coal co-firing is also used as concrete or asphalt filler [25]. However, several existing standards exclude the use of BFA in cement. For example, ASTM C-618 explicitly states that the fly ash used in the concrete industry must be completely derived from coal [181,184]; EN 197-1 [225] and BS 12 [226] state that fly ash should be obtained by electrostatic or mechanical precipitation of dust-like particles from the flue gases of furnaces fired with pulverized coal, and the ash obtained by other methods cannot be used in cement. Although the revised EN 450-1:2012 permits

less than 30% of ash derived from co-combustion material with a high co-firing ratio of 40% (for green wood, up to 50%) to be used in cement, it lists a set of requirements, including $\text{SiO}_2 + \text{Al}_2\text{O}_3 + \text{Fe}_2\text{O}_3 \geq 70\%$; reactive $\text{SiO}_2 \geq 25\%$; reactive $\text{CaO} \leq 10\%$; $\text{MgO} \leq 4\%$; total alkalis $\leq 5\%$; $\text{SO}_3 \leq 3\%$; $\text{Cl}^- \leq 0.1\%$; soundness $\leq 10\text{ mm}$; LOI equal or less than 5, 7, and 9 for categories A, B, and C, respectively; and an initial setting lower than twice that for the test cement alone [227,228]. In addition, EN 450-1 defines that fly ash has to be derived from the burning of pulverized coal with or without a co-combustion material [224,227]. This means that the ash from a dedicated boiler where the finely ground fuel is burned above 1300 °C can be used, whereas ash from grate furnaces and fluidized bed boilers cannot be used.

Ash as a blended cement component shares some of the requirements of both raw materials and direct concrete admixture use. However, given that little or no adjustment can be provided at the concrete mixing stage, its utilization in blended cements must involve consistent and uniform chemical and physical characteristics [200]. **Table 11** provides a summary of the main Portland cement standards, which provide useful guidelines for ash selection and pretreatment. For example, Cl^- , alkalis, and unburned carbon (which are higher in biomass ash than in coal ash and seriously compromise the durability of the cement-based material) can be removed [177,185,201] or partially replaced [177] before use. According to the standards of EN 197-1:2000 [225], GB175-2007 [230], and JIS R 5210-1997 [231], the content of SO_3 should be equal to or lower than 4.0, 3.5, and 3.0, respectively; the content of Cl^- should be equal to or lower than 0.1, 0.06, and 0.02, respectively; the equivalent alkalis should be lower than or within the range of 0.60–0.75; and the LOI should not exceed 5.0 (EN 197-1:2000), 3.0 (GB175-2007), and 2.5 (ASTM C150-07). For more standard limits, refer to **Table 11**.

Table 10

Current utilization practices for biomass ash and co-firing ash (IEA Bioenergy Task 32) (adapted from reference 25).

Ash origination	Utilization
Bottom ash/coarse fly ash from (wood fired) grate, BFB or CFB	Fertilizer; Liming agent on agricultural/forest soils; Additives to compost production; Cement production; Disposal
Fly ash from (wood fired) furnace, BFB or CFB	Cement production; Brick production; Construction material at landfills; Concrete filler; Asphalt filler; Minc; Soil stabilization; Disposal
Bottom ash from co-firing peat and biomass in BFB or CFB	Disposal
Fly ash from co-firing peat and biomass in BFB or CFB	Fertilizer; Grouting mines; Soil stabilization; Disposal
ashes from straw fired CHP plants	Fertilizer; Disposal
ashes from domestic fireplaces, stoves and pellet boilers	Land spreading on gardens; Composting own garden; Disposal own garden; Disposal household waste; landfill
Bottom ashes from co-firing up to 20 wt% biomass/coal	Concrete aggregate
Fly ashes from co-firing up to 20 wt% biomass/coal	Additive in cement; Concrete filler

Table 11

Comparison of the properties of common Portland cement from various countries or standards.

ASTM C150-07 [229]									BS EN 197-1:2000 [225]		GB175-2007 [230]		JIS R 5210-1997 [231]		
Type ^a	I	IA	II	IIA	III	IIIA	IV	V	I	II	-	-	-	-	
Standard chemical composition required															
MgO /%	≤6.0								≤5.0		≤5.0	≤5.0	≤5.0	≤5.0	
Al ₂ O ₃ /%	-	-	≤6.0	≤6.0	-	-	-	-	-	-	-	-	-	-	
Fe ₂ O ₃ /%	-	-	≤6.0	≤6.0	-	-	-	-	-	-	-	-	-	-	
SO ₃ /%	≤3.0 ^b /3.5 ^c	≤3.0/3.5	≤3.0/-	≤3.0/-	≤3.5/4.5	≤3.5/4.5	≤2.3/-	≤2.3/-	≤3.5 ^d /4.0 ⁱ		≤3.5	≤3.5	≤3.0		
Cl ⁻ /%	-	-	-	-	-	-	-	-	≤0.1		≤0.06	≤0.06	≤0.02		
CaO/SiO ₂ /m/m	-	-	-	-	-	-	-	-	≥2.0		≥2.0	≥2.0	-		
LOI /%	≤3.0						≤2.5	≤3.0	≤5.0		≤3.0	≤3.5	-		
Insoluble residue /%	≤0.75								≤5.0		≤0.75	≤1.5	-		
Equivalent alkalis /%	≤0.60								-		≤0.60	≤0.60	≤0.75		
Minor additional constituents /%	0								≤5.0		≤5.0	≤5.0	≤5.0		
Standard physical requirements															
Air content of mortar /V%	≤12	16–22	≤12	16–22	≤12	16–22	≤12	≤12	-	-	-	-	-		
Autoclave expansion /% and mm ^j	≤0.80								≤10		≤5.0	≤5.0	≤10.0		
Time of setting /min	45–375								≥75 for 32.5N/R ≥ 60 for 42.5N/R ≥45 for 52.5N/R		45–390	45–390	60–600		
Compressive strength /Mp	1 day	-	-	-	-	≥12.0	≥10.0	-	-	No limitation for 32.5N	-	-	-		
	3(2 ^g) days	≥12.0	≥10.0	≥10.0	≥8.0	≥24.0	≥19.0	-	≥8.0	≥10.0 for 32.5R ≥10.0 for 32.5R ≥10.0 for 42.5N ≥20.0 for 42.5R ≥20.0 for 52.5N ≥30.0 for 52.5R	≥17.0 for 42.5 ^f ≥22.0 for 42.5R ≥23.0 for 52.5 ≥27.0 for 52.5R ≥28.0 for 62.5 ≥32.0 for 62.5R	≥12.5			
	7 days	≥19.0	≥16.0	≥17.0	≥14.0	-	-	≥7.0	≥15.0	≥16.0 for 32.5N 32.5–52.5 for 32.5N/R 42.5–62.5 for 42.5N/R ≥52.5 for 52.5N/R	-	≥22.5			
	28 days	-	-	-	-	-	-	≥17.0	≥21.0	≥21.0 for 42.5 and 42.5R ≥52.5 for 52.5 and 52.5R	≥42.5 for 42.5 and 42.5R ≥52.5 for 52.5 and 52.5R	≥42.5	≥42.5		
Flexural strength /Mp	3 days	-	-	-	-	-	-	-	-	≥3.5 for 42.5 ^f	-				
		-	-	-	-	-	-	-	-	≥4.0 for 42.5R	-				
		-	-	-	-	-	-	-	-	≥4.0 for 52.5	-				
		-	-	-	-	-	-	-	-	≥5.0 for 52.5R	-				
		-	-	-	-	-	-	-	-	≥5.0 for 62.5	-				
	28 days	-	-	-	-	-	-	-	-	≥5.5 for 62.5R	-				
		-	-	-	-	-	-	-	-	≥6.5 for 42.5 and 42.5R ^f	-				
		-	-	-	-	-	-	-	-	≥7.0 for 52.5 and 52.5R ^f	-				
		-	-	-	-	-	-	-	-	≥8.0 for 62.5 and 62.5R ^f	-				
Fineness /m ² /kg	Average ^d	≥160	≥160	160–240 ^e	160–240 ^e	-	-	160–240	≥160	-	-	-	-		
Turbidimeter test	Any one sample	≥150	≥150	150–245 ^e	150–245 ^e	-	-	150–245	≥150	-	-	-	-		
Fineness /m ² /kg	Average ^d	≥280	≥280	280–420 ^e	280–420 ^e	-	-	280–420	≥280	-	≥300	-	≥250		
Air permeability test	Any one sample	≥260	≥260	260–400 ^e	260–400 ^e	-	-	260–400	≥260	-	-	-	-		

^a Type I: For use when the special properties specified for any other type are not required; Type IA : air-entrained cement for the same uses as Type I, where air-entrained is desired;

Type II: for general use, more especially when moderate sulfate resistance or moderated heat of hydration is desired; Type IIA: air-entrained cement for the same uses as Type II, where air-entrained is desired;

Type III: for use when high early strength is desired; Type IIIA: air-entrained cement for the same uses as Type III, where air-entrained is desired;

Type IV: for use when a low heat of hydration is desired; Type V: for use when high sulfate resistance is desired.

^b When 3CaO·Al₂O₃ is 8% or less.^c When 3CaO·Al₂O₃ is more than 8%.^d Average value shall be determined on the last consecutive five samples from the source.^e Maximum average ad maximum single sample fineness limes do not apply if the sum of C₃S+4.75C₃A is less than or equal to 90.^f Corresponding compressive strength at 28 days, representing the classes of standard strength.^g for EN 197-1.^h For cement 32.5N, 32.5R, 42.5N.ⁱ For cement 42.5R, 52.5N, 52.5R.^j ASTM adopts %, others adopt mm.

4.2.2. BFA

Many types of BFA such as those from wood [177,181], olive residue [182], rice husk [232], and sugar cane straw [233] have similar pozzolanic properties as coal fly ash and have been added in concrete to improve performance. Aside from the economic feasibility, fly ash use has a number of other positive effects on the resulting concrete when used as an additive to Portland cement. Such positive effects include improved pumpability, reduced water demand and water/cement ratio, low heat evolution, strong and stable protection cover to the embedded steel framework against natural weathering action, increased corrosion and abrasion resistance, improvement in the packing of particles, and reduced air entrainment in the concrete [200]. However, reduced air entrainment adversely affects the initial freeze and the durability of the concrete. However, if the fly ash concrete is allowed to cure fully, the effects would be minimal, and the concrete mix will perform satisfactorily [200]. Generally, biomass ashes contain high quantities of alkali and alkaline earth metals. Soluble alkali metal salts (KCl and K_2SO_4) in ash cause the precipitation of gypsum and portlandite during the first hydration stages of the pastes and consequently enhance their apparent viscosity. CaO and MgO present in ash could potentially improve the 28d strength, provided that the silica content in the ashes is higher than that in the cement [184]. In contrast, a high alkali content in biomass ash can cause a serious alkali silica reaction (ASR) and expansion of the cement [181], and the alkali reaction coupled with a progressive dissolution of K salts present in the starting ashes causes a long term decline in the material's mechanical behavior [184]. In addition, high LOI or unburned carbon leads to an unstable air content and decreased binding properties when used in construction, leading to poor durability if not dealt with properly [181,191,202].

Wang et al. [181] conducted durability research on BFA concrete, where the fly ash includes co-fired fly ash from biomass/coal co-firing, wood fly ash, and blended fly ash (wood fly ash mixing with coal fly ash). Freezing and thawing tests showed that all types of fly ash concrete have a statistically equal or lower weight loss

than pure cement concrete. Furthermore, all types of fly ash concrete have lower chloride permeability. Cuenca et al. [182] studied the effect of olive residue BFA as a filler in self-compacting concrete and pointed out that BFA concrete has a compressive strength that is equal to or greater than that of conventional concrete.

Maschio et al. [184] systematically studied the compressive strength of mortar pastes obtained by replacing a commercial cement with the equivalent mass of 5, 10, 20, and 30 wt.% of BFA or BBA from fir chips combustion (Fig. 50). They observed that the materials containing 5 wt.% ash (used as the reference composition) have acceptable compression strength after 28 days; however, a progressive increase in ash causes a continuous decline in material strength because of increased water adsorption. Moreover, the samples tested after 180 days display a marked decline in compressive strength because of potassium elution and alkali silica reaction during curing. Rajamma et al. [201] characterized cement-based materials, where cement is replaced by BFA from a grate furnace and a bubbling fluidized bed at proportions of 10, 20, and 30 wt.%. They found that the basic strengths (both flexural and compressive) maintained with 10% fly ash decrease by 25% at 20% replacement ratio. Fernandez-Pereira et al. [179] also pointed out that the addition of 20% BFA to a clay mixture reduces strength, but the material can be used commercially as low-density clay masonry units with good thermal insulating capacity. Therefore, the maximum amount of ash that can be used to replace cement is approximately 5–10 wt.%; large quantities do not lead to good physico-mechanical behaviors.

4.2.3. BBA

Carrasco et al. [177] evaluated the potential of bottom ash from a biomass plant (mixture of olive pomace and agricultural residue) as a mass replacement in proportions ranging from 10% to 90% for cement in building blocks. They reported that the addition of BBA increases the material's porosity and consequentially decreases its thermal conductivity and compressive strength, as shown in Fig. 51. Meanwhile, with a 1:1 Si/Ca ratio, both the compressive strength

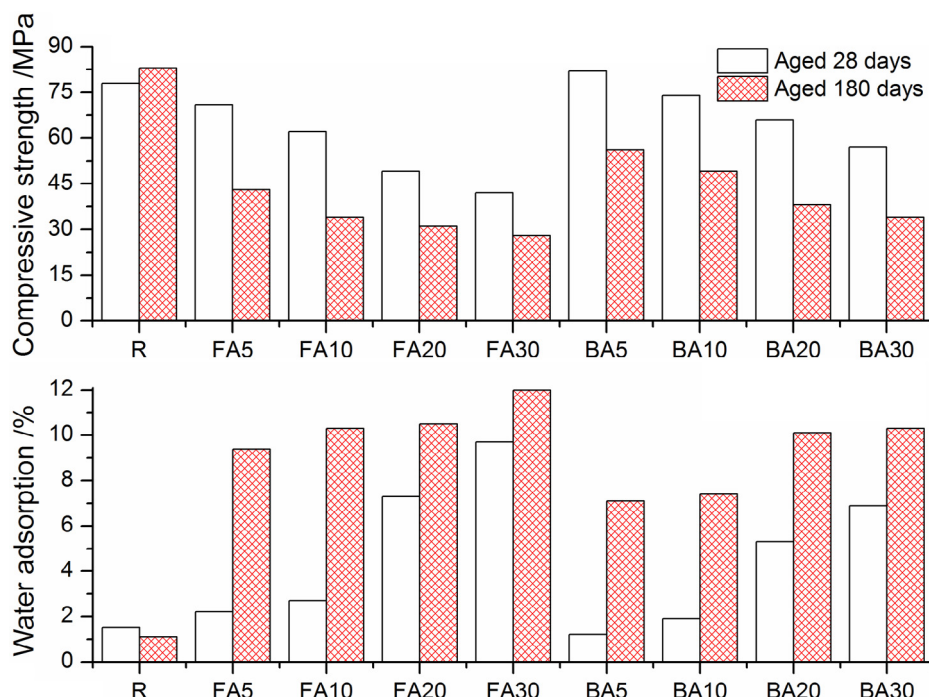


Fig. 50. Water adsorption and compressive strength of pastes aged 28 days and 180 days in water at room temperature by replacing cement with BFA and BBA (adapted from reference 184).

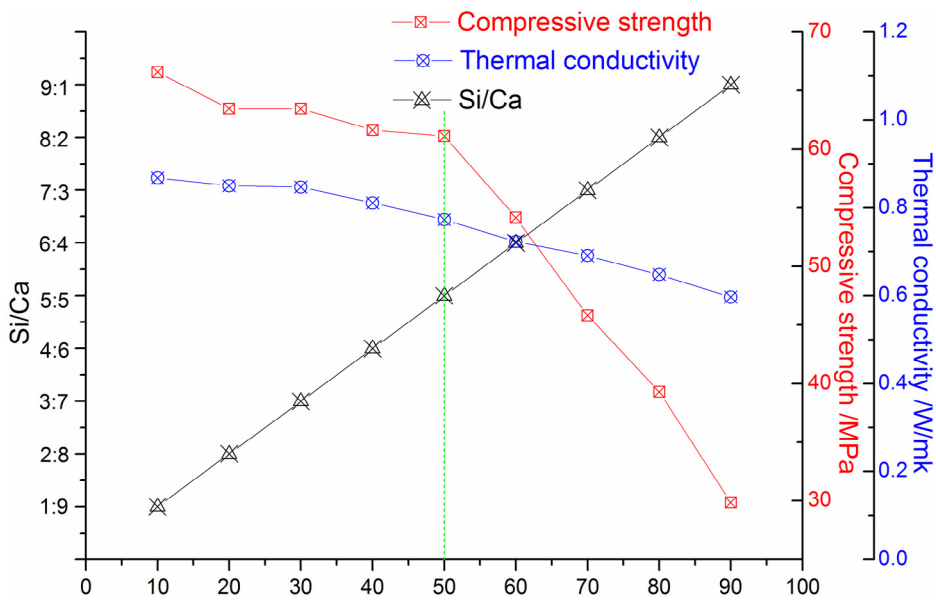


Fig. 51. Effects of BBA and Si/Ca ratio on the compressive strength and thermal conductivity of BBA/Portland cement mixtures (adapted from reference 177).

(61.11 MPa) and thermal conductivity ($0.773 \text{ W m}^{-1} \text{ K}^{-1}$) are acceptable and can potentially be utilized in products, such as blocks. Cabrera et al. [180] reported that BBA, as stated in the Spanish technical specification PG-3 that assesses the potential of using BBA in construction materials, has acceptable properties to be used as a filler material in road embankments and that, by reducing the level of organic matter, can be used in a wider range of civil infrastructures projects. However, if BBA contains high amounts of organic matter, Hinojosa et al. [185] suggested that it should not be used in building materials because the high chloride content from the organic matter is disadvantageous for the manufacture of reinforced concrete. However, it can be utilized in bulk concrete at a defined percentage of replacement. Rajamma et al. [201] agreed with Hinojosa et al.'s suggestion and pointed out that the presence of chlorides and sulfates in cement materials can reduce durability by causing deterioration of the microstructure.

4.2.4. Biomass/coal co-fired ash

Wang et al. [181] conducted durability research on BFA concrete, where the fly ash includes co-fired fly ash from biomass/coal co-firing and blended fly ash (wood fly ash mixing with coal fly ash). They reported that all types of fly ash concrete have a statistically equal or less weight loss and lower chloride permeability than pure cement concrete. Biomass/coal co-fired ash normally does

not noticeably alter the bulk cement chemistry, and the produced materials have equal or even better performance (strength, alkali silica reaction, durability, deformation, and permeability) than that of coal ashes [178].

In our previous research [26], we found that the cement characteristics of the fly ash produced by agricultural/forestry residue co-firing in a PC furnace are more dependent on the primary fuel coal; a modest co-firing ratio (<20 wt.%) does not affect the fly ash used for cement alternative significantly. The detailed results are presented in Table 12. With or without co-firing, the condensation starting/ending times, expansion and water demand ratio satisfy GB/T1596-2005, although compressive and flexural strengths, as well as the activity index, are lower than the indicators of GB/T1596-2005. Notably, the compressive and flexural strengths and activity index of the fly ash of co-firing (approximately 6% decline) are comparable with the corresponding parameters of the fly ash of coal, and other researchers have presented similar results [138], where co-firing also resulted in decreased compressive and flexural strengths and activity index even though the testing results satisfy GB/T1596-2005; compressive strength and activity index decreased by 5%–6% with co-firing ratio of 9.68 wt.% and 22.7 wt.%.

Given that coal ash as a replacement for cement can improve durability [186,187,194], strength [191,192], abrasion resistance [189], heat evolution [188] and shrinkage [190], we believe that biomass

Table 12

Test results of key parameters for the mortar characteristics of fly ash^a (reprinted from reference 26, with permission of MDPI).

Parameters	Unit	PC	Burner B	Burner D	Burner F	Contrast	Criterion
Condensation starting time	min	234	214	240	225	-	>45
Condensation ending time	h	4.6	4.38	4.47	4.55	-	<10
Expansion	mm	1.9	1.1	1.9	1.6	-	<5
Water demand ratio	%	88.8	93.6	91.2	94.4	-	<95
Flexural strength (7 days)	MPa	4.3	4.4	4.3	4.4	6.2	-
Compressive strength (7 days)	MPa	17.5	16.6	17.1	16.4	27.3	-
Flexural strength (28 days)	MPa	5.9	5.7	5.2	5.4	7.2	≥5.5
Compressive strength (28 days)	MPa	26.2	23.8	24.9	25.1	44.6	≥32.5
Flexural strength (90 days)	MPa	7.2	6.7	7.2	6.9	9.1	-
Compressive strength (90 days)	MPa	38.9	37.2	37.5	37.8	50.1	-
Activity index	%	58.7	53.4	55.8	56.3	100	≥70

^a PC represents dedicated PC combustion; Burner B, D and F mean co-firing by burner B, D and F; Contrast is 100% cement. Activity index: the ratio of the compressive strength of the tested mortar and the standard contrast mortar (28 days). Tests are conducted according to Chinese standard GB/T1596-2005, GSB 14-1510, and GB/T17671-1999.

ash also can be widely used in special constructions after adequate research on selection and various pretreatments.

4.3. Utilization in agriculture and other fields

Soil acidification is aggravated by the extensive use of nitrogen fertilizers. Lime has been widely utilized as an effect approach to neutralize or optimize the soil pH value to 6.5–7.0, a value that is preferred by most crops and maximizes the availability of most nutrients to plants [176,196]. However, its application contributes to global warming because, as the Intergovernmental Panel on Climate Change (IPCC) assumes, all carbon in agricultural lime is finally released as CO₂ to the atmosphere [197]. Therefore, the use of fly ash as an effective substituent for lime in soil improvement has been recommended to reduce net CO₂ emission and global warning [197,234]. Fly ash used as a soil ameliorant brings not only economic benefits but also environmental and ecological benefits compared with conventional disposal, which leads to the degradation of arable land and contamination of ground water [195]. Moreover, the use of fly ash as a soil ameliorant significant promotes the growth and yield of plants [196,235–240] because of the high concentration or increased availability of nutritional elements (K, Na, Zn, Ca, Mg, Fe, etc.) [176,197].

As summarized in Table 13, which shows the application of fly ash to improve problematic soil systems, the effects of FA on soil (shown below) are extensive.

- (1) Optimization of the pH value. FA as a substitute for lime can be utilized to buffer the soil pH between 6.5 and 7.0 [176,234], which is essential to plant growth. At very low pH, i.e., acidic soil, Mn and Al are toxic to plants because of their dissolution and resultant bioavailability [176].
- (2) Alteration of soil texture. Soil and FA mixtures tend to have lower bulk density, higher porosity, higher water-holding capacity, and lower hydraulic conductivity than soil alone [197,220,222,241,242].
- (3) Biota improvement. FA can activate microorganisms in acidic soil [243] and improve enzymatic activity such as invertase, amylase, dehydrogenase, and protease [244].
- (4) Accommodation of plant nutrients. FA in soil can improve the availability of sulfate, carbonate, bicarbonate, chloride, P, K, Ca, Mg, Mn, etc. [222,240] but decrease the amount of Ni, C, Pb, etc. [222].
- (5) Stabilization/immobilization of heavy metal. For heavy metal-contaminated soil, FA addition can inhibit the transport of contaminants into deeper soil layers and into groundwater by metal immobilization [176] and alkalizing effects, which are more significant in acidic soils [245].
- (6) Reduction in global warming. FA is a feasible alternative to lime for treating acidic soil, and lime brings additional CO₂ emission [197,234]. And so on.

Although FA has numerous benefits for soil amendment and crop growth, almost all studies are related to coal FA. Research on BFA is scarce, and extensive research is urgently needed.

Aside from its use as construction materials (cement substituent/additive and aggregate) and in soil amelioration, biomass ash can be utilized in other fields such as flue gas cleaning (as adsorbents for SO_x, NO_x, mercury, and other toxic metals), wastewater treatment (removal of dyes and heavy metals), synthesis of zeolite, production of ceramic, mine backfill, forestry, and wasteland reclamation. All these applications have been reviewed comprehensively in references 176,178,195,200; thus, a review of the literature is not made in this paper.

4.4. Barriers and counterplans for the utilization of biomass ash

Although there are numerous utilization approaches for biomass ash, and many studies have verified their feasibility, the majority of biomass ash is discarded. Technical, economic, institutional, and legal regulations should be established to address the lack of utilization of biomass ash.

Technical verification is essential for the practical use of biomass ash. However, several key parameters such as biomass ash yield, ash properties, commercial validation, user requirements, and related specifications and standards are scarce and sporadic.

Economic balance is another key barrier. For biomass ash utilization that brings extra income, whether or not the income can overcome the logistical costs is the key factor for the producer. Therefore, economic incentives play an important role in biomass ash utilization.

Institutional and legal regulations serve as guidelines for the utilization of biomass ash. Besides the lack of knowledge on potential ash utilization, compositional inconsistencies and changes in the products, belief that other raw materials are readily available, and scarce data on environment and health effects, the lack of state guidelines and laws and rigid or incomplete industry and environment regulations further limit the utilization of biomass ash.

To promote the extensive utilization of biomass ash, firstly, the state or local government should formulate or revise relevant legal regulations to force the implementation of recycling and establish incentive policies that can act as a strong driving force for businesses to strengthen their technological research, various application verification, and market development. Secondly, the cooperation between biomass-fired power plants and other industries should be strengthened; this is the bridge between biomass ash utilization and extending/developing/introducing new applications. Thirdly, technical research on existing potential approaches (e.g., use of biomass ash as construction materials, soil ameliorant, and adsorbents and use in metal recovery) should be intensified. Finally, the logistics between the operator of biomass-fired plants and the users of the ash should be improved concerning ash removal, treatment, storage and transport. At last, ensuring stable biomass and ash qualities is also essential for biomass ash utilization.

5. Conclusions

Although biomass firing and co-firing power plants have been rapidly developed around the world, these power plants continue to face various challenges that arise during combustion. This study focused on intractable ash-related issues, namely, alkali-induced slagging, silicate melt-induce slagging (ash fusion), agglomeration, corrosion, and ash utilization, as well as potential remedies, including the use of additives, co-firing, leaching, alloying, and others.

For alkali-induced slagging, which is mainly associated with alkali metals especially alkali chlorides and sulfates, preliminary alkali-salt generation and transformation mechanisms have been presented to clarify the alkali chemistry during biomass combustion. Alkali chemistry is affected significantly by the fuel species, ash components (such as the concentrations of alkalis, S, Cl, Si, Al, etc. as well as the ratios of alkali/Cl and S/Cl), combustion temperature, and combustion atmosphere (concentrations of SO₂, O₂, H₂O, etc.). The formation of alkali-induced slagging, shown as an alternating overlapping multi-layered structure, and its growth mechanisms are discussed in detail. The formation is highly dependent on the re-enrichment of fine particles containing high concentrations of K, Na, Cl, and S in the forms of alkali chloride and sulfates, the re-capture of coarse particles containing high Si, Al, etc., and the existence of an initial slagging layer primarily containing fine alkali chloride and sulfate particles. The criterion numbers or evaluation indexes, particularly the Cl ratio (Cl + K₂O + Na₂O)/(SiO₂ + Al₂O₃)

Table 13

Application of fly ash to improve problematic soil system (improved on the basis of the summary of Pandey and Singh [176]).

Amendments ^a	FA doses range	Soil type	Remarks	References
FA + soil	FA added to the top 0.15 m coarse textured (sandy) soil 0, 2.5, 5.0, 10.0, 25.0, 50.0 V%	Acidic soil; Duplex soil	Reduce hydraulic conductivity by 25% and improve water-holding capacity	[196]
FA + soil	Greenfield sandy loam; Domino loam; Reyes silty clay; Redding sandy loam; Merced sandy clay loam		At application rates > 25%, there was a consistent increase in water-holding capacity (except domino loam), and a decrease in bulk density and modulus of rupture in all soil tested. The hydraulic conductivity increased with small amounts of fly ash, but declined rapidly as fly ash volume increased. At a low applicant rate, fly ash amendment appeared useful in improving certain agronomic properties of soils.	[220]
FA + soil	0, 9, 20, 28.5, 35.5, 41.2, 46 wt%	-	Fly ash addition reduced density and swelling, and increased void ratio, shear strength and value of cohesion. The fly ash may be effectively utilized in soil to get improvement in shear strength, cohesion, and thus improvement in the bearing capacity.	[221]
FA + soil	0, 10, 20, 30, 40, 50, 60, 70, 80, 90, 100 V%	Filled soil from Aligarh	Increased the porosity, water holding capacity, pH, conductivity, sulfate, carbonate, bicarbonate, chloride, O, K, Ca, Mg, Cu, Zn and B. While significant reduced N content. Plant growth, yield, carotenoids, and chlorophylls were mostly enhanced in the treatment with 40–80% fly ash, being optimal at 50 or 60%. From 60 or 70% onward, the measured parameters tended to reduce, and considerably reduced at 100% fly ash.	[222]
FA + lime + acidic coal spoil	FA:0, 10, 20, 30, 40 g/kg; Lime:0, 10, 20, 40, 80 g/kg	Acidic coal spoils	All rates of lime tested and FA rates at or above 20 g/kg increased the spoil pH, and FA is a feasible alternative to lime for treating acidic coal spoils in the regio.	[234]
FA, CF, FA + CF, FYM + CF, FA + FYM + CF, L + FYM + CF, PFS + CF, FA + PFS + CF, L + PFS + CF, CR + CF, FA + CR + CF	FA:10 t/ha; Organic sources (FYM, PFS and CR):30 g/Nha; Lime: 2 t/ha	Acid lateritic soil	The application 10 t, a of FA in combination with organic sources and chemical fertilizer increased the grain yield and nutrient uptake of rice and pod yield of peanut compared to chemical fertilizers alone.	[235]
FA + acid lateritic soils	-	Sandy loam acid lateritic soil	Integrated use of fly ash, organic wastes and chemical fertilizers was beneficial in improving crop yield, soil pH, organic carbon and available N, P and K in sandy loam acid lateritic soil.	[236]
FA + soil	0, 40, 80, 120 Mg/ha	Loamy fine sand	FA can be a good soil amendment for rice production without B toxicity.	[237]
FA + soil	0, 1, 2.5, 5, 10, 15 Mg/ha	Sandy soil; Sandy loam	Improved physical properties of soil and growth and yield of rice at 10Mg/, ha	[238]
FA + soil	0, 20, 20, 40, 80, 100 V%	Filled soil from Aligarh	40% fly ash caused a higher increase in growth and yield than did 20%; while 60%, 80%, and 100% fly ash had an adverse effect on growth and yield	[239]
FA + soil	20, 40, 60, 80 t/ha	Sandy loam soil	The application of fly ash at 40 t/ha in conjunction with <i>P. striata</i> inoculation improved the bean yield and P uptake by grain. The available phosphorus of soil also showed an upward trend. The fly ash did not exert any detrimental effect on the population of inoculated bacteria.	[240]
FA + soil	0, 280, 560, 1120Mg/ha	-	Improved physical properties of soils (water-holding capacity, plant available water, and water retention capacity)	[241]
FA + soil; Biogas slurry + soil	FA:0, 4, 8, 12 Mg/ha Biogas slurry: 0, 4.5Mg/ha, 15 Mg/ha	Ustochrept	Both types of amendments reduced bulk density, and increased saturated hydraulic conductivity and moisture retention capacity of soil.	[242]
FA + soil; FA + soil + sludge(5%)	0, 5, 10, 20 wt%	Silt loam soil	High rates of FA to soil may hinder normal decomposition and nutrient cycling processes.	[243]
FA + soil	0, 10, 12.5, 15, 17.5, 20 t/ha	Sandy-loam	Invertase, amylase, dehydrogenase and protease activity increased with increasing application of fly-ash up to 10 t/ha, but decreased with higher levels of FA application.	[244]
FA + soil; Soil + (Zn, Cu, Ni and Cd); FA + soil + (Zn, Cu, Ni and Cd)	3%	Poorly buffered acidic soils	Alkalizing effects of FA can be utilized to reduce plant accumulation of potentially toxic elements, particularly in poorly buffered acidic soils.	[245]
FA + soil	3, 5, 12 wt%	Sandy loam soil	3% FA amendment on sandy loam soil enhanced decomposition rate of soil organic carbon in comparison to control.	[246]
FA + soil; FA + soil + FTM(5 g/, kg)	80, 160 g/kg	Acid alfisol	Higher microbial activities in soil amended with up to 8% FA and combined application of FYM and FA proved to be beneficial in augmenting proliferation and activity of microorganisms in acid soil.	[247]
FA + soil	0, 10, 20, 30, 40 wt%	Clayey; Sandy- clay-loam; Sandy; Sandy-loam	FA incorporation in texturally variant soils modifies the soil physical and physico-chemical environment that in turn may influence the crop yields.	[248]
FA + soil	0, 2, 5, 10, 15, 20%	Acidic soil	Helped to reduce metal solubility and availability to plants	[249]
FA + soil	10, 25, 50%	-	Improved physico-chemical properties of soil and plant grown, net primary productivity, leaf area and photosynthetic pigments.	[250]
FA + soil	0, 3, 6, 12, 30 wt%	Sandy soil; Sandy loam	The electrical conductivity and pH of both recipient soils were raised, but more so for the sandy soil. The increase in electrical conductivity may limit the availability of soil water because of the high osmotic pressure and the increased pH would alter the availability of micro-elements to plants.	[251]
FA + soil	0, 3, 6, 12%	Calcareous heavy loam soil (Ustarents)	FA at the highest rate raised the pH of sandy soil and sandy loam from 7.3 and 6.7 to 9.7 and 8.6, respectively. Both accumulation and reduction of metals in plant tissue were significantly correlated with the pH of FA-amended soils.	[252]
FA + soil	FA depths: 5, 7 and 10 cm in bottom of pots; total depths of growth substrate: 15 cm; mycorrhizal treatments	Two paddy soils of contrasting textures	Arbuscular mycorrhizal (AM) fungi may make a substantial contribution to successful crop establishment in soils overlying areas of coal fly ash.	[253]
FA + phospho-gypsum + soil	FA + phospho-gypsum (50:50, w/w) mixture: 0, 20, 40, 60 Mg/ha	Silt loam; Loamy sand	FA + phospho-gypsum should reduce P loss from rice paddy soils due to the high Ca content in this mixture, which might convert water-soluble P to less soluble forms by precipitation process and increase soil fertility.	[254]

^a FA: Fly ash; FYM: farmyard manure; CF: chemical fertilizer; I: lime; PFS: paper factory sludge; CR: crop residue.

and S ratio ($S_{\text{volatile}} + K_2O + Na_2O$)/($SiO_2 + Al_2O_3$), that influence the formation and growth of slagging are also discussed. Subsequently, considerable attention should be focused on research into the kinetics of R 1–R 15, which are essential for the transformation, and sequestration of alkali species. Meanwhile, further evaluation and improvement on the existing criterion numbers of alkali-induced slagging based on industry practice are necessary.

Silicate melt-induced slagging (ash fusion) depends not only on the elemental composition, where the initial deformation temperature increases as the contents of MgO , CaO , Fe_2O_3 , and Al_2O_3 increase and decrease with increasing K_2O and SiO_2 contents in the ash, but also on the mineral components, where refractory minerals (such as quartz, metakaolinite, and mullite) increase ash fusion temperatures and fluxing minerals (such as anhydrite, calcium silicate, and hematite) reduce them. The effects and evolution of both elemental and mineral components during combustion should be addressed together. In addition, the pseudo 4D phase diagrams of (Ma_2O) -MaeO- P_2O_5 - Al_2O_3 and (Ma_2O) -MaeO- SiO_2 - Al_2O_3 can serve as effective tools to forecast the ash fusion characteristics or the potential properties of melt-induced slagging; however, the diagrams should be constructed according to statistical data from real biomass ashes rather than from simulated ashes obtained by the addition of partial metal oxides to biomass/biomass ashes or the direct mixing of metal oxides. A combination of heterogeneous chemical kinetics and multiphase equilibrium models is essential to estimate the speciation, saturation levels, and the presence of melt of ash-forming matter and to obtain reliable guidance.

Agglomeration, which typically occurs in FB, results from the interaction between ash-forming elements in the fuel and the bed particles. For fuels containing K and relatively low Si content, bed agglomeration is initiated by molten potassium silicates formed on the bed particle surfaces by reaction with gaseous or liquid K compounds. The bed material plays an active role in the agglomeration processes. For fuels with high alkali metal and organically bound Si or P content, bed agglomeration is initiated by the direct adhesion of bed particles by partly molten ash-derived potassium silicate particles/droplets and potassium phosphates particles/droplets; agglomeration is more dependent on the compositions of the fuel ash. The former is called “coating-induced” agglomeration, and the latter is called “melt-induced” agglomeration. Generally, quartz and natural sand bed materials are problematic when fuels with high alkali metal content are combusted. Olivine and blast-furnace slag can be successfully used as bed material substituent. However, the optimal solution for agglomeration requires further study, particularly to find effective combinations of fuels and bed materials, as well as practical agglomeration indicators.

Corrosion that occurs in biomass combustion is initiated by Cl_2 , gaseous alkali chlorides, solid/deposited alkali chlorides, molten alkali chlorides, molten alkali sulfates, molten alkali carbonates, and sulfation/silication of alkali chlorides. High temperatures improve the diffusion of gas reactants (Cl_2 and O_2) and gaseous reaction products (KCl and $CrCl_2$) and, thus, result in accelerated corrosion. For certain alkali chlorides, the corrosion strength of the molten state is the highest followed by that of the solid state; the gaseous state causes the smallest degree of corrosion. The presence of potassium induces initial oxidation acceleration with potassium chromate formed as the intermediate. The presence of chlorides and chlorine is essential for corrosion to continue. For molten state corrosion, high Cr content accelerates corrosion by forming low-melting $K_2Cr_2O_7$ and eutectic $KCl-K_2CrO_4$. For other types of corrosion related to active oxidation to some extent, high Cr content inhibits the process by forming a protective Cr_2O_3 oxide layer because of higher Cr supply than loss by evaporation. Aside from Cr, research on Si, Al, and Co, which exhibit high corrosion resistance when used as coating or alloying elements, should be strengthened. Meanwhile, heavy metals

such as Zn and Pb, which may form low melting chlorides and accelerate corrosion, need scrupule.

Alkali chlorides and sulfates, as the dominant alkali species responsible for the mentioned ash-related issues, can be controlled by using additives, co-firing, and leaching. Lime/calcite, kaolin, zeolites, and sulfur are effective additive candidates for certain problems; however, in practice, the combined effect of these additives on all aspects of the ash-related problems should be balanced. For example, sulfur can reduce corrosion initiated by chlorine present in deposits, but it may result in a high deposit formation rate and could worsen slagging. Co-firing, as the most effective remedy, also requires further industrial practice verification. Through leaching, the elements (K, Na, Cl, and S) that cause significant problems during combustion can be completely removed, solving the ash-related problems. However, a proper leaching process (including water amount, water application rate, and leaching duration/time) should be implemented because of the combined effect of both diffusion control and mechanical processes. In addition, as a supplement for technical leaching, natural leaching by rain and snow during the field drying period should be encouraged as an option in bio-fuel quality optimization.

With the rapid development of biomass combustion power generation, the large volumes of ash produced as a by-product have become an intractable problem throughout the world. The majority of biomass ashes is discarded because the standards for ash utilization of various countries are restrictive; in particular, in the two main potential fields of construction material and agricultural soil ameliorant. To promote the extensive utilization of biomass ash, legal regulations, cooperation between biomass-fired power plants and other industries, potential technical research and logistics should be strengthened.

Lastly, alkali-induced slagging, silicate melt-induced slagging (ash fusion), agglomeration, and corrosion occur concurrently and should thus be investigated jointly rather than separately.

Acknowledgements

Y Niu conceived and performed the whole research; collected and analyzed the data; and wrote the paper. H Tan and S Hui were involved in the design of Sections 2.2.1–2.2.3. The present work was supported by National Natural Science Foundation of China (51406149), the Fundamental Research Funds for the Central Universities (2014ghz08), and China Postdoctoral Science Foundation funded project (2014T70921). The authors would like to thank Xiaolin Wei from Chinese Academy of Sciences for providing the original illustrations of Fig. 4a and 4b; Haitao Ma from Dalian University of Technology for providing the original illustrations of Figs. 35a, 35b, and 42; Håkan Kassman from Chalmers University of Technology for providing the original illustration of Fig. 22; Qinghai Li from Tsinghua University for providing the original sub-illustration of Fig. 1; and Jesper Liske from Chalmers University of Technology for providing the original illustration of Fig. 45. Also, the authors thank Xing Liu, a PHD candidate in Xi'an Jiaotong University, for his assistance with reproduction of Figs. 31–33. Note also that we are sorry for the possible slight differences between the reproduced illustrations (Figs. 17, 21, 28–33, 37, 38, 43–47) and the original that show low resolution.

References

- [1] Scheffer K, Stulpnagel R. Biomass for Energy, London: Pergamon; 2002.
- [2] Yifu C. Rental market analysis of biomass power generation equipment, (translated from Chinese). <http://blog.sina.com.cn/s/blog_4985aeed0100c5g7.html>; 2009 [accessed 14.10.15].
- [3] Li L, Yu C, Huang F, Bai J, Fang M, Luo Z. Study on the deposits derived from a biomass circulating fluidized-bed boiler. *Energ Fuel* 2012;26:6008–14.

- [4] National Development and Reform Comission. Mid-long term development plan for renewable energy. *Renew Energ Resour* 2007;25:1–5.
- [5] Rycroft M, editor. Co-firing biomass with coal for power generation. EE Publishers; 2015.
- [6] Niu YQ, Tan HZ, Ma L, Pourkashanian M, Liu ZN, Liu Y, et al. Slagging Characteristics on the superheaters of a 12 MW biomass-fired boiler. *Energ Fuel* 2010;24:5222–7.
- [7] Li QH, Zhang YG, Meng AH, Li L, Li GX. Study on ash fusion temperature using original and simulated biomass ashes. *Fuel Process Technol* 2013;107:107–12.
- [8] Yu C, Tang Z, Zeng L, Chen C, Gong B. Experimental determination of agglomeration tendency in fluidized bed combustion of biomass by measuring slip resistance. *Fuel* 2014;128:14–20.
- [9] Xiong SJ, Burvall J, Orberg H, Kalen G, Thyrel M, Ohman M, et al. Slagging characteristics during combustion of corn stovers with and without kaolin and calcite. *Energ Fuel* 2008;22:3465–70.
- [10] Bowie D. Operational experience with a high fouling biomass fuel. In: Livingston B, editor. Ash related issues in biomass combustion. Glasgow, Scotland: ThermalNet; 2006.
- [11] Baxter LL. Influence of ash deposit chemistry and structure on physical and transport properties. *Fuel Process Technol* 1998;56:81–8.
- [12] Niu Y, Zhu Y, Tan H, Hui S, Jing Z, Xu W. Investigations on biomass slagging in utility boiler: criterion numbers and slagging growth mechanisms. *Fuel Process Technol* 2014;128:499–508.
- [13] Ohman M, Boman C, Hedman H, Nordin A, Bostrom D. Slagging tendencies of wood pellet ash during combustion in residential pellet burners. *Biomass Bioenerg* 2004;27:585–96.
- [14] Melissari B. Ash related problems with high alkali biomass and its mitigation-experimental evaluation. *Memoria Investigaciones en Ingeniería (Mem Invest Eng)* 2014;31:44.
- [15] Niu YQ, Tan HZ, Wang XB, Liu ZN, Liu HY, Liu Y, et al. Study on fusion characteristics of biomass ash. *Bioresour Technol* 2010;101:9373–81.
- [16] Niu Y, Du W, Tan H, Xu W, Liu Y, Xiong Y, et al. Further study on biomass ash characteristics at elevated ashing temperatures: the evolution of K, Cl, S and the ash fusion characteristics. *Bioresour Technol* 2013;129:642–5.
- [17] De Geyter S, Ohman M, Bostrom D, Eriksson M, Nordin A. Effects of non-quartz minerals in natural bed sand on agglomeration characteristics during fluidized bed combustion of biomass fuels. *Energ Fuel* 2007;21:2663–8.
- [18] Piispanen MH, Niemela ME, Tiainen MS, Laitinen RS. Prediction of bed agglomeration propensity directly from solid biofuels: a look behind fuel indicators. *Energ Fuel* 2012;26:2427–33.
- [19] Ohman M, Nordin A, Skrifvars BJ, Backman R, Hupa M. Bed agglomeration characteristics during fluidized bed combustion of biomass fuels. *Energ Fuel* 2000;14:169–78.
- [20] Visser HJM. The influence of fuel composition on agglomeration behaviour in fluidised-bed combustion. ECN-C-04-054, Sep. 2004.
- [21] Viklund P, Hjornhede A, Henderson P, Stalenheim A, Pettersson R. Corrosion of superheater materials in a waste-to-energy plant. *Fuel Process Technol* 2013;105:106–12.
- [22] Nielsen HP, Frandsen FJ, Dam-Johansen K, Baxter LL. The implications of chlorine-associated corrosion on the operation of biomass-fired boilers. *Prog Energ Combust* 2000;26:283–98.
- [23] Ma HT, Zhou CH, Wang L. High temperature corrosion of pure Fe, Cr and Fe-Cr binary alloys in O₂-containing trace KCl vapour at 750 degrees C. *Corros Sci* 2009;51:1861–7.
- [24] Khan AA, de Jong W, Jansens PJ, Spliethoff H. Biomass combustion in fluidized bed boilers: potential problems and remedies. *Fuel Process Technol* 2009;90:21–50.
- [25] van Eijk RJ, Obernberger I, Supancic K. Options for increased utilization of ash from biomass combustion and co-firing. IEA Bioenergy Task 32: Biomass combustion and co-firing. Arnhem, Netherlands 2012.
- [26] Xu W, Niu Y, Tan H, Wang D, Du W, Hui S. A new agro/forestry residues co-firing model in a large pulverized coal furnace: technical and economic assessments. *Energies* 2013;6:4377–93.
- [27] Elled AL, Davidsson KO, Amand LE. Sewage sludge as a deposit inhibitor when co-fired with high potassium fuels. *Biomass Bioenerg* 2010;34:1546–54.
- [28] Livingston WR. Biomass ash characteristics and behavior in combustion systems. Workshop on ash related issues in biomass combustion. Glasgow: IEA Task 32; 2006, 9.
- [29] Livingston WR. Biomass ash deposition, erosion and corrosion processes. Workshop on ash related issues in biomass combustion. Glasgow: IEA Task 32/Thermalnet Workshop; 2006.
- [30] Liu H, Feng Y, Wu S, Liu D. The role of ash particles in the bed agglomeration during the fluidized bed combustion of rice straw. *Bioresour Technol* 2009;100:6505–13.
- [31] Nutalapati D, Gupta R, Moghtaderi B, Wall TF. Assessing slagging and fouling during biomass combustion: a thermodynamic approach allowing for alkali/ash reactions. *Fuel Process Technol* 2007;88:1044–52.
- [32] Niu YQ, Liu YY, Tan HZ, Xiong YY, Xu TM. Origination and formation of NH₄Cl in biomass-fired furnace. *Fuel Process Technol* 2013;106:262–6.
- [33] Tonn B, Thumm U, Lewandowski I, Claupein W. Leaching of biomass from semi-natural grasslands – Effects on chemical composition and ash high-temperature behaviour. *Biomass Bioenerg* 2012;36:390–403.
- [34] Lindstrom E, Larsson SH, Bostrom D, Ohman M. Slagging characteristics during combustion of woody biomass pellets made from a range of different forestry assortments. *Energ Fuel* 2010;24:3456–61.
- [35] Werkelin J, Skrifvars BJ, Hupa M. Ash-forming elements in four Scandinavian wood species. Part 1: summer harvest. *Biomass Bioenerg* 2005;29:451–66.
- [36] Garba MU, Ingham DB, Ma L, Porter RTJ, Pourkashian M, Tan HZ, et al. Prediction of potassium chloride sulfation and its effect on deposition in biomass-fired boilers. *Energ Fuel* 2012;26:6501–8.
- [37] Aho M. Reduction of chlorine deposition in FB boilers with aluminium-containing additives. *Fuel* 2001;80:1943–51.
- [38] Jimenez S, Ballester J. Influence of operating conditions and the role of sulfur in the formation of aerosols from biomass combustion. *Combust Flame* 2005;140:346–58.
- [39] Reichelt J, Pfarrang-Stotz G, Bergfeldt B, Seifert H, Knapp P. Formation of deposits on the surfaces of superheaters and economisers of MSW incinerator plants. *Waste Manage* 2013;33:43–51.
- [40] Tran QK, Steenari BM, Iisa K, Lindqvist O. Capture of potassium and cadmium by kaolin in oxidizing and reducing atmospheres. *Energ Fuel* 2004;18:1870–6.
- [41] Steenari BM, Lindqvist O. High-temperature reactions of straw ash and the anti-sintering additives kaolin and dolomite. *Biomass Bioenerg* 1998;14:67–76.
- [42] Raclavska H, Juchelkova D, Roubicek V, Matysek D. Energy utilisation of biowaste – Sunflower-seed hulls for co-firing with coal. *Fuel Process Technol* 2011;92:13–20.
- [43] Khan AA, Aho M, de Jong W, Vainikka P, Jansens PJ, Spliethoff H. Scale-up study on combustibility and emission formation with two biomass fuels (B quality wood and pepper plant residue) under BFB conditions. *Biomass Bioenerg* 2008;32:1311–21.
- [44] Werkelin J, Skrifvars BJ, Zevenhoven M, Holmbom B, Hupa M. Chemical forms of ash-forming elements in woody biomass fuels. *Fuel* 2010;89:481–93.
- [45] Turn SQ, Kinoshita CM, Ishimura DM. Removal of inorganic constituents of biomass feedstocks by mechanical dewatering and leaching. *Biomass Bioenerg* 1997;12:241–52.
- [46] Li YS, Spiegel M, Shimada S. Corrosion behaviour of various model alloys with NaCl-KCl coating. *Mater Chem Phys* 2005;93:217–23.
- [47] Uusitalo MA, Vuoristo PMJ, Mantyla TA. High temperature corrosion of coatings and boiler steels below chlorine-containing salt deposits. *Corros Sci* 2004;46:1311–31.
- [48] Bostrom D, Skoglund N, Grimm A, Boman C, Ohman M, Brostrom M, et al. Ash transformation chemistry during combustion of biomass. *Energ Fuel* 2012;26:85–93.
- [49] Liu RP. Slagging characteristics and alkali migration during straw combustion: Southeast University; 2008 (Chinese).
- [50] Wang L, Hustad JE, Gronli M. Sintering characteristics and mineral transformation behaviors of corn cob ashes. *Energ Fuel* 2012;26:5905–16.
- [51] Glarborg P, Marshall P. Mechanism and modeling of the formation of gaseous alkali sulfates. *Combust Flame* 2005;141:22–39.
- [52] Davidsson KO, Amand LE, Steenari BM, Elled AL, Eskilsson D, Leckner B. Countermeasures against alkali-related problems during combustion of biomass in a circulating fluidized bed boiler. *Chem Eng Sci* 2008;63:5314–29.
- [53] Oleschko H, Muller M. Influence of coal composition and operating conditions on the release of alkali species during combustion of hard coal. *Energ Fuel* 2007;21:3240–8.
- [54] Diaz-Ramirez M, Boman C, Sebastian F, Royo J, Xiong S, Bostrom D. Ash characterization and transformation behavior of the fixed-bed combustion of novel crops: poplar, brassica, and cassava fuels. *Energ Fuel* 2012;26:3218–29.
- [55] Vanvuka D, Zografas D, Alevizos G. Control methods for mitigating biomass ash-related problems in fluidized beds. *Bioresour Technol* 2008;99:3534–44.
- [56] Brus E, Ohman M, Nordin A, Bostrom D, Hedman H, Eklund A. Bed agglomeration characteristics of biomass fuels using blast-furnace slag as bed material. *Energ Fuel* 2004;18:1187–93.
- [57] Chen AH, Yang XM, Lin WG. Thermodynamic equilibrium analysis on release characteristics of chlorine and alkali metals during combustion of biomass residues. *Chin J Process Eng* 2007;989–98.
- [58] Xiong SJ, Ohman M, Zhang YF, Lestander T. Corn stalk ash composition and its melting (slagging) behavior during combustion. *Energ Fuel* 2010;24:4866–71.
- [59] Jia Y, Lighty JS. Ash particulate formation from pulverized coal under oxy-fuel combustion conditions. *Environ Sci Technol* 2012;46:5214–21.
- [60] Niu YQ, Tan HZ, Wang XB, Liu ZN, Liu Y, Xu TM. Study on deposits on the surface, upstream, and downstream of bag filters in a 12 MW biomass-fired boiler. *Energ Fuel* 2010;24:2127–32.
- [61] Wei XL, Schnell U, Hein KRG. Behaviour of gaseous chlorine and alkali metals during biomass thermal utilisation. *Fuel* 2005;84:841–8.
- [62] Mu L, Zhao L, Liu L, Yin H. Elemental distribution and mineralogical composition of ash deposits in a large-scale wastewater incineration plant: a case study. *Ind Eng Chem Res* 2012;51:8684–94.
- [63] Lindberg D, Backman R, Chartrand P, Hupa M. Towards a comprehensive thermodynamic database for ash-forming elements in biomass and waste combustion – Current situation and future developments. *Fuel Process Technol* 2013;105:129–41.
- [64] Brus E, Ohman M, Nordin A. Mechanisms of bed agglomeration during fluidized-bed combustion of biomass fuels. *Energ Fuel* 2005;19:825–32.
- [65] Grimm A, Skoglund N, Bostrom D, Ohman M. Bed agglomeration characteristics in fluidized quartz bed combustion of phosphorus-rich biomass fuels. *Energ Fuel* 2011;25:937–47.
- [66] Vassilev SV, Kitano K, Takeda S, Tsurue T. Influence of mineral and chemical-composition of coal ashes on their fusibility. *Fuel Process Technol* 1995;45:27–51.

- [67] Niu Y, Zhu Y, Tan H, Wang X, Hui S, Du W. Experimental study on the coexistent dual slagging in biomass-fired furnaces: alkali- and silicate melt-induced slagging. *P Combust Inst* 2015;35:2405–13.
- [68] Olson JG, Jaglid U, Pettersson JBC, Hald P. Alkali metal emission during pyrolysis of biomass. *Energ Fuel* 1997;11:779–84.
- [69] Blomberg T. A thermodynamic study of the gaseous potassium chemistry in the convection sections of biomass fired boilers. *Mater Corros* 2011;62:635–41.
- [70] Thy P, Jenkins BM, Grundvig S, Shiraki R, Lesher CE. High temperature elemental losses and mineralogical changes in common biomass ashes. *Fuel* 2006;85:783–95.
- [71] Dayton DC, Milne TA. Laboratory measurements of alkali metal containing vapors released during biomass combustion. In: Baxter L, DeSollar R, editors. Applications of advanced technology to ash-related problems in boilers. Waterville Valley: 1996. p. 161–85.
- [72] Kai XP. The influence of sulfur on the migration characteristics of alkali during biomass and coal co-combustion. Shenyang Aerospace University; 2010 (Chinese).
- [73] Pettersson A, Amand LE, Steenari BM. Chemical fractionation for the characterisation of fly ashes from co-combustion of biofuels using different methods for alkali reduction. *Fuel* 2009;88:1758–72.
- [74] Sengelov LW, Hansen TB, Bartolome C, Wu H, Pedersen KH, Frandsen FJ, et al. Sulfation of condensed potassium chloride by SO₂. *Energ Fuel* 2013;27:3283–9.
- [75] Matsuda H, Ozawa S, Naruse K, Ito K, Kojima Y, Yanase T. Kinetics of HCl emission from inorganic chlorides in simulated municipal wastes incineration conditions. *Chem Eng Sci* 2005;60:545–52.
- [76] Henriksson M, Wärnqvist B. Kinetics of formation of HCl(g) by the reaction between NaCl(s) and SO₂, O₂, and H₂O(g). *Ind Eng Chem Process Des Dev* 1979;18:249–54.
- [77] Boonsongsup L, Iisa K, Frederick WJ. Kinetics of the sulfation of NaCl at combustion conditions. *Ind Eng Chem Res* 1997;36:4212–16.
- [78] Li B, Sun Z, Li Z, Alden M, Jakobsen JG, Hansen S, et al. Post-flame gas-phase sulfation of potassium chloride. *Combust Flame* 2013;160:959–69.
- [79] Kassman H, Bafver L, Amand L-E. The importance of SO₂ and SO₃ for sulphation of gaseous KCl – An experimental investigation in a biomass fired CFB boiler. *Combust Flame* 2010;157:1649–57.
- [80] Wang X, Liu Y, Tan H, Ma L, Xu T. Mechanism research on the development of ash deposits on the heating surface of biomass furnaces. *Ind Eng Chem Res* 2012;51:12984–92.
- [81] Liu HY, Tan HZ, Liu Y, Liu ZN, Ma L, Pourkashanian M, et al. Study of the layered structure of deposit in a biomass-fired boiler (case study). *Energ Fuel* 2011;25:2593–600.
- [82] Zhou H, Zhou B, Dong K, Ding JZ, Cen KF. Research on the slagging characteristics of easy to slagging coal in a pilot scale furnace. *Fuel* 2013;109:608–15.
- [83] Jenkins B, Baxter L, Miles T Jr, Miles T. Combustion properties of biomass. *Fuel Process Technol* 1998;54:17–46.
- [84] Wang S, Jiang XM, Han XX, Wang H. Fusion characteristic study on seaweed biomass ash. *Energ Fuel* 2008;22:2229–35.
- [85] Ye Y. Research on the characteristics of biomass ash and agglomeration mechanism [D]: Huazhong University of Science & Technology; 2007.
- [86] Hu Y, Cheng S, Sun P, Xie J, Zhang H. Research on fusion behavior of ash from mixedly burning biomass with coal. *Therm Power Gen* 2011;40:8–12.
- [87] Wang L, Skjervik G, Hustad JE, Grønli MG. Effects of sewage sludge and marble sludge addition on slag characteristics during wood waste pellets combustion. *Energ Fuel* 2011;25:5775–85.
- [88] Folgueras MB, Diaz RM, Xiberta J, Garcia MP, Pis JJ. Influence of sewage sludge addition on coal ash fusion temperatures. *Energ Fuel* 2005;19:2562–70.
- [89] van Dyk JC. Understanding the influence of acidic components (Si, Al, and Ti) on ash flow temperature of South African coal sources. *Miner Eng* 2006;19:280–6.
- [90] Gray VR. Prediction of ash fusion temperature from ash composition for some New Zealand coals. *Fuel* 1987;66:1230–9.
- [91] Nuutinen LH, Tiainen MS, Virtanen ME, Enestam SH, Laitinen RS. Coating layers on bed particles during biomass fuel combustion in fluidized-bed boilers. *Energ Fuel* 2004;18:127–39.
- [92] Morey G, Kracek F, Bowen N. The ternary system K₂O-CaO-SiO₂. *J Soc Glass Technol* 1930;14:149–87.
- [93] Ricker R, Osborn E. Additional phase equilibrium data for the system CaO-MgO-SiO₂. *J Am Ceram Soc* 1954;37:133–9.
- [94] Seggiani M. Empirical correlations of the ash fusion temperatures and temperature of critical viscosity for coal and biomass ashes. *Fuel* 1999;78:1121–5.
- [95] Ozbayoglu G, Ozbayoglu ME. A new approach for the prediction of ash fusion temperatures: a case study using Turkish lignites. *Fuel* 2006;85:545–52.
- [96] Gilbe C, Lindstrom E, Backman R, Samuelsson R, Burvall J, Ohman M. Predicting slagging tendencies for biomass pellets fired in residential appliances: a comparison of different prediction methods. *Energ Fuel* 2008;22:3680–6.
- [97] Xiao RR, Chen XL, Wang FC, Yu GS. The physicochemical properties of different biomass ashes at different ashing temperature. *Renew Energ* 2011;36:244–9.
- [98] Thy P, Lesher CE, Jenkins BM. Experimental determination of high-temperature elemental losses from biomass slag. *Fuel* 2000;79:693–700.
- [99] Vamvuka D, Zografos D. Predicting the behaviour of ash from agricultural wastes during combustion. *Fuel* 2004;83:2051–7.
- [100] Johansen JM, Jakobsen JG, Frandsen FJ, Glarborg P. Release of K, Cl, and S during pyrolysis and combustion of high-chlorine biomass. *Energ Fuel* 2011;25:4961–71.
- [101] Olofsson G, Ye ZC, Bjerle I, Andersson A. Bed agglomeration problems in fluidized-bed biomass combustion. *Ind Eng Chem Res* 2002;41:2888–94.
- [102] Grimm A, Ohman M, Lindberg T, Fredriksson A, Bostrom D. Bed agglomeration characteristics in fluidized-bed combustion of biomass fuels using olivine as bed material. *Energ Fuel* 2012;26:4550–9.
- [103] Laitinen R, Nuutinen L, Tiainen M, Virtanen M. An improved bed material for the BFB-boilers. Case 2: Combustion of fuel with high Na content. 5th European Conference on Industrial Furnaces and Boilers. Porto, Portugal, 11–14 April 2000.
- [104] Lind T, Valmari T, Kauppinen E, Nilsson K, Sfiris G, Maenhaut W. Ash formation mechanisms during combustion of wood in circulating fluidised beds. 28th International Symposium on Combustion. Edinburgh 30 July–4 August 2000.
- [105] Visser HJM, Hofmans H, Huijnen H, Kastelein R, Kiel JHA. Biomass ash bed material interaction leading to agglomeration in fluidised bed combustion and gasification. Blackwell Science; 2001.
- [106] Latva-Somppi J, Kurkela J, Tapper U, Kauppinen EI, Jokiniemi JK, Johansson B. Ash Deposition on Bed Material Particles during Fluidized Bed Combustion of Wood-Based Fuels ABC '98 International Conference on Ash Behaviour Control in Energy Conversion Systems Yokohama, Japan; 1998. p. 110–18.
- [107] Niu YQ, Tan HZ, Wang XB, Xu TM, Liu ZN, Liu Y. Fusion characteristics of capsicum stalk ash. *Asia Pac J Chem Eng* 2011;6:679–84.
- [108] Bapat DW, Kulkarni SV, Bhandarkar VP. Design and operating experience on fluidized bed boiler burning biomass fuels with high alkali ash. The 14th International Conference on Fluidized Bed Combustion. New York: ASME; 1997. p. 165–74.
- [109] Bostrom D, Grimm A, Boman C, Bjornbom E, Ohman M. Influence of kaolin and calcite additives on ash transformations in small-scale combustion of oat. *Energ Fuel* 2009;23:5184–90.
- [110] Steenari BM, Lundberg A, Pettersson H, Wilewska-Bien M, Andersson D. Investigation of ash sintering during combustion of agricultural residues and the effect of additives. *Energ Fuel* 2009;23:5655–62.
- [111] Kassman H, Pettersson J, Steenari B-M, Amand L-E. Two strategies to reduce gaseous KCl and chlorine in deposits during biomass combustion – injection of ammonium sulphate and co-combustion with peat. *Fuel Process Technol* 2013;105:170–80.
- [112] Davidsson KO, Korsgren JG, Pettersson JBC, Jaglid U. The effects of fuel washing techniques on alkali release from biomass. *Fuel* 2002;81:137–42.
- [113] Dayton DC, Jenkins BM, Turn SQ, Bakker RR, Williams RB, Belle-Oudry D, et al. Release of inorganic constituents from leached biomass during thermal conversion. *Energ Fuel* 1999;13:860–70.
- [114] Arvelakis S, Vourliotis P, Kakaras E, Koukios EG. Effect of leaching on the ash behavior of wheat straw and olive residue during fluidized bed combustion. *Biomass Bioenerg* 2001;20:459–70.
- [115] Eldabbagh F, Ramesh A, Hawari J, Hutny W, Kozinski JA. Particle-metal interactions during combustion of pulp and paper biomass in a fluidized bed combustor. *Combust Flame* 2005;142:249–57.
- [116] Lindstrom E, Sandstrom M, Bostrom D, Ohman M. Slagging characteristics during combustion of cereal grains rich in phosphorus. *Energ Fuel* 2007;21:710–17.
- [117] Zevenhoven M, Yrjas P, Skrifvars B-J, Hupa M. Characterization of ash-forming matter in various solid fuels by selective leaching and its implications for fluidized-bed combustion. *Energ Fuel* 2012;26:6366–86.
- [118] Boström D, Skoglund N, Grimm A, Boman C, Ohman M, Broström M, et al. Ash transformation chemistry during combustion of biomass. *Energ Fuel* 2011;26:85–93.
- [119] Folgueras MB, Diaz RM, Xiberta J. Sulphur retention during co-combustion of coal and sewage sludge. *Fuel* 2004;83:1315–22.
- [120] Thy P, Jenkins BM, Lesher CE. High-temperature melting behavior of urban wood fuel ash. *Energ Fuel* 1999;13:839–50.
- [121] Wang L, Becidan M, Skreiber Ø. Sintering behavior of agricultural residues ashes and effects of additives. *Energ Fuel* 2012;26:5917–29.
- [122] Lindstrom E, Ohman M, Backman R, Bostrom D. Influence of sand contamination on slag formation during combustion of wood derived fuels. *Energ Fuel* 2008;22:2216–20.
- [123] Zheng Y, Jensen PA, Jensen AD. A kinetic study of gaseous potassium capture by coal minerals in a high temperature fixed-bed reactor. *Fuel* 2008;87:3304–12.
- [124] Tran KQ, Iisa K, Steenari BM, Lindqvist O. A kinetic study of gaseous alkali capture by kaolin in the fixed bed reactor equipped with an alkali detector. *Fuel* 2005;84:169–75.
- [125] Kassman H, Brostrom M, Berg M, Amand LE. Measures to reduce chlorine in deposits: application in a large-scale circulating fluidised bed boiler firing biomass. *Fuel* 2011;90:1325–34.
- [126] Aho M, Silvennoinen J. Preventing chlorine deposition on heat transfer surfaces with aluminium-silicon rich biomass residue and additive. *Fuel* 2004;83:1299–305.
- [127] Aho M, Ferrer E. Importance of coal ash composition in protecting the boiler against chlorine deposition during combustion of chlorine-rich biomass. *Fuel* 2005;84:201–12.
- [128] Bridgeman TG, Jones JM, Williams A, Waldron DJ. An investigation of the grindability of two torrefied energy crops. *Fuel* 2010;89:3911–18.
- [129] Livingston WR. Biomass ash and the mixed ashes from co-firing biomass with coal. Co-firing biomass with coal workshop. Drax Power Station, UK: IEA Clean Coal Workshop; 2011.
- [130] Savolainen K. Co-firing of biomass in coal-fired utility boilers. *Appl Energ* 2003;74:369–81.

- [131] Baxter L. Biomass-coal co-combustion: opportunity for affordable renewable energy. *Fuel* 2005;84:1295–302.
- [132] Shaw Y, Wang J, Preto F, Zhu J, Xu C. Ash deposition in biomass combustion or co-firing for power/heat generation. *Energies* 2012;5:5171–89.
- [133] Tariq AS, Purvis MRI. NO_x emissions and thermal efficiencies of small scale biomass-fuelled combustion plant with reference to process industries in a developing country. *Int J Energ Res* 1996;20:41–55.
- [134] National Renewable Energy Laboratory, Department of Energy (DOE), U.S. Biopower Factsheet – Biomass Cofiring: A Renewable Alternative for Utilities (DOE/GP-102000-1055). 2000.
- [135] Nordin A. Optimization of sulfur retention in ash when cocombusting high sulfur fuels and biomass fuels in a small pilot scale fluidized bed. *Fuel* 1995;74:615–22.
- [136] Sandberg J, Karlsson C, Fdhila RB. A 7 year long measurement period investigating the correlation of corrosion, deposit and fuel in a biomass fired circulated fluidized bed boiler. *Appl Energ* 2011;88:99–110.
- [137] Huang Y, McIlveen-Wright D, Rezvani S, Wang YD, Hewitt N, Williams BC. Biomass co-firing in a pressurized fluidized bed combustion (PFBC) combined cycle power plant: a techno-environmental assessment based on computational simulations. *Fuel Process Technol* 2006;87:927–34.
- [138] Wang XB, Tan HZ, Niu YQ, Pourkashanian M, Ma L, Chen EQ, et al. Experimental investigation on biomass co-firing in a 300 MW pulverized coal-fired utility furnace in China. *P Combust Inst* 2011;33:2725–33.
- [139] Patumsawad S. Co-firing Biomass with Coal for Power Generation. Fourth Biomass-Asia Workshop "Biomass: Sources of Renewable Bioenergy and Biomaterial". Shah Alam, Malasia, 2007.
- [140] Zactruba J, Stonecypher L, editor. Cofiring biomass – what to look for if considering. Fuel: Bright HUB; 2011.
- [141] Willeboer W. Biomass-coal cofiring in present and future power blocks. Workshop on Increasing Biomass Cofiring Percentages in Existing Power Plants. Geertruidenberg, Netherlands: IEA; 2008.
- [142] Dai JJ, Sokhansanj S, Grace JR, Bi XT, Lim CJ, Melin S. Overview and some issues related to co-firing biomass and coal. *Can J Chem Eng* 2008;86:367–86.
- [143] Livingston WR. The direct co-firing of biomass at high co-firing ratios. Workshop on High Percentage Biomass Cofiring in New Power Plants. Hamburg, Germany; 2009.
- [144] Biomass Energy Centre. Co-firing technology: Conversion technologies. <http://www.biomassenergycentre.org.uk/portal/page?_pageid=75,41182&_dad=portal&_schema=PORTAL>; 2014.
- [145] Hughes EE, Tillman DA. Biomass cofiring: status and prospects 1996. In: Engineering-Foundation Conference Biomass Usage for Utility and Industrial Power. Snowbird, Utah: Elsevier Science Bv; 1996. p. 127–42.
- [146] Sander B. Properties of Danish biofuels and the requirements for power production. *Biomass Bioenerg* 1997;12:177–83.
- [147] Tonn B, Dengler V, Thumm U, Piepho HP, Claupein W. Influence of leaching on the chemical composition of grassland biomass for combustion. *Grass Forage Sci* 2011;66:464–73.
- [148] Liaw SB, Wu H. Leaching characteristics of organic and inorganic matter from biomass by water: differences between batch and semi-continuous operations. *Ind Eng Chem Res* 2013;52:4280–9.
- [149] Bakker RR, Jenkins BM, Williams RB. Fluidized bed combustion of leached rice straw. *Energ Fuel* 2002;16:356–65.
- [150] Wu H, Yip K, Kong Z, Li C-Z, Liu D, Yu Y, et al. Removal and recycling of inherent inorganic nutrient species in mal lee biomass and derived biochars by water leaching. *Ind Eng Chem Res* 2011;50:12143–51.
- [151] Ho YS, Harouna-Oumarou HA, Fauduet H, Porte C. Kinetics and model building of leaching of water-soluble compounds of *Tilia* sapwood. *Sep Purif Technol* 2005;45:169–73.
- [152] Liu H, Zhang L, Han Z, Xie B, Wu S. The effects of leaching methods on the combustion characteristics of rice straw. *Biomass Bioenerg* 2013;49:22–7.
- [153] Smith DM, Brown DM. Rainfall-induced leaching and leaf losses from drying alfalfa forage. *Agron J* 1994;86:503–10.
- [154] Enestam S, Bankiewicz D, Tuiremo J, Makela K, Hupa M. Are NaCl and KCl equally corrosive on superheater materials of steam boilers? *Fuel* 2013;104:294–306.
- [155] Srivastava M, Balraj JN, Ravisankar B, Anandan C, Grips VKW. High temperature oxidation and corrosion behaviour of Ni/Ni-Co-Al composite coatings. *Appl Surf Sci* 2012;263:597–607.
- [156] Metsajoki J, Huttunen-Saarivirta E, Lepisto T. Elevated-temperature corrosion of uncoated and aluminized 9–12% Cr boiler steels beneath KCl deposit. *Fuel* 2014;133:173–81.
- [157] Lehmusto J, Yrjas P, Skrifvars Bj, Hupa M. High temperature corrosion of superheater steels by KCl and K₂CO₃ under dry and wet conditions. *Fuel Process Technol* 2012;104:253–64.
- [158] Uusitalo MA, Vuoristo PMJ, Mantyla TA. High temperature corrosion of coatings and boiler steels in oxidizing chlorine-containing atmosphere. *Mat Sci Eng A* 2003;346:168–77.
- [159] Persson K, Brostrom M, Carlsson J, Nordin A, Backman R. High temperature corrosion in a 65 MW waste to energy plant. *Fuel Process Technol* 2007;88:1178–82.
- [160] Grabke HJ, Reese E, Spiegel M. The effects of chlorides, hydrogen-chloride, and sulfur-dioxide in the oxidation of steel below deposits. *Corros Sci* 1995;37:1023–43.
- [161] Bankiewicz D, Enestam S, Yrjas P, Hupa M. Experimental studies of Zn and Pb induced high temperature corrosion of two commercial boiler steels. *Fuel Process Technol* 2013;105:89–97.
- [162] Pettersson C, Pettersson J, Asteman H, Svensson JE, Johansson LG. KCl-induced high temperature corrosion of the austenitic Fe-Cr-Ni alloys 304L and Sanicor 28 at 600 degrees C. *Corros Sci* 2006;48:1368–78.
- [163] Lehmusto J, Skrifvars Bj, Yrjas P, Hupa M. Comparison of potassium chloride and potassium carbonate with respect to their tendency to cause high temperature corrosion of stainless 304L steel. *Fuel Process Technol* 2013;105:98–105.
- [164] Li YS, Niu Y, Spiegel M. High temperature interaction of Al/Si-modified Fe-Cr alloys with KCl. *Corros Sci* 2007;49:1799–815.
- [165] Brostrom M, Enestam S, Backman R, Makela K. Condensation in the KCl-NaCl system. *Fuel Process Technol* 2013;105:142–8.
- [166] Cutler AJB, Raask E. External corrosion in coal-fired boilers – assessment from laboratory data. *Corros Sci* 1981;21:789–800.
- [167] Spiegel M, Biedenkopf P, Grabke HJ. Corrosion of iron base alloys and high alloy steels in the Li₂CO₃-K₂CO₃ eutectic mixture. *Corros Sci* 1997;39:1193–210.
- [168] Nishina T, Uchida I, Selman JR. Gas electrode-reactions in molten-carbonate media .5. Electrochemical analysis of the oxygen reduction-mechanism at a fully immersed gold electrode. *J Electrochem Soc* 1994;141:1191–8.
- [169] Huttunen-Saarivirta E, Kalidakis S, Stott FH, Rohr V, Schutze M. The erosion-corrosion resistance of uncoated and aluminized 12% chromium ferritic steels under fluidized-bed conditions at elevated temperature. *Mater Corros* 2005;56:897–906.
- [170] Qiao M, Zhou C. Hot corrosion behavior of Co modified NiAl coating on nickel base superalloys. *Corros Sci* 2012;63:239–45.
- [171] Mayer P, Manolescu AV. Influence of hydrogen-chloride on corrosion of boiler steels in synthetic flue-gas. *Corrosion* 1980;36:369–73.
- [172] Opila EJ. Volatility of common protective oxides in high-temperature water vapor: current understanding and unanswered questions. *Mater Sci Forum* 2004;461–464:765–73.
- [173] Vassilev SV, Baxter D, Andersen LK, Vassileva CG. An overview of the composition and application of biomass ash. Part 1. Phase-mineral and chemical composition and classification. *Fuel* 2013;105:40–76.
- [174] American Coal Ash Association(ACAA). Coal Combustion Products Production & Use Statistics. <<http://www.acaa-usa.org/Publications/Production-Use-Reports>>; 2014.
- [175] European Coal Ash Association (ECOBA). Production and Utilisation of CCPs in Europe(EU15). <<http://www.acaa-usa.org/Publications/Production-Use-Reports>>; 2014.
- [176] Pandey VC, Singh N. Impact of fly ash incorporation in soil systems. *Agric Ecosyst Environ* 2010;136:16–27.
- [177] Carrasco B, Cruz N, Terrados J, Corpas FA, Perez L. An evaluation of bottom ash from plant biomass as a replacement for cement in building blocks. *Fuel* 2014;118:272–80.
- [178] Vassilev SV, Baxter D, Andersen LK, Vassileva CG. An overview of the composition and application of biomass ash. Part 2. Potential utilisation, technological and ecological advantages and challenges. *Fuel* 2013;105:19–39.
- [179] Fernandez-Pereira C, de la Casa JA, Gomez-Barea A, Arroyo F, Leiva C, Luna Y. Application of biomass gasification fly ash for brick manufacturing. *Fuel* 2011;90:220–32.
- [180] Cabrera M, Galvin AP, Agrela F, Dolores Carvajal M, Ayuso J. Characterisation and technical feasibility of using biomass bottom ash for civil infrastructures. *Constr Build Mater* 2014;58:234–44.
- [181] Wang SZ, Llamazos E, Baxter L, Fonseca F. Durability of biomass fly ash concrete: freezing and thawing and rapid chloride permeability tests. *Fuel* 2008;87:359–64.
- [182] Cuencia J, Rodriguez J, Martin-Morales M, Sanchez-Roldan Z, Zamorano M. Effects of olive residue biomass fly ash as filler in self-compacting concrete. *Constr Build Mater* 2013;40:702–9.
- [183] Babu KG, Rao GSN. Efficiency of fly ash in concrete with age. *Cement Concrete Res* 1996;26:465–74.
- [184] Maschio S, Tonello G, Piani L, Furlani E. Fly and bottom ashes from biomass combustion as cement replacing components in mortars production: rheological behaviour of the pastes and materials compression strength. *Chemosphere* 2011;85:666–71.
- [185] Hinojosa MJR, Galvin AP, Agrela F, Perianes M, Barbudo A. Potential use of biomass bottom ash as alternative construction material: conflictive chemical parameters according to technical regulations. *Fuel* 2014;128:248–59.
- [186] Esteves TC, Rajamma R, Soares D, Silva AS, Ferreira VM, Labrincha JA. Use of biomass fly ash for mitigation of alkali-silica reaction of cement mortars. *Constr Build Mater* 2012;26:687–93.
- [187] Atis CD. Accelerated carbonation and testing of concrete made with fly ash. *Constr Build Mater* 2003;17:147–52.
- [188] Atis CD. Heat evolution of high-volume fly ash concrete. *Cement Concrete Res* 2002;32:751–6.
- [189] Atis CD. High volume fly ash abrasion resistant concrete. *J Mater Civil Eng* 2002;14:274–7.
- [190] Atis CD. High-volume fly ash concrete with high strength and low drying shrinkage. *J Mater Civil Eng* 2003;15:153–6.
- [191] Atis CD. Strength properties of high-volume fly ash roller compacted and workable concrete, and influence of curing condition. *Cement Concrete Res* 2005;35:1112–21.
- [192] Atis CD, Sevim UK, Ozcan F, Bilim C, Karahan O, Tanrikulu AH, et al. Strength properties of roller compacted concrete containing a non-standard high calcium fly ash. *Mater Lett* 2004;58:1446–50.

- [193] Mehta PK. High-performance, high-volume fly ash concrete for sustainable development. Proceedings of the International Workshop on Sustainable Development and Concrete Technology. 2004;3–14.
- [194] Nath P, Sarker P. Effect of Fly Ash on the Durability Properties of High Strength Concrete. Proceedings of the Twelfth East Asia-Pacific Conference on Structural Engineering and Construction (Easec12). 2011;14:1149–56.
- [195] Jala S, Goyal D. Fly ash as a soil ameliorant for improving crop production – a review. *Bioresour Technol* 2006;97:1136–47.
- [196] Yunusa IAM, Eamus D, DeSilva DL, Murray BR, Burchett MD, Skilbeck GC, et al. Fly-ash: an exploitable resource for management of Australian agricultural soils. *Fuel* 2006;85:2337–44.
- [197] Basu M, Pande M, Bhadoria PBS, Mahapatra SC. Potential fly-ash utilization in agriculture: a global review. *Prog Nat Sci* 2009;19:1173–86.
- [198] American Coal Ash Association (ACAA). What are CCPs: Fly ash. <<http://www.acaa-usa.org/About-Coal-Ash/What-are-CCPs/Fly-Ash>>; 2014.
- [199] American Coal Ash Association (ACAA). What are CCPs: Bottom ash. <<http://www.acaa-usa.org/About-Coal-Ash/What-are-CCPs/Bottom-Ash>>; 2014.
- [200] Ahmaruzzaman M. A review on the utilization of fly ash. *Prog Energ Combust* 2010;36:327–63.
- [201] Rajamma R, Ball RJ, Tarelho LAC, Allen GC, Labrincha JA, Ferreira VM. Characterisation and use of biomass fly ash in cement-based materials. *J Hazard Mater* 2009;172:1049–60.
- [202] James AK, Thring RW, Helle S, Ghuman HS. Ash management review—applications of biomass bottom ash. *Energies* 2012;5:3856–73.
- [203] Laurendeau NM. Heterogeneous kinetics of coal char gasification and combustion. *Prog Energ Combust* 1978;4:221–70.
- [204] Vassilev SV, Baxter D, Andersen LK, Vassileva CG. An overview of the chemical composition of biomass. *Fuel* 2010;89:913–33.
- [205] Wang S, Miller A, Llamazos E, Fonseca F, Baxter L. Biomass fly ash in concrete: mixture proportioning and mechanical properties. *Fuel* 2008;87:365–71.
- [206] Chen WM, Jiang N. Calculation of ash fusion temperature using ash compositions. *Coal Process Compr Util* 1995;13–17.
- [207] Bouzoubaa N, Lachemi M. Self-compacting concrete incorporating high volumes of class F fly ash – preliminary results. *Cement Concrete Res* 2001;31:413–20.
- [208] Marku J, Dumi I, Lico E. The characterization and the utilization of cement kiln dust (CKD) as partial replacement of Portland cement in mortar and concrete production. *Zastita Mater* 2012;53.
- [209] Lanzerstorfer C. Chemical composition and physical properties of filter fly ashes from eight grate-fired biomass combustion plants. *J Environ Sci (China)* 2015;30:191–7.
- [210] Lanzerstorfer C. Chemical and physical characterization of cyclone fly ashes from five grate-fired biomass combustion plants. *Carpath J Earth Env* 2014;9:129–35.
- [211] Steenari BM, Schelander S, Lindqvist O. Chemical and leaching characteristics of ash from combustion of coal, peat and wood in a 12 MW CFB – a comparative study. *Fuel* 1999;78:249–58.
- [212] Poykio R, Ronkkomaki H, Nurmesniemi H, Peramaki P, Popov K, Valimaki I, et al. Chemical and physical properties of cyclone fly ash from the grate-fired boiler incinerating forest residues at a small municipal district heating plant (6 MW). *J Hazard Mater* 2009;162:1059–64.
- [213] Nurmesniemi H, Makela M, Poykio R, Manskinen K, Dahl O. Comparison of the forest fertilizer properties of ash fractions from two power plants of pulp and paper mills incinerating biomass-based fuels. *Fuel Process Technol* 2012;104:1–6.
- [214] Page A, Elseewi AA, Straughan I. Physical and chemical properties of fly ash from coal-fired power plants with reference to environmental impacts. In: Residue reviews. Springer; 1979. p. 83–120.
- [215] Killingley J, McEvoy S, Dokumcu C, Stauber J, Dale L. Trace element leaching from fly ash from Australian power stations. End of Grant Report, Australian Coal Association Research Program; 2000.
- [216] Poykio R, Nurmesniemi H, Peramaki P, Kuokkanen T, Valimaki I. Leachability of metals in fly ash from a pulp and paper mill complex and environmental risk characterisation for eco-efficient utilization of the fly ash as a fertilizer. *Chem Spec Bioavailab* 2005;17:1–9.
- [217] Melotti R, Santagata E, Bassani M, Salvo M, Rizzo S. A preliminary investigation into the physical and chemical properties of biomass ashes used as aggregate fillers for bituminous mixtures. *Waste Manage* 2013;33:1906–17.
- [218] Vassilev SV, Vassileva CG. A new approach for the classification of coal fly ashes based on their origin, composition, properties, and behaviour. *Fuel* 2007;86:1490–512.
- [219] Asokan P, Saxena M, Asolekar SR. Coal combustion residues – environmental implications and recycling potentials. *Resour Conserv Recy* 2005;43:239–62.
- [220] Chang AC, Lund LJ, Page AL, Warneke JE. Physical-properties of fly ash amended soils. *J Environ Qual* 1977;6:267–70.
- [221] Prabakar J, Dendorkar N, Morchhale RK. Influence of fly ash on strength behavior of typical soils. *Constr Build Mater* 2004;18:263–7.
- [222] Khan MR, Khan MW. The effect of fly ash on plant growth and yield of tomato. *Environ Pollut* 1996;92:105–11.
- [223] Péra J, Husson S, Guilhot B. Influence of finely ground limestone on cement hydration. *Cement Concrete Comp* 1999;21:99–105.
- [224] European Committee for Standardization. Cement – Part 1: Composition, specifications and conformity criteria for common cements (EN 450-1:2005+A1:2007). 2007.
- [225] European Committee for Standardization. Cement – Part 1: Composition, specifications and conformity criteria for common cements (BS EN 197-1:2000). 2000.
- [226] British Standard Institution. Specification for Portland cement. 1996.
- [227] European Committee for Standardization. Cement – Part 1: Composition, specifications and conformity criteria for common cements (EN 450-1:2012). 2012.
- [228] Caldas-Vieira F, Feuerborn H-J, Saraber A. European product standards—update on status and changes with relevance to CCPs. World of Coal Ash (WOCA) conference, Lexington, KY, USA, 2013.
- [229] American Society for Testing and Materials. ASTM C15: Standard Specification for Portland Cement. 2007.
- [230] General Administration of Quality Supervision, Inspection and Quarantine of the People's Republic of China, Standardization Administration of the People's Republic of China. Common Portland Cement (GB175-2007). 2007.
- [231] Japanese Standards Association (JSA). Portland Cement (JIS R5210:2003). 2003.
- [232] Yu QJ, Sawayama K, Sugita S, Shoya M, Isojima Y. The reaction between rice husk ash and Ca(OH)₂ solution and the nature of its product. *Cement Concrete Res* 1999;29:37–43.
- [233] Martirena F, Middendorf B, Day RL, Gehrke M, Roque P, Martinez L, et al. Rudimentary, low tech incinerators as a means to produce reactive pozzolan out of sugar cane straw. *Cement Concrete Res* 2006;36:1056–61.
- [234] Taylor EM, Schuman GE. Fly-ash and lime amendment of acidic coal spoil to aid revegetation. *J Environ Qual* 1988;17:120–4.
- [235] Mittra BN, Karmakar S, Swain DK, Ghosh BC. Fly ash – a potential source of soil amendment and a component of integrated plant nutrient supply system. *Fuel* 2005;84:1447–51.
- [236] Rautaray SK, Ghosh BC, Mittra BN. Effect of fly ash, organic wastes and chemical fertilizers on yield, nutrient uptake, heavy metal content and residual fertility in a rice-mustard cropping sequence under acid lateritic soils. *Bioresour Technol* 2003;90:275–83.
- [237] Lee SB, Lee YB, Lee CH, Hong CO, Kim PJ, Yu C. Characteristics of boron accumulation by fly ash application in paddy soil. *Bioresour Technol* 2008;99:5928–32.
- [238] Mishra M, Sahu RK, Padhy RN. Growth, yield and elemental status of rice (*Oryza sativa*) grown in fly ash amended soils. *Ecotoxicology* 2007;16:271–8.
- [239] Singh LP, Siddiqui ZA. Effects of fly ash and *Helminthosporium oryzae* on growth and yield of three cultivars of rice. *Bioresour Technol* 2003;86:73–8.
- [240] Gaind S, Gaur AC. Impact of fly ash and phosphate solubilising bacteria on soybean productivity. *Bioresour Technol* 2002;85:313–15.
- [241] Adriano DC, Weber JT. Influence of fly ash on soil physical properties and turfgrass establishment. *J Environ Qual* 2001;30:596–601.
- [242] Garg RN, Pathak H, Das DK, Tomar RK. Use of flyash and biogas slurry for improving wheat yield and physical properties of soil. *Environ Monit Assess* 2005;107:1–9.
- [243] Pichtel JR, Hayes JM. Influence of fly-ash on soil microbial activity and populations. *J Environ Qual* 1990;19:593–7.
- [244] Sarangi PK, Mahakur D, Mishra PC. Soil biochemical activity and growth response of rice *Oryza sativa* in flyash amended soil. *Bioresour Technol* 2001;76:199–205.
- [245] Scotti IA, Silva S, Botteschi G. Effect of fly ash on the availability of Zn, Cu, Ni and Cd to chicory. *Agric Ecosyst Environ* 1999;72:159–63.
- [246] Wong MH, Wong JWC. Effects of fly-ash on soil microbial activity. *Environ Pollut A* 1986;40:127–44.
- [247] Lal JK, Mishra B, Sarkar AK. Effect of fly ash on soil microbial and enzymatic activity. *J Indian Soc Soil Sci* 1996;44:77–80.
- [248] Kalra N, Hari RC, Sharma SK. Effect of flyash incorporation on soil properties of texturally variant soils. *Bioresour Technol* 2000;75:91–3.
- [249] Shende A, Juwarkar AS, Dara SS. Use of fly-ash in reducing heavy-metal toxicity to plants. *Resour Conserv Recy* 1994;12:221–8.
- [250] Ajaz S, Tiyagi S. Effect of different concentrations of fly-ash on the growth of cucumber plant, *Cucumis sativus*. *Arch Agron Soil Sci* 2003;49:457–61.
- [251] Wong MH, Wong JWC. Germination and seedling growth of vegetable crops in fly ash-amended soils. *Agric Ecosyst Environ* 1989;26:23–35.
- [252] Wong JWC, Wong MH. Effects of fly ash on yields and elemental composition of two vegetables, *Brassica parachinensis* and *B. chinensis*. *Agric Ecosyst Environ* 1990;30:251–64.
- [253] Bi YL, Li XL, Christie P, Hu ZQ, Wong MH. Growth and nutrient uptake of arbuscular mycorrhizal maize in different depths of soil overlying coal fly ash. *Chemosphere* 2003;50:863–9.
- [254] Lee CH, Lee YB, Lee H, Kim PJ. Reducing phosphorus release from paddy soils by a fly ash-gypsum mixture. *Bioresour Technol* 2007;98:1980–4.